ADVANCES IN ANATOMY, EMBRYOLOGY AND CELL BIOLOGY

Ricardo Insausti
Sandra Cebada-Sánchez
Pilar Marcos

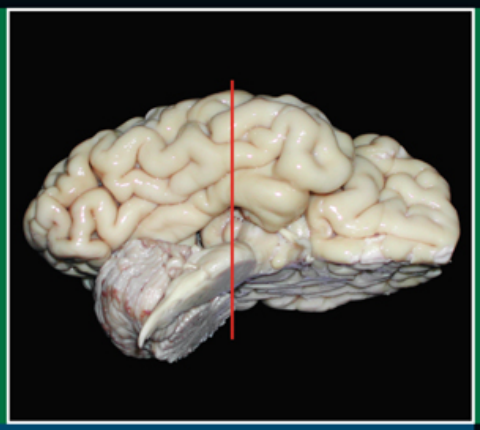

Postnatal Development of the Human Hippocampal Formation

Springer

Reviews and critical articles covering the entire field of normal anatomy (cytology, histology, cyto- and histochemistry, electron microscopy, macroscopy, experimental morphology and embryology and comparative anatomy) are published in Advancesin Anatomy, Embryology and Cell Biology. Papers dealing with anthropology and clinical morphology that aim to encourage cooperation between anatomy andrelated disciplines will also be accepted. Papers are normally commissioned. Original papers and communications may be submitted and will be considered for publication provided they meet the requirements of a review article and thus fit into the scope of "Advances". English language is preferred.
It is a fundamental condition that submitted manuscripts have not been and will not simultaneously be submitted or published elsewhere. With the acceptance of a manuscript for publication, the publisher acquires full and exclusive copyright for all languages and countries.
Twenty-five copies of each paper are supplied free of charge.

Manuscripts should be addressed to

206
Advances in Anatomy, Embryology and Cell Biology

Ricardo Insausti, Sandra Cebada-Sánchez, Pilar Marcos

Postnatal Development of the Human Hippocampal Formation

With 23 figures

Springer

Dr. Ricardo Insausti
Universidad Castilla-La Mancha
CRIB
Fac. Medicina
Avda. Almansa, 14
02006 Albacete
Spain
e-mail: ricardo.insausti@uclm.es

Dr. Pilar Marcos
Universidad Castilla-La Mancha
CRIB
Fac. Medicina
Avda. Almansa, 14
02006 Albacete
Spain
e-mail: pilar.marcos@uclm.es

Dr. Sandra Cebada-Sánchez
Universidad Castilla-La Mancha
CRIB
Fac. Medicina
Avda. Almansa, 14
02006 Albacete
Spain
e-mail: sandra.cebada@uclm.es

ISSN 0301-5556
ISBN 978-3-642-03660-6 e-ISBN 978-3-642-03661-3
DOI 10.1007/978-3-642-03661-3
Springer Heidelberg Dordrecht London New York

Library of Congress Control Number: 2009936783

Cover design: WMXDesign GmbH, Heidelberg, Germany

Printed on acid-free paper

Springer is part of Springer Science+Business Media (www.springer.com)

To Sofía.

Preface

Ume Eder Bat (A beautiful child) (popular song from Basque folklore)

The aim of this monograph is to introduce the postnatal development of morphological features that are relevant to readers interested in the neurobiology and pathology of the hippocampal formation in terms of the complex phenomena that underlie the progressive anatomical and functional maturation of this brain region. This review focuses on the morphological aspects, while more detailed basic phenomena associated with neuronal maturation—which are undoubtedly also of great interest—are only marginally referred to, although a selection of behavioral and clinical aspects will also be briefly addressed in an attempt to illustrate real situations in different clinical specialties.

The creation of this monograph is justified by the increasing importance and growing awareness shown in recent years of neurodevelopmental disorders in children. This awareness is leading to increasing refinement in clinical examinations of patients that may suffer from different neurodevelopment-related diseases, such as autism, epilepsy, memory disorders, etc. To the best of our knowledge, this work is the first comprehensive description of the postnatal changes in the hippocampal formation in its different constituent fields. Given the growing sensitivity and accuracy of neuroradiological examinations, particularly MRI, we also sought to offer a glimpse at the MRI aspects related to the development of the hippocampal formation in the human infant. Some caution must be exercised here, as our data deal with the anatomo-radiological correlation in ex vivo MRI images taken in fixed, normal human infant brains from routinely obtained necropsies in different hospitals across Spain. In this regard, we would like to show our appreciation of the uninterested help offered by the Pathology and Radiological Services of the Albacete University Hospital Complex (Drs. Atiénzar, Pascual, Cros and Mansilla, as well as their technician Francisca Cortés, who provided immensely valuable help), Drs. Tuñón and García-Bragado from Navarra's Department of Health, Dr. Rábano from Alcorcón Foundation Hospital, and we extend a very special thanks to the Pathology Service of Virgen del Rocío Hospital in Seville, in particular Drs.

Rivas, Chinchón and Fernández, for their tremendous help in providing human infant tissue.

This work is dedicated with kindness to those parents who gave their consent to perform necropsies on their beloved little ones at difficult moments. We hope that they will find comfort in the knowledge that their altruism will improve the health of other children.

Ricardo Insausti

P.S. To my inspiring mentor and friend, Prof. David G. Amaral, whose dedication to autistic children is an example of translational research, from basic science to clinical situations.

Acknowledgements

The authors wish to thank the great work carried out by the technical team of the Human Neuroanatomy Laboratory of the University of Castilla-La Mancha in Albacete (Spain), as well as the help of the technicians of the Virgen del Rocío Hospital in Seville (Spain) in the manipulation and preparation of the human brains and sections used in this study. This work has been supported by grants PI-2006/14 and PCI08-0113 by Junta de Comunidades de Castilla-La Mancha, Spain, and by grants FIS 01/0688 from the Ministry of Health, and G-2007_C/07 from FISCAM, JJCCM, Spain.

Abstract

The postnatal development of the human hippocampal formation (HF) is subject of increasing interest due to its implication in important pathologies that hamper the normal development of children. In this work, we present a glimpse of the main events that constitute important milestones in the development and shaping of some of the most important psychological capabilities such as autobiographical memory. We analyzed a total of 21 brains ranging from 27 gestational weeks to 14 years. Although we examined some cases in the last trimester of gestation, our description starts at birth, around 40 gestational weeks. Serial sections stained with thionin for Nissl analysis revealed that all fields of the HF were present and identifiable at birth. However, the relative growth of the cortical mantle was much higher relative to the HF. The main structural changes took place during the first postnatal year, in particular in the dentate gyrus and in the entorhinal cortex. At subsequent ages, a growth in size was noted in all components of the HF. This growth was more evident at the body and tail of the hippocampus, as evidenced by measurements of the neuroanatomical series. In addition, we examined in some cases the MRI appearance of the HF at different postnatal ages obtained by post-mortem imaging. MRI neuroanatomical series provided anatomically identified landmarks useful for the MRI identification of different components of the HF during postnatal development.

List of Contents

Abbreviations

A	Amygdala
AC-PC line	Anterior–posterior commissure line
ADHD	Attention-deficit/hyperactivity disorder
AHTA	Amygdalo-hippocampal transition area
ALA	Amniotic liquid aspiration
CA1	CA1 (*cornus ammonis*, Ammon's horn) field of the hippocampus
CA2	CA2 (*cornus ammonis*, Ammon's horn) field of the hippocampus
CA3	CA3 (*cornus ammonis*, Ammon's horn) field of the hippocampus
CD	Caudate nucleus
CHD	Congenital hearth disease
chf	Choroidal fissure
CL	Claustrum
COS	Childhood-onset schizophrenia
cs	Collateral sulcus
DG	Dentate gyrus
DIC	Disseminated intravascular coagulation
DNMS	Delayed-non-matching to sample
EC	Entorhinal cortex
EI	Intermediate subfield of the entorhinal cortex
ELc	Lateral caudal subfield of the entorhinal cortex
EMI	Medial intermediate subfield of the entorhinal cortex
f	Fimbria
fx	Fornix
GA	Gyrus ambiens
GIL	Gyrus intralimbicus
GS	Gyrus semilunaris
H	Hippocampus
HF	Hippocampal formation
hf	Hippocampal fissure
HMD	Hyaline membrane disease
IC	Insular cortex
irs	Intrarhinal sulcus
IQ	Intellectual quotient
its	Inferior temporal sulcus
IVC	Intraventricular communication

las	Lateral sulcus
LGN	Lateral geniculate nucleus
MAP	Microtubule associated protein
MRI	Magnetic resonance imaging
MTL	Medial temporal lobe
mts	Middle temporal sulcus
NIH	National Institutes of Health
ots	Occipito-temporal sulcus
p	Polymorphic cell layer
PAC	Periamygdaloid cortex
PaS	Parasubiculum
PB	Phosphate buffer
PBS	Phosphate buffered saline
PE	Pulmonary edema
PHR	Parahippocampal region
PIR	Piriform cortex
PPH	Posterior parahippocampal cortex
PRC	Perirhinal cortex
PrS	Presubiculum
pul	Pulvinar
PUT	Putamen
RFDH	Respiratory failure by diaphragmatic hernia
rs	Rhinal sulcus
S	Subiculum
SDCO	Sudden death of cardiac origin
SE-HR	Spin eco-high resolution
SMI31	High molecular weight phosphorilated neurofilaments
so	*Stratum oriens* (hippocampus)
sp	Splenium of corpus callosum
sr	*Stratum radiatum* (hippocampus)
ssa	Sulcus semiannularis
sts	Superior temporal sulcus
T	Tesla
TCS	Tissue collection solution
TE	Area TE of Bailey and von Bonin
TF	Area TF of Bailey and von Bonin
TH	Area TH of Bailey and von Bonin
TIR	"Tiempo de inversión-recuperación" in English "Inversion-recovery time"
V	Lateral ventricle
Vc	Sublayer Vc of the entorhinal cortex
w	White matter
WME	Without morphological expression
II	Layer II of the entorhinal cortex
III	Layer III of the entorhinal cortex

Chapter 1
Introduction

At birth, infants have fully developed brains—at least from a macroscopic point of view—and the constituents of the brain are easily recognizable in both humans (Arnold and Trojanowski 1996) and nonhuman primates (Rakic and Nowakowski 1981). However, many events need to occur in various areas of the brain once the child is born in order for it to achieve full maturity, and the human hippocampal formation (HF) is no exception. Although the HF is almost completely developed—macroscopically and structurally—by the time of birth, it does mature. This process of maturation includes absolute growth through the expansion of its constituents (Gogtay et al. 2006; Evans 2006), and the functional refinement of its circuitry at both the anatomic and physiologic levels.

However, even given this period of protracted development until full maturity, the anatomical appearance of the infant HF differs from that of the adult in only rather subtle ways. This fact does not preclude the development and maturation of a system that is most strongly associated with memory function, while, from a pathological point of view, epilepsy probably accounts for most of the clinical problems related to the HF.

For the sake of concision and brevity, we will not provide basic notions of the cell layers and fiber tracts that reside in the HF here, but we will assume that the reader knows how to navigate along its anterior–posterior dimension (the rostrocaudal axis, more commonly known as the septotemporal axis, especially in the rodent-related literature; i.e., Amaral and Witter 1989). Likewise, the medial-to-lateral axis implies a starting point in the dentate gyrus (DG), and unfolds from the medial extreme to the most lateral point, which is marked in humans by the border near to the transition with the neocortex. This lateral border of the HF varies along the anterior–posterior dimension such that the entorhinal cortex (EC) occurs rostrally and the parasubiculum caudally, and the presubiculum occurs near the end of the hippocampus (i.e., Fig. 23.15 in Insausti and Amaral 2004).

It seems reasonable to start by defining what is included under the term HF. As is the case in the adult human brain, we recognize a number of structures that are mainly linked by unidirectional connections. These have a starting point, namely

the DG, and an end point, the EC. This scheme, which was laid out by the great Spanish neuroanatomist Santiago Ramón y Cajal, is still valid today. Axons of the superficial cellular layers of the EC (layers II and III) innervate the DG and field CA3 of the hippocampus proper through the perforant path, and form the main source of afferents to the DG. DG cells project to CA3 through the mossy fiber system that forms the stratum lucidum, a special stratum that is specific to CA3. CA3, in turn, projects to CA1 through the system of Schaffer collaterals. CA1 projects to the subiculum, and this in turn projects to the presubiculum and parasubiculum. Finally, a converging input terminates in the EC, at the deep layers (layers V and VI) from CA1 (but not CA3) and the subiculum, while the presubiculum and very likely the parasubiculum project to layer III. Under normal circumstances no cells in CA3 innervate the DG, CA3 does not receive innervation from CA1, and CA1 is not innervated by the subiculum. In this way, the hippocampal input and output follows a defined stepwise set of connections that reach the EC, to be ultimately distributed to the neocortex. This system lies at the core of the declarative memory system.

The layout of the neural circuits that subserve the declarative memory system has been derived largely from experimental studies, mostly of rodents and to a lesser extent the nonhuman primate brain. There are a number of reviews in the literature that describe the details of this basic circuitry (Witter et al. 1989; rodent: Witter and Amaral 2004; human: Insausti and Amaral 2004) that have been applied to the human infant by extrapolating the experimental data, particularly from studies carried out in nonhuman primates (Lavenex et al. 2007) as the homology is closer than with rodent species, although the basic mechanisms may be similar.

Although the whole set of macroscopic components of the HF is complete when a child is born, a number of connectivity maturation phenomena occur after this that are extremely important in normal development. Another important phenomenon that may take place in humans, and has been known about for several decades in rodents (Sidman and Rakic 1973), is neurogenesis in the DG of the hippocampus. Although this has been demonstrated in humans (Eriksson et al. 1998), little is known about its contribution to the postnatal development of the human HF.

Yet another important issue is the presence of pathologies related specifically to neurodevelopmental disorders. Those disorders, which have been recognized for a long time, manifest themselves as epileptic seizures in the temporal lobe (cryptogenetic seizures), and more subtle disorders such as developmental amnesia (Vargha-Kadem at al. 1994, 1997), schizophrenia (Arnold et al. 1991a, b; Conrad et al. 1991; Heckers et al. 1991; Abel et al. 1992; Cannon et al. 1994; Arnold et al. 1995), autism (Bauman and Kemper 1985; Raymond et al. 1996; Saitoh et al. 2001), Down syndrome (Insausti et al. 1998c; Uecker et al. 1993; de la Monte and Hedley-Whyte 1990; Ferrer and Gullotta 1990; Weis 1991; Raz et al. 1995; Tanzi

1996), fetal alcohol syndrome (West et al. 1994), Williams syndrome (Galaburda et al. 1994), as well as other less frequent syndromes associated with genetic causes, such as velo-cardio-facial syndrome (22q11 deletion syndrome), where memory function impairment and a higher risk for schizophrenia are observed in association with decreased hippocampal volume (Debbane et al. 2006a, b).

Chapter 2
Materials and Methods

A total of 21 human brains (from individuals ranging from 27 gestational weeks to 14 years of age) were included in this study. The brains were collected during routine autopsies performed at several pathology departments. Standardized sanitary protocols that complied with Spanish regulations were followed, and informed consent was obtained from the families of the deceased. Postmortem intervals ranged from 12 to 24 h after death. Diagnostic procedures were performed by the respective trained neuropathologists, and all cases were free of neurological or psychological disorders. Data on age, sex and cause of death for the deceased are presented in Table 2.1.

Brains were fixed by immersion in 10% buffered formalin at the respective pathology departments after taking samples from cortical and subcortical structures for diagnostic purposes. The remainder of the brain was available for study. The brains of newborns and infants in general lack the consistency and firmness of adult brain tissue, at least until they reach two years or so. For this reason, the brains were postfixed in 4% paraformaldehyde in phosphate buffer (PB), pH 7.4, in our laboratory until processing. The total fixation procedure lasts at least one month (4–6 weeks).

The complete brain was obtained in some cases, but more often only one hemisphere was obtained. In the latter case, they were sectioned in slabs 1 cm thick, orthogonal to the anterior–posterior commissure line (AC–PC line), as described previously (Insausti et al. 1995). The remaining cases were received presectioned in the coronal plane, so the plane of section was not exactly orthogonal to the anterior–posterior commissure line.

Every brain was photographed at the time it was received. If the brain had already been blocked for neuropathological study, the blocks were reconstructed to create photographic records of the overall external aspect of the brain, and both the anterior and posterior faces of the individual blocks were photographed. Intact brains (or, more commonly, just one hemisphere) were photographed before and after blocking according to the plane of section described above. Blocks

Table 2.1 List of cases examined in the present study

Case	Age	Sex	Cause of death	MRI
1	27 gestational weeks	Female	Cardiac malformation	–
2	27 gestational weeks	Male	Bronchopneumonia	–
3	28 gestational weeks	Male	HMD	–
4	30 gestational weeks	Male	HMD	Yes
5	35 gestational weeks	?	?	–
6	37 gestational weeks	Male	ALA	–
7	38 gestational weeks	Male	DIC	Yes
8	40 gestational weeks	Male	ALA	Yes
9	40 gestational weeks	Female	WME	Yes
10	40 gestational weeks	Male	Bronchopneumonia	Yes
11	41 gestational weeks	Male	RFDH	Yes
12	14 postnatal days	Male	CHD	Yes
13	22 days	Male	Bronchopneumonia	Yes
14	5 months	Female	IVC	–
15	1 year	?	Sepsis	–
16	1.5 years	Male	SDCO	Yes
17	5 years	Male	Sepsis	–
18	5 years	Male	Sepsis/PE	Yes
19	5 years	Male	Sepsis	Yes
20	12 years	Female	Hypovolemic shock	–
21	14 years	Female	Lymphoma	Yes

containing the temporal lobe were dissected out and cryoprotected in graded sucrose solutions (15–30% sucrose in phosphate-buffered saline) before being sectioned. A series of 50 μm thick sections were obtained with a sliding microtome attached to a unit with a freezing stage. In cases where the tissue was more fragile (usually stillborns and newborns), 60 μm thick sections were obtained for a better histological appearance. One in five sections were immediately mounted onto gelatin-coated slides, air dried, and Nissl stained with 0.25% thionin at intervals of 250 or 300 μm (in cases sectioned at 60 μm) for cytoarchitectonic analysis. The intervening sections were collected in 24-well plates in tissue collection solution (TCS: 20% glycerol, 20% ethyleneglycol in 0.05 M PB) and stored at 4°C. Sections adjacent to the thionin-stained series were used for further immunohistochemical studies (Cebada-Sánchez et al., in preparation).

Analysis of the Nissl-stained series was performed by drawing the sections with the aid of a camera lucida on a Leica MZ stereomicroscope (Heidelberg, Germany). The borders of the different HF fields were charted on the camera lucida drawings and analyzed in more detail with a Nikon Eclipse 80*i* microscope. Low-power photomicrographs were taken with a photographic camera attached to densitometry apparatus (MCID, Paris) or with a digital Nikon camera attached to a Nikon Eclipse 80*i*. Microphotographs were only adjusted for brightness and contrast using Adobe Photoshop software; there was no other image manipulation.

MRI images were obtained for 12 brains (Table 2.1). The brains were retrieved from the storage solution and briefly rinsed in distilled water to remove excess

paraformaldehyde. For brains sectioned for neuropathologic examination, the brain was reconstructed from the blocks and embedded in 1.5% agar in lukewarm distilled water; the agar, once solidified, held the slabs together during MRI acquisition. This procedure did not alter the properties of the brain tissue for further tissue processing.

MRI images were obtained with a 1.5 T Philips Intera scanner at the Department of Radiology, Albacete University Hospital. Whenever possible, the coronal plane was placed orthogonal to the anterior–posterior commissure line, although, especially in the stillborns and newborns, it was not always easy to identify. In such cases an approximation was used. Further methodological details are presented in the MRI correlation section.

Both the MRI scans and the histological series were compared, with distances measured from the temporal pole to a number of medial temporal lobe structures such as the limen insulae, the beginning of the temporal horn of the lateral ventricle, the hippocampal head, the end of the uncal hippocampus (gyrus intralimbicus), and the tail of the hippocampus (caudal end of the hippocampus). The lateral geniculate nucleus (LGN) was also included in some cases as an extrahippocampal landmark that indicates the end of the EC (as in the adult brain, see Insausti and Amaral 2004).

Chapter 3
General Organization of the HF Fields Related to Macroscopic Anatomy

Macroscopically, both premature cases (not illustrated) and newborns have completely formed brains. Telencephalic structures, such as lobules and commissures and the general topography and disposition of the brain are present. The HF lies at the same position as in the adult: at the ventromedial aspect of the temporal lobe. A gross examination of the brain reveals that the full set of macroscopic landmarks is present in the newborn brain. The utility of this group of gross anatomical landmarks in the segmentation of the HF and the surrounding cortex of the parahippocampal region (PHR, namely the cortical areas around the HF, beginning with the temporopolar cortex, and followed in the caudal direction by the perirhinal and posterior parahippocampal cortices) has been reported previously (Insausti et al. 1998b; Insausti and Amaral 2004).

3.1
Gross Anatomical Landmarks

Proceeding rostrally to caudally, this set of gross anatomical landmarks comprises:

- The temporal pole, which constitutes the rostral extreme of the temporal lobe and hence of the PHR (see above). The temporopolar cortex continues ventrally, and is limited rostrally by the perirhinal cortex (PRC, Brodmann areas 35 and 36). Dorsally, it continues the cortex of the superior temporal gyrus and adjoining fields limiting with the insular cortex (parainsular cortex).
- The rostral limit of the PRC is marked by the start of the collateral sulcus (Figs. 3.1b, 3.2, 3.3), which is usually well marked in the most medial part at the ventral aspect of the temporal lobe.
- Shortly after, there is the beginning of the limen insulae (frontotemporal junction). At the level of the limen insulae there is a short transitional part that lies rostral to the amygdaloid complex where the temporal lobe presents

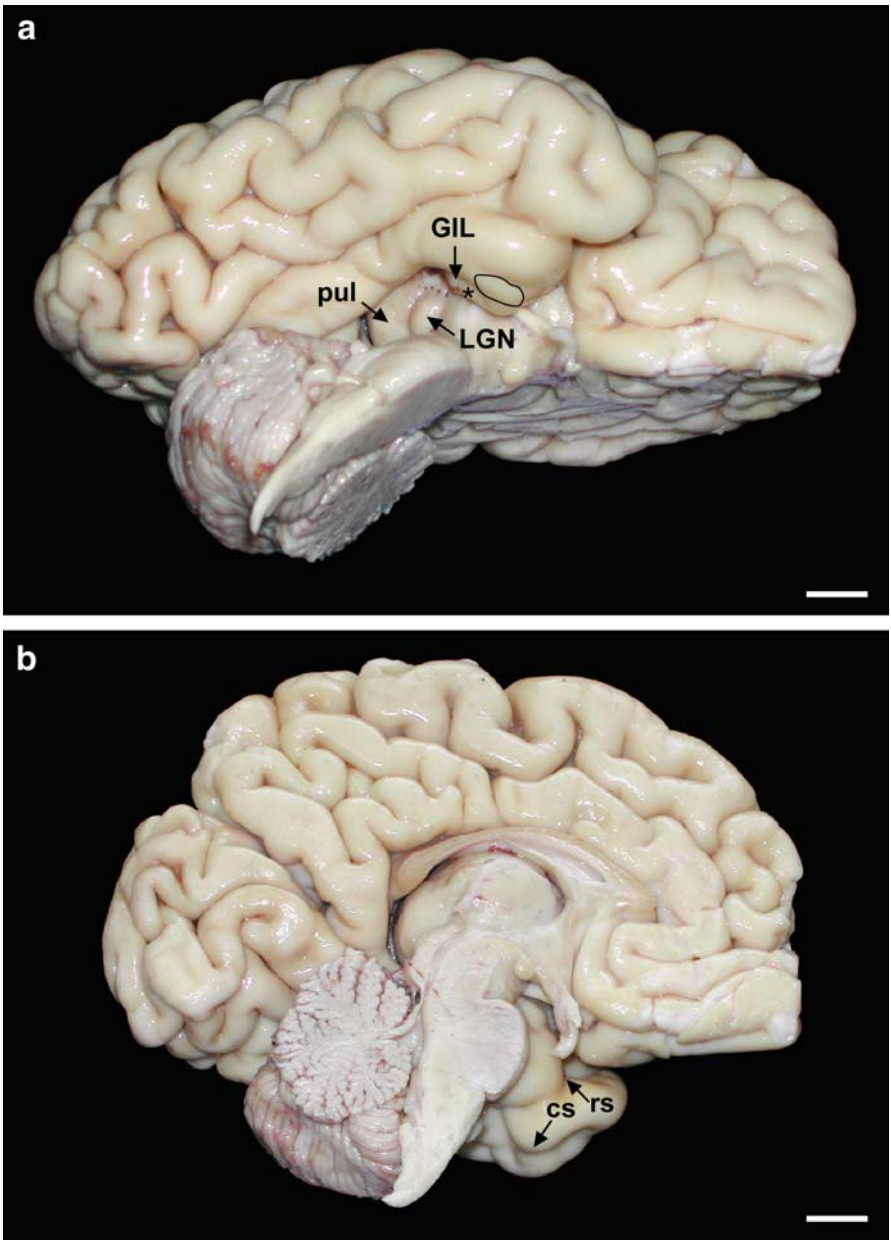

Fig. 3.1 Photographs showing the macroscopic aspect of a newborn brain. (**a**) Lateral view; (**b**) midsagittal view. Overall, the appearance of the newborn brain is reminiscent of that of the adult brain, other than the limited growth of the cortical mantle. Compare the size of the whole telencephalon to that of the brainstem in the photographs. Other than that, the convolutions (gyri) and the sulci are well developed, including the temporal lobe.

the middle and inferior temporal gyri. At this point, the EC appears as the rostralmost component of the HF, a few millimeters in front of the rostral pole of the amygdaloid complex, which also occurs in the human adult brain sectioned orthogonal to the AC–PC line (Insausti and Amaral 2004, Fig. 23.4).

- At this level, the rhinal sulcus is noticeable, and child brains show the same degree of variability of the rhinal sulcus as adult brains (Fig. 3.1b). The rhinal sulcus is continuous with the collateral sulcus in approximately less than half of the cases (Hanke 1997), and, as in adults, when the collateral sulcus reaches the temporal pole, the rhinal sulcus is short and becomes progressively less prominent until it disappears on the surface of the EC (Fig. 3.1b); conversely, when the collateral sulcus is short, the rhinal sulcus joins the collateral sulcus at some point. This situation is similar to that in the adult (Insausti et al. 1995).
- Further caudally, the rostromedial aspect of the medial temporal lobe (MTL) presents some bulges or prominences along the dorsomedial corner of the MTL. The presence of the sulcus semiannularis defines the gyrus semilunaris, which consists of periamygdaloid cortex (PAC), dorsally; the gyrus ambiens lies ventral to the sulcus semiannularis and is the medialmost portion of the EC. The gyrus ambiens is a medial intermediate subfield (EMI, see Insausti et al. 1995 for the labeling of EC subfields) of the EC that Brodmann (1909) labeled area 34, thus indicating a different cytoarchitectonic area, distinct from area 28 or EC proper. The gyrus ambiens is demarcated by the intrarhinal sulcus (or the inferior rhinal sulcus of Retzius 1898, Insausti and Amaral 2004) that can be clearly seen in the ventromedial aspect of the EC in Fig. 3.1a. These prominences, when examined in the neuroanatomical series of sections, match closely with those described for the adult brain, and will be used as gross anatomical landmarks to signal relevant structures in the HF and MTL in general. The overall spatial relationship of those elements is shown in Fig. 3.4a, b, which are magnified photomicrographs of sections that are slightly caudal to the limen insulae in a newborn; the gyrus semilunaris (Figs. 3.4a, b) and the gyrus ambiens (Fig. 3.4b) are indicated. In addition, they depict how the EC completely enwraps the rostral portion of the amygdaloid complex.
- The gyrus semilunaris and the gyrus ambiens (circled in Fig. 3.1a) are continuous caudally with the very rostral portion of the uncus, forming the gyrus uncinatus (Fig. 3.1a, asterisk) The sulcus semiannularis is no longer present at this point, and the EC lies ventral to the opening of the choroidal fissure medially (Fig. 3.4b). The lateral border of the EC is indicated by the collateral sulcus. At birth, the limit between the entorhinal and perirhinal cortices occurs

Fig. 3.1 (continued) The *asterisk in* **a** indicates the gyrus uncinatus and the *circled area* includes the gyrus ambiens, rostral to the gyrus uncinatus. The position of the LGN in the thalamus (*arrow*) is apparent, as the weight of the brainstem reveals the ventral aspect of the newborn thalamus. The LGN is an extrahippocampal landmark that is used to calculate distances between components of the HF, which are useful in MRI examinations (see text). *Scale bar* equals 1 cm

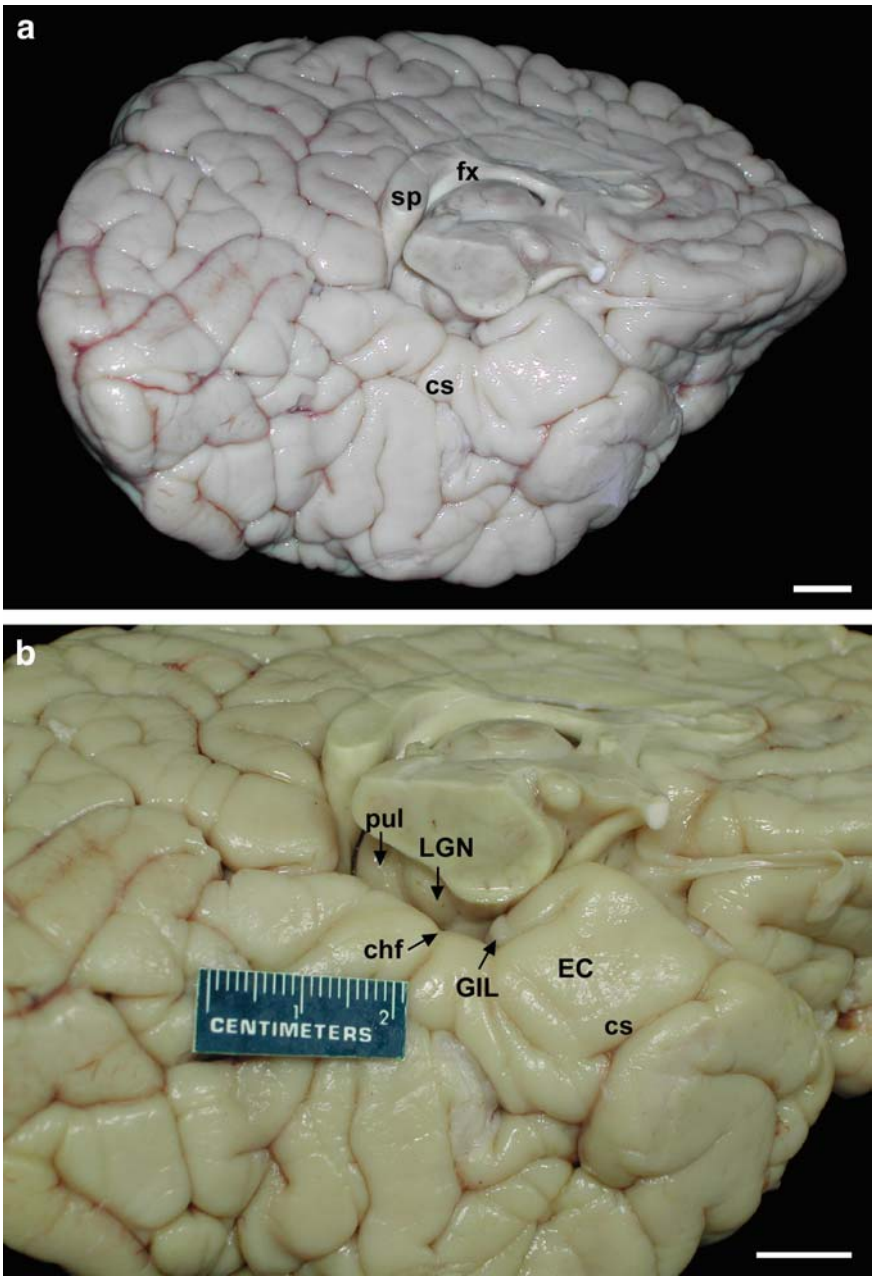

Fig. 3.2 (**a**) Ventromedial view of the brain in an 18 month old. (**b**) Close-up view of the same case. Note the growth of the whole cortical mantle, including the HF in the ventromedial aspect of the temporal lobe. Just as in newborns, the external aspect of the brain looks like an adult. The brainstem was removed, so from this view the LGN is easily observed, as well as the mammillary bodies and part of the optic chiasm. In the temporal lobe, the parahippocampal gyrus is readily distinguishable at higher magnification (**b**), as is the head of the uncus in the most rostral part of this gyrus. *Scale bar* equals 1 cm

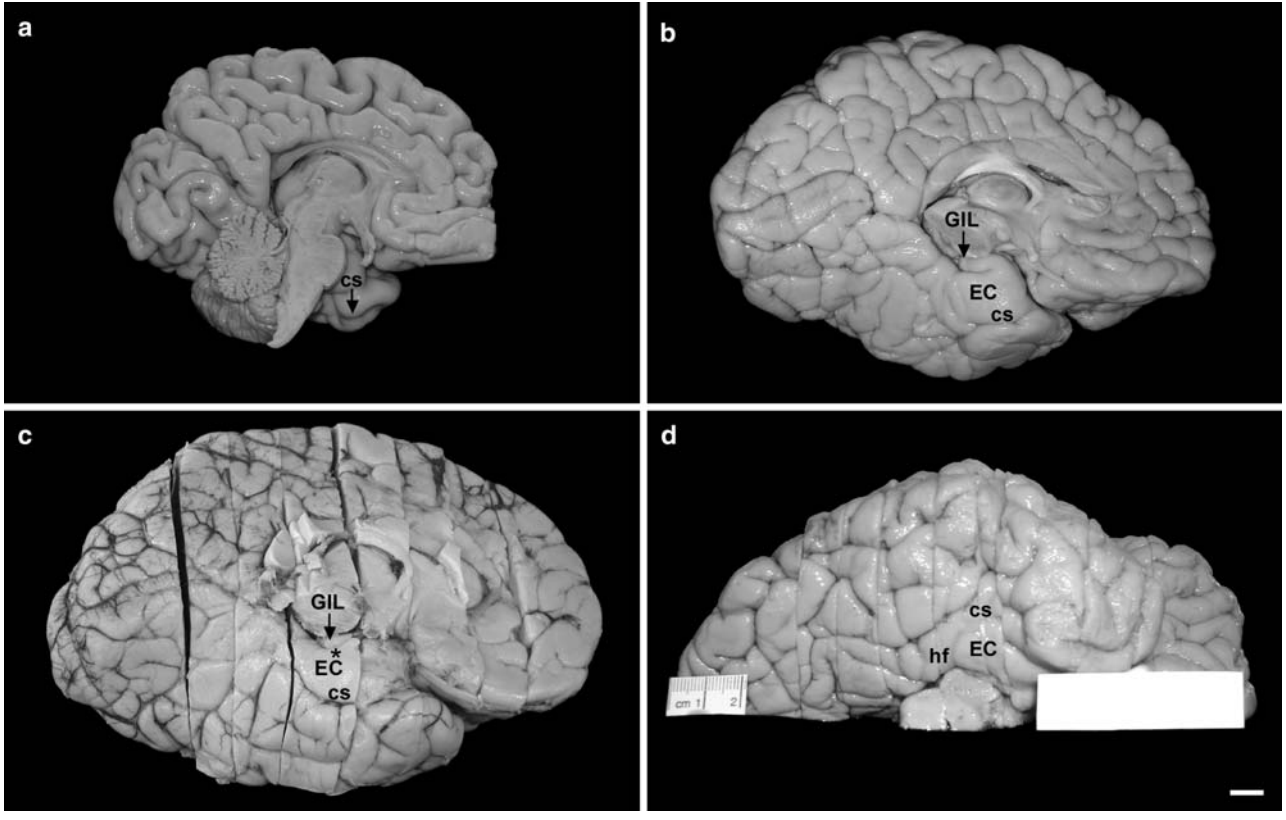

Fig 3.3 Comparison of the macroscopic aspects of the ventromedial (**a**, **b**, **c**) or ventral (**d**) surfaces of the brain in a newborn (**a**), an 18 month old (**b**), a five year old (**c**), and a 14 year old (**d**). From this macroscopic point of view, the growth of the cortical mantle relative to the more limited growth of the medial temporal lobe structures can be observed. The a*sterisk* in **c** shows the gyrus ambiens. *Scale bar* equals 1 cm in all panels

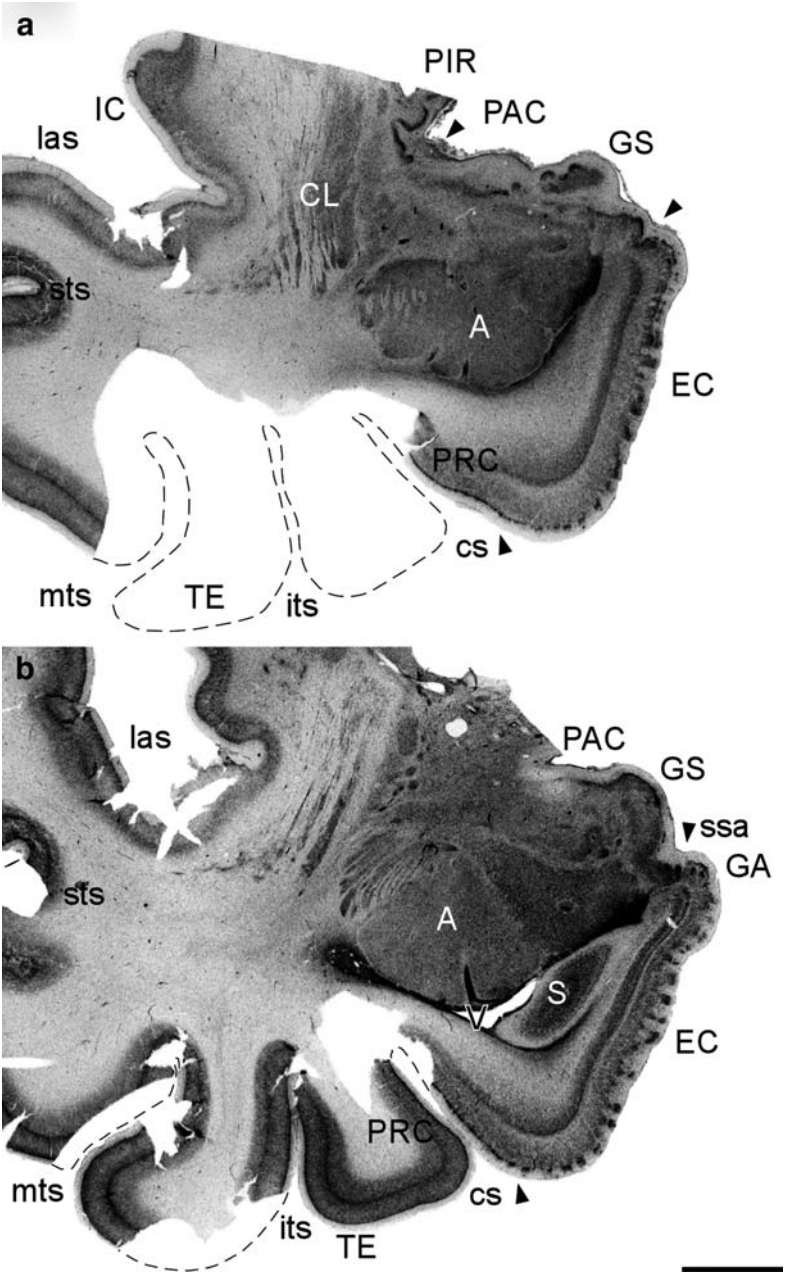

Fig. 3.4 (continued)

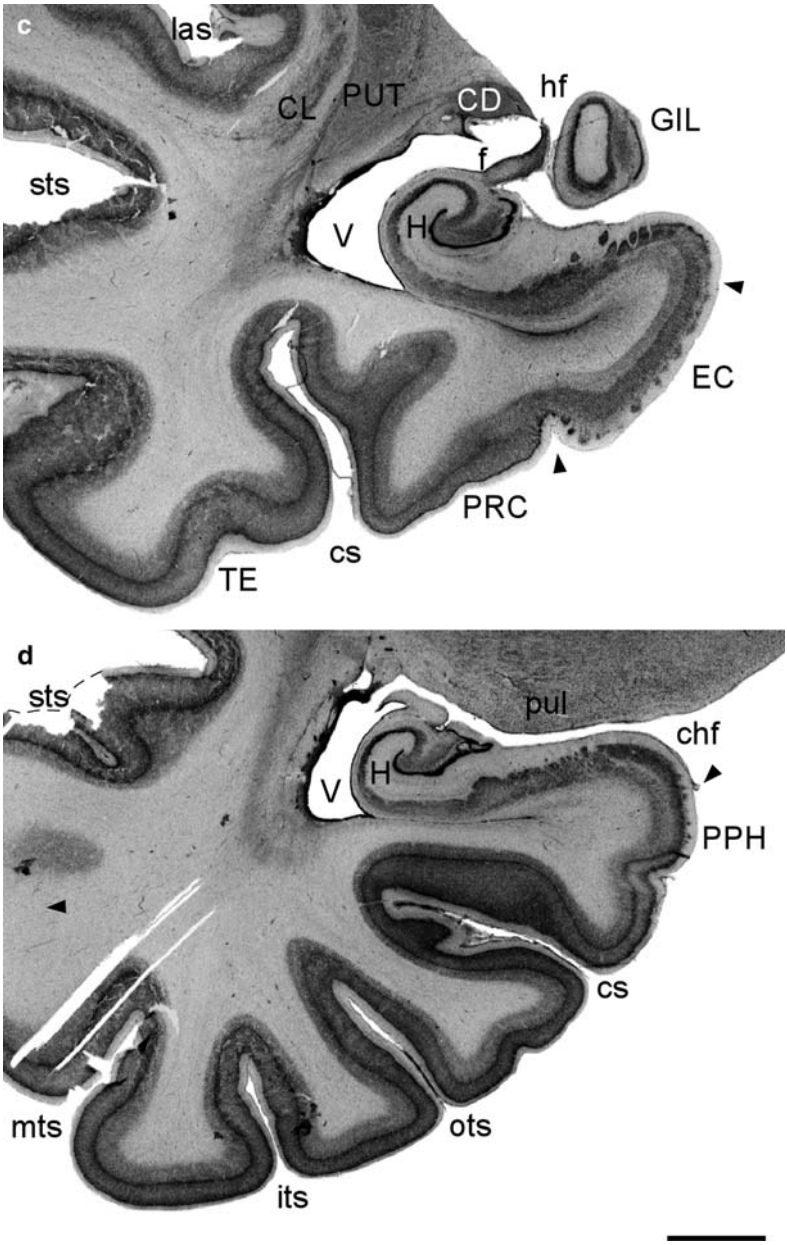

Fig. 3.4 Low-power microphotographs of the HF in coronal sections from rostral (**a**) to caudal (**d**) in a newborn. **a** is slightly behind the limen insulae, and shows the rostral amygdaloid complex and the rostral EC. In addition, the piriform cortex (PIR) and periamygdaloid cortices (PAC) as well as the prominence of the gyrus semilunaris (GS)

at the medial bank of the collateral sulcus, as in the adult. Figure 3.4c shows the relationship between the lateral border of the EC and the PRC at the medial bank of the collateral sulcus at a level rostral to the gyrus intralimbicus. The surface of the EC is smooth and totally devoid of the verrucae gyri hippocampi described in the adult (Klingler 1948).

- The lateral ventricle appears as a small slit underneath the amygdala (Fig. 3.4b), and is followed shortly after by the most anterior aspect of the hippocampal head, which mostly consists of the subiculum. The same spatial relationship is present in the adult human brain (Insausti and Amaral 2004).
- The subiculum starts at mid level of the amygdala. The first indication of the hippocampal head occurs as a tangential section through the rostralmost portion of the subiculum (Fig. 3.4b). The CA1 and CA3 fields appear in the hippocampal head until the DG presents itself (Fig. 3.4c).
- The DG (gyrus dentatus) becomes apparent at midportions of the hippocampal head. The DG first appears as a darkly stained band that is roughly circular or elliptical in shape. The DG encloses the hilar region, one of the layers of the DG. The DG granule cell layer (responsible for the dark band observed at low magnification, see below) is surrounded by the molecular layer of the DG, a band of white matter that wraps completely around the DG granule cell layer. The dark band of the granule cell layer of the DG splits into two or more "fingers" or extensions that follow the digitationes hippocampi. This feature of the hippocampal head consists of a variable number of flexures of all structures of the hippocampal head (DG, CA3, CA1 and subiculum) located at the rostral part of the uncus, reaching as far as the start of the hippocampal fissure (Gertz 1972).
- As mentioned, at this point the hippocampal head presents a variable number of flexures, and it is not known whether this number is fixed from birth or develops postnatally. Nonetheless, we have observed the presence of several digitationes hippocampi at the time of birth. The medialmost flexure forms the caudal part of the uncus, and particularly the gyrus uncinatus, which presents an overall appearance that is very similar to the adult brain (Fig. 3.1). The uncus displays the same rostrocaudal progression of structures as seen in adults.

Fig. 3.4 (continued) are apparent, much like in the adult. Also, the indentation between the EC and the PAC (*upper arrowhead*) is visible. The *broken lines* indicate the approximate locations of the inferior and middle temporal gyri. The inferior (*its*), medial (*mts*) and superior (*sts*) temporal sulci are distinguishable, as is the area TE, which is lateral to the PRC. In **b**, the beginning of the head of the hippocampus can be distinguished, as well as the intermediate portion of the EC. **c** is a section at the end of the uncus, where the gyrus intralimbicus is present. **d** is at the mid-rostrocaudal level of the body of the hippocampus, and depicts the typical appearance of the hippocampus. Overall, the small size of the cortical mantle of the temporal lobe relative to the HF is one of the main features of the neonatal brain. *Scale bar* equals 4 mm

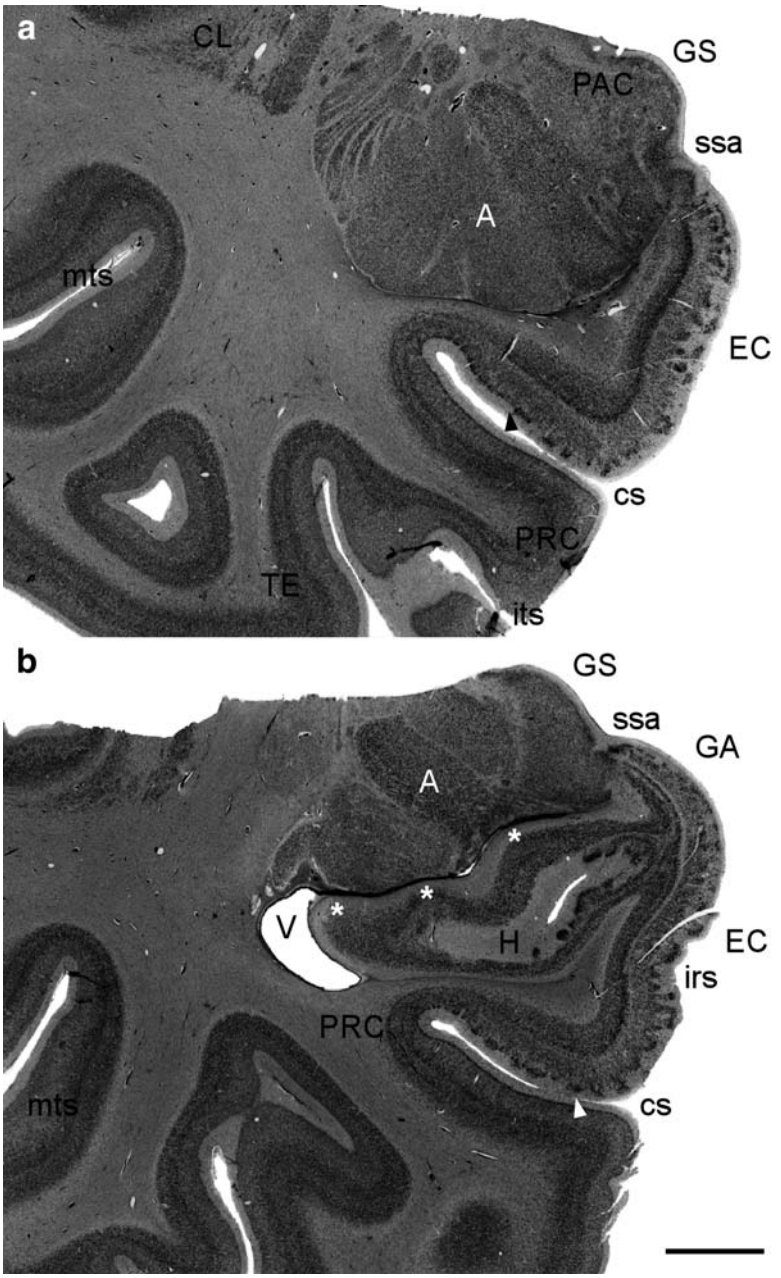

Fig. 3.5 (continued)

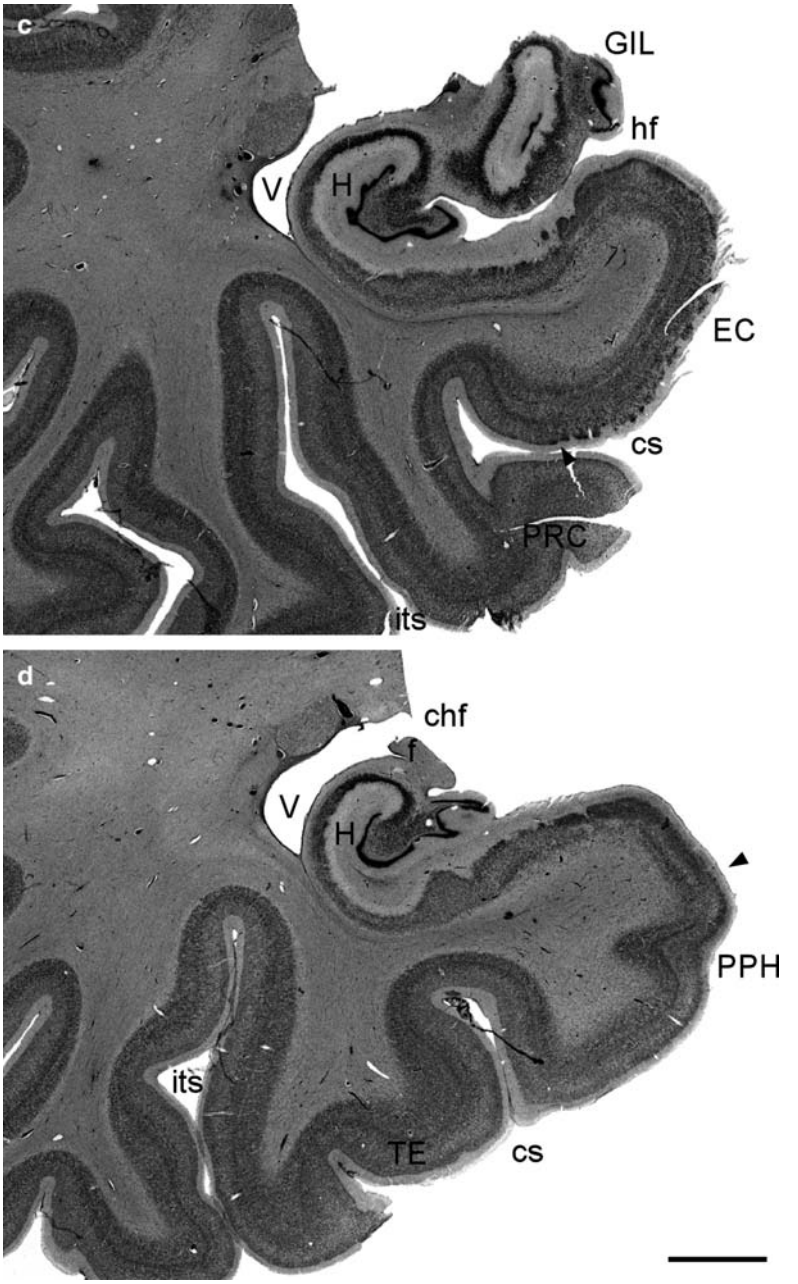

Fig. 3.5 Series of low-power photomicrographs in a 12 month old case. Note the relative growth of the cortical mantle in the temporal lobe compared to the smaller growth of the HF. (**a**) presents a mid-amygdaloid level with the gyrus semilunaris (GS), formed by PAC and separated from the EC by the sulcus semiannularis (*ssa*). The rostral EC extends as far

- The transition with the remainder of the uncus occurs at the caudalmost portion of the gyrus uncinatus, which represents the transition zone between the amygdala and the hippocampus. This transition zone is also known as the amygdalo-hippocampal transitional area (AHTA of Rosene and Van Hoesen 1987; Insausti and Amaral 2004). More caudally, this field is continued by the medialmost flexure of the DG, which is known as the band of Giacomini. The caudal end of the uncus is a rounded prominence that ends in a cul-de-sac, mostly consisting of CA3 cells that form the gyrus intralimbicus. The gyrus intralimbicus is an important hallmark in the topography of HF medial temporal lobe structures, as it points to the caudal end of the uncus (GIL in Figs. 3.1a, 3.2b, 3.3b, c, 3.4c, 3.5c, 3.6c, 3.7c). The body of the hippocampus starts from this point caudally. The gyrus intralimbicus is an important landmark in structural MRI studies of adults (Insausti et al. 1998b), and it has proven very useful in the MRI identification of MTL structures in the infant brain (see below).
- Once the gyrus intralimbicus has been traversed in the caudal direction, the remainder of the hippocampus—the body of the hippocampus—follows, and is located just lateral to the choroidal fissure (panel d in Figs. 3.4–3.7). The choroidal fissure widens and includes the point of access to the ventricular cavity of the lateral ventricle in the MTL. The temporal horn of the lateral ventricle is closed by the tela choroidea, the point of access to the ventricular cavity. The ependymal lining of the lateral ventricle is continuous with the tip of the fimbria, and thus closes the ventricular space containing spinocerebral fluid medially (Figs. 3.4c, 3.5d, 3.6d, 3.7c, d).
- The body of the hippocampus extends caudally for a variable distance. Depending on the age considered, the body can vary from less than 1 cm (newborn) to twice that length (1.75 cm) by one and a half years old, relative to that of an adult (2.8 cm) (Fig. 5.4). The body of the hippocampus continues imperceptibly with the tail of the hippocampus, which forms the caudalmost portion of the HF. This portion is not parallel to the long axis of the brain, but is instead directed upwards and medially; this upwards tilt of the tail of the hippocampus explains why it appears tangentially cut in the coronal plane. The body and tail of the hippocampus are not visible on the external part of the brain. They are hidden by the posterior portion of the posterior parahippocampal cortex (PPH), which starts at the ventral part of the choroidal fissure. This cortical portion of the PHR corresponds to areas TH and TF of Bailey and von Bonin (1951). The caudal end of the hippocampus is highly irregular and forms special bulges known as gyri Andreae Retzii, consisting of field CA1 of the hippocampus;

Fig. 3.5 (continued) as the mid-distance of the medial bank of the collateral sulcus (cs). (**b**) depicts the gyrus ambiens (GA), which is formed from subfield EMI of the EC, as in adults. The hippocampal head with the digitationes hippocampi (*asterisks*) is apparent. (**c**) is at the level of the gyrus intralimbicus end of the uncus (GIL). (**d**) shows a section at the midlevel of the body of the hippocampus. *Scale bar* equals 4 mm

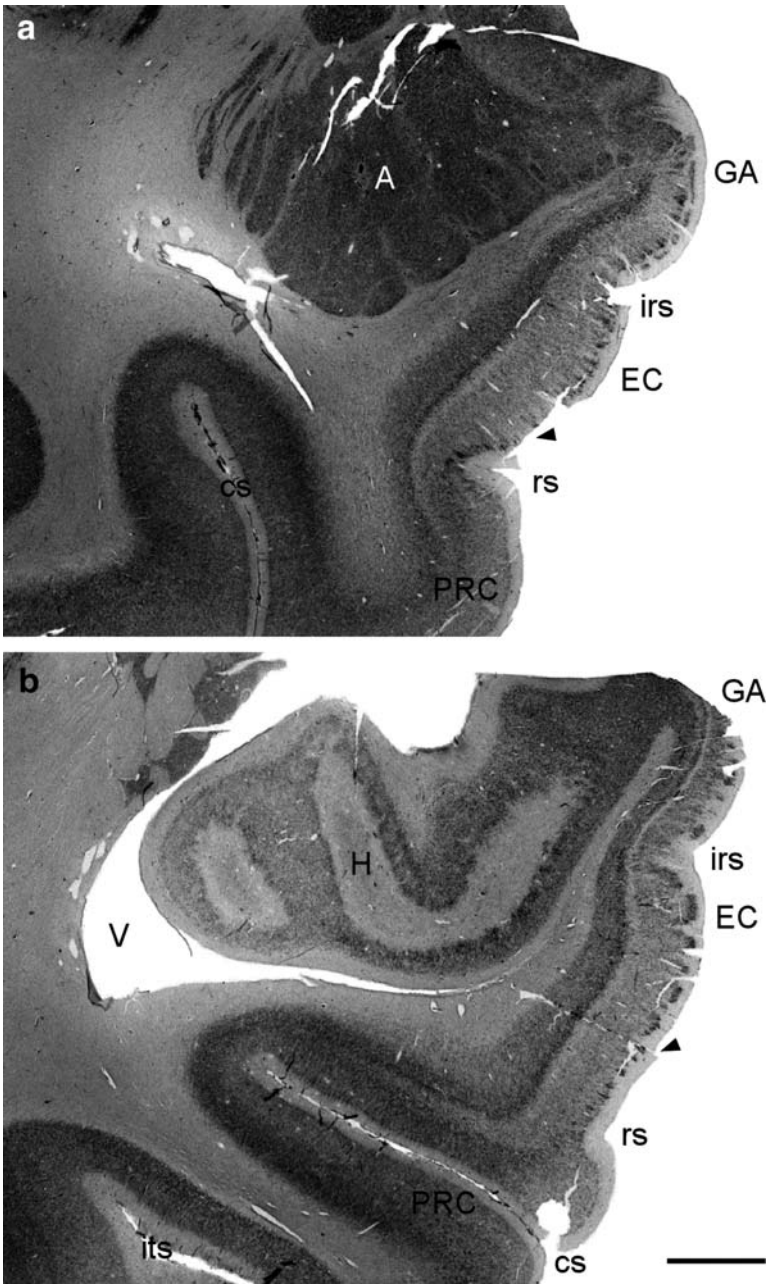

Fig. 3.6 (continued)

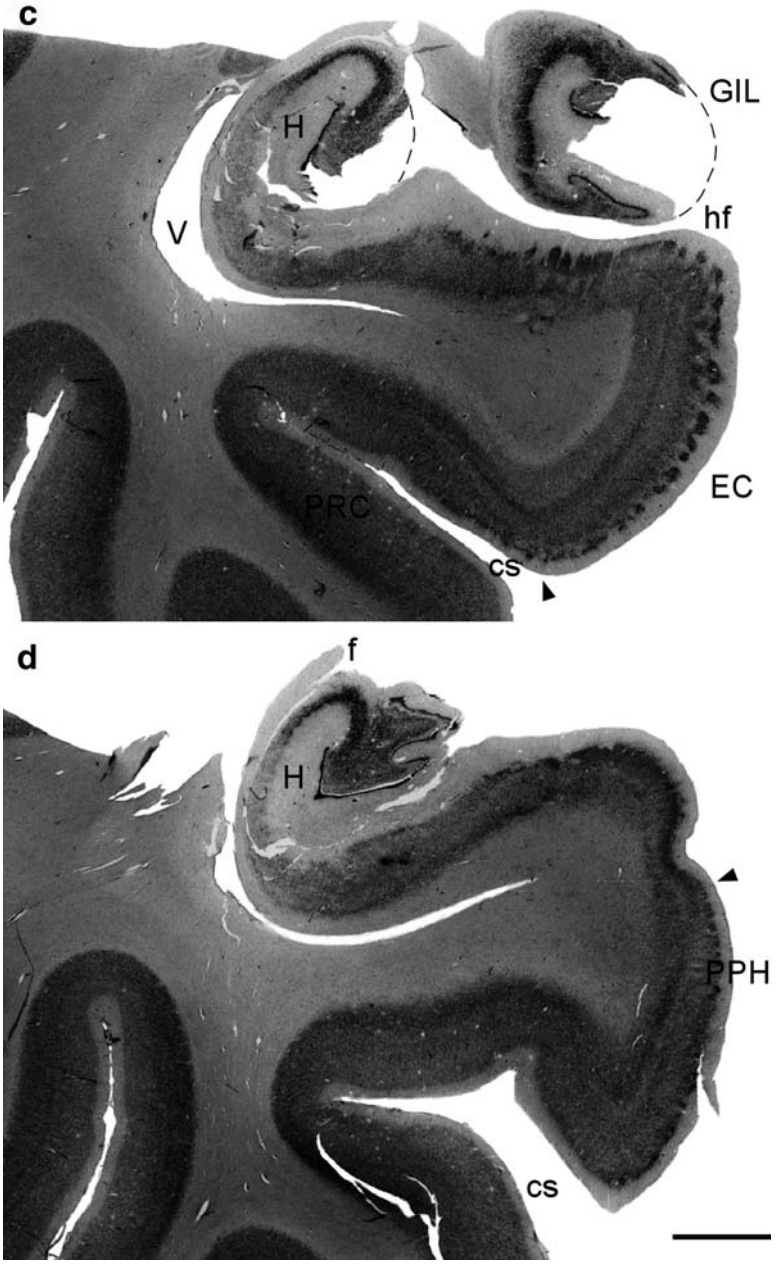

Fig. 3.6 Low-power photomicrographs of a series of coronal sections in a five year old. Note that the sizes of the HF and the amygdaloid complex are very similar to those seen in adults. Four different levels are shown, beginning with the mid-amygdaloid and rostral part of the intermediate portion of the EC (**a**). (**b**) shows the hippocampal head and the digitationes hippocampi. **c** is at the level of the gyrus intralimbicus (slightly broken and completed with *dashed lines*). **d** shows the midportion of the hippocampal body. *Scale bar* equals 4 mm

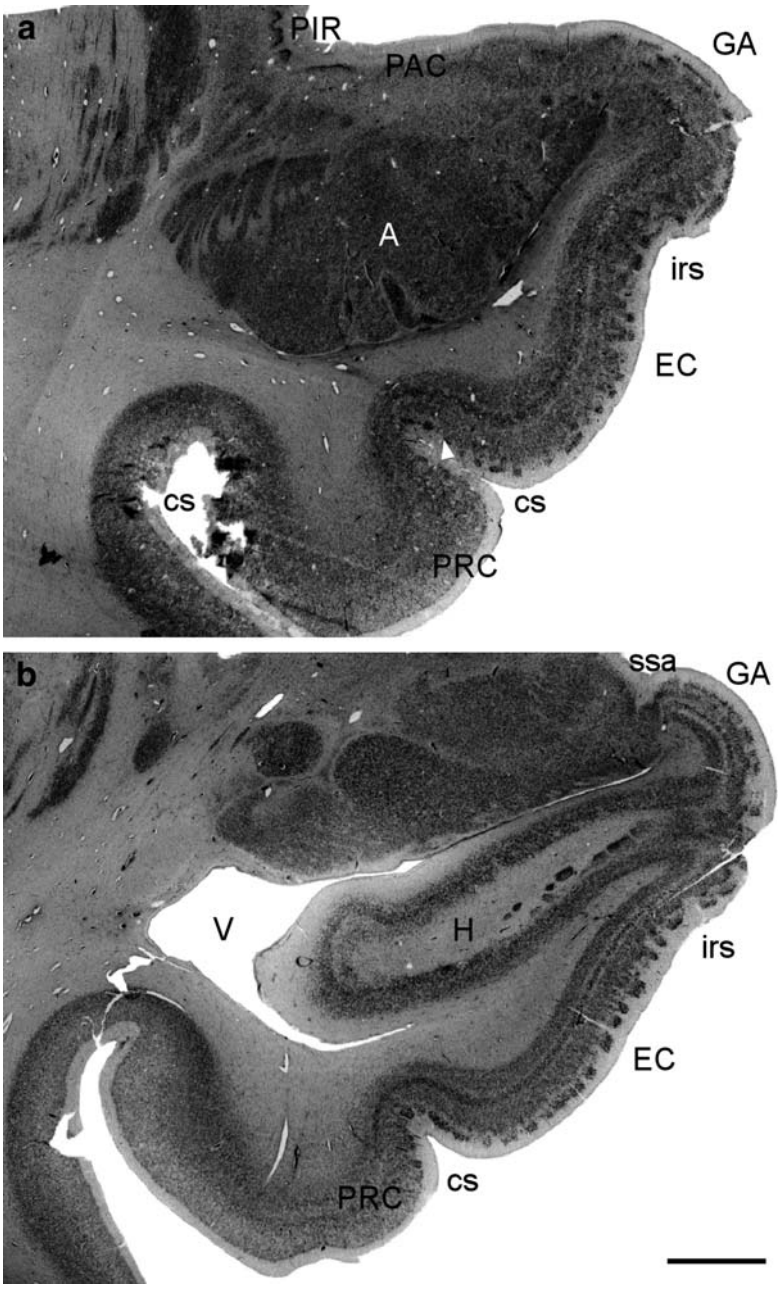

Fig. 3.7 (continued)

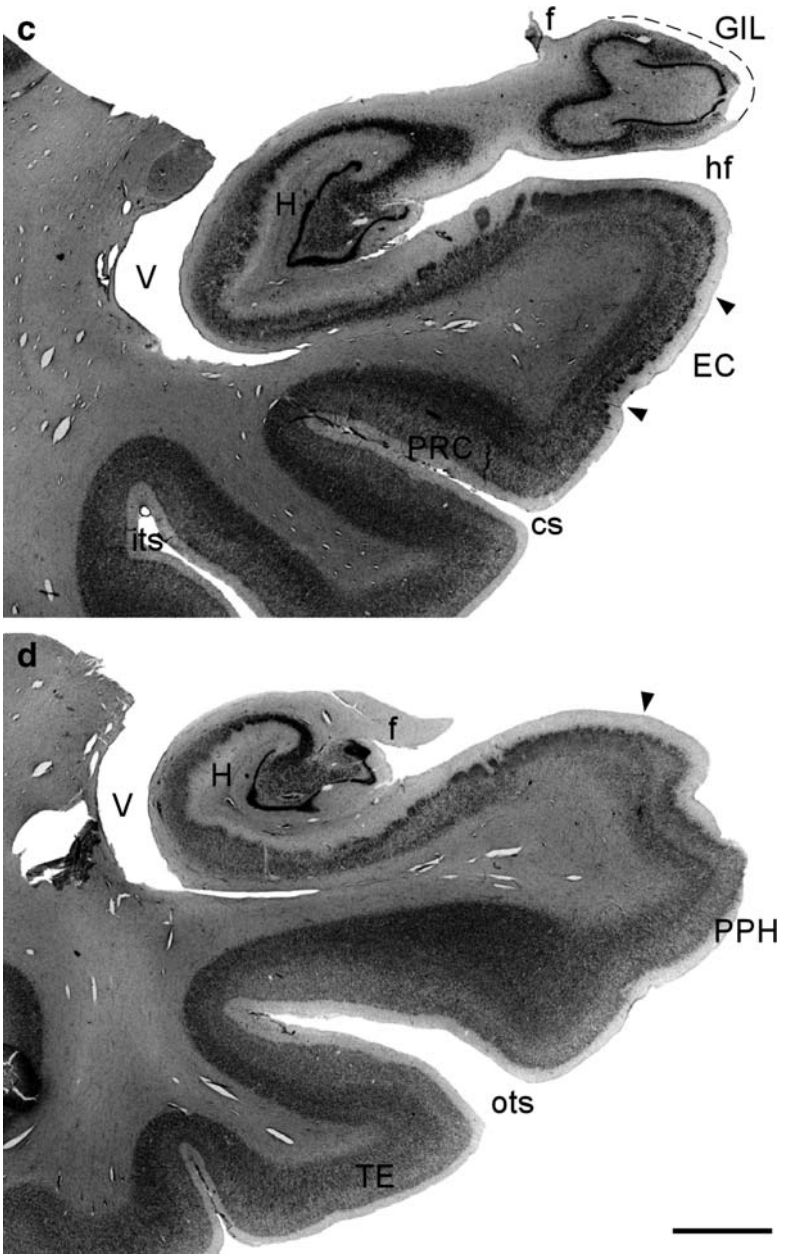

Fig. 3.7 Series of low-power photomicrographs showing coronal sections through the HF in a 14 year old case. The rostralmost section (**a**) is at the level of the amygdaloid complex; it also shows the rostral level of the EC with an incipient gyrus ambiens (GA) as well as the characteristic indentation of the intrarhinal sulcus (*irs*); in this case, a shallow collateral

further medially, two small protrusions are present: the more medial of the two is the fasciola cinerea (caudal end of the DG) and the more lateral is the gyrus fasciolaris (end of CA3, not shown). The caudal hippocampus is directed towards the splenium of the corpus callosum, and a hippocampal rudiment known as the induseum griseum continues dorsally above the corpus callosum. Neither the fasciola cinerea nor the gyrus fasciolaris are very visible; they are more apparent on the medial surface of the brain once the ventricular surface of the hippocampus has been exposed. Although present from birth, those structures are not easy to identify on structural MRI examinations. Instead, following the tilt of the long axis of the hippocampus, the obliquely cut fimbria is a useful landmark that points to the end of the hippocampus.

Regarding the growth of the HF relative to the increase in size of the remainder of the brain, the hippocampus is still incomplete at birth, especially its mid- and caudal portions. The HF grows steadily during postnatal development, but proportionally speaking, the cortical surface grows to a much greater extent. As an indication of the more extensive growth of the neocortex relative to the HF, while the size of the neocortex hides the ventral surface of the diencephalon and precludes direct exposure of the ventral thalamus in the adult brain, in young children—from newborns until two years of age approximately—the ventrolateral surface of the thalamus is exposed at the ventral aspect of the brain due to the incomplete growth of the neocortex at these ages (Figs. 3.1, 3.2, 3.3a, b). This is a clear indication of the protracted development of the surrounding cortex, and in particular the PHR. At these early ages, the bulge produced by the LGN on the ventral aspect of the thalamus is clearly visible in the ventral aspect of the newborn brain (LGN in Fig. 3.1a). By the same token, the pulvinar appears disproportionately large relative to the adult human brain (Figs. 3.1a, 3.2b; compare with Figure 23.1 in Insausti and Amaral 2004).

In summary, a gross macroscopic examination of the newborn human brain shows that all of the components of the HF are present, with the same topology and spatial relationship as seen in the adult, although its relative size is reduced. Likewise, the neocortex is still at an early stage of development, and rapid growth continues in the subsequent months of postnatal life.

Fig. 3.7 (continued) sulcus makes the border with PRC, and the characteristic cell islands in layer II of the EC. More caudally (**b**), the gyrus semilunaris (GS) and GA are separated by the sulcus semiannularis (*ssa*). The hippocampus (H) is at the level of the rostral portion of the hippocampal head. More caudally, (C) the typical appearance of the hippocampus at the level of the gyrus intralimbicus (GIL) is shown. The hippocampal fissure (*hf*) is open and the lateral ventricle (V) is then clearly visible. The EC (*the space between the arrowheads*) is present in its caudal portion. The caudalmost level (**d**) shows the EC continued caudally by the PPH. *Scale bar* is 4 mm

Macroscopic photographs of the infant brain at different ages are presented in Figs. 3.1–3.3. The rapid growth of the neocortex becomes apparent upon comparing macroscopic photographs of the brain of a newborn (Fig. 3.3a) with that of a one year old (Fig. 3.3b). The growth of the neocortex is clear, both near to and farther from the HF, so that by one and a half years of age the macroscopic appearance of the brain is closer in appearance to the adult human brain (Fig. 3.2). In Fig. 3.3, photographs of the brains of a newborn (a), a one and a half years old (b), a five year old (c), and a 14 year old (d) taken at the same magnification are presented, so that differences in the growth of the whole brain can be appreciated (note that the cases shown in a, c and d correspond to the age series shown in microphotographs in subsequent figures). It is apparent that the largest increase in size takes place in the first postnatal year, between birth and two years of age (compare Fig. 3.3a, b). Thereafter, the increase in size is much more gradual (Fig. 3.3c–d). It would be difficult to distinguish the infant brains using any macroscopic developmental feature other than size.

One and a half years of age, the brain looks much more mature (Fig. 3.3b). At first glance, the major difference compared to the newborn brain is the relative high growth of the neocortex compared to that of the medial temporal lobe cortex. Figure 3.5 shows a series of coronal sections through the medial temporal lobe at one year of age. Compared to a similar series of sections for a newborn (Fig. 3.4), the expansion of the temporal neocortex produced during the first postnatal year is most evident. In Fig. 3.5a, b, the prominence of the gyrus semilunaris and gyrus ambiens, separated by a noticeable sulcus semiannularis, is clearly seen. The amygdaloid complex, located dorsal to the EC, shows increased size and well-defined nuclei (Fig. 3.5a). The hippocampal head presents clearer indentations of the digitationes hippocampi and includes the rostralmost extreme of the presubiculum (Fig. 3.5b). The uncus, with its portions, shows no obvious differences from that of the newborn (Figs. 3.4c, 3.5c), while the hippocampal body continues for some distance without variation until it reaches the tail of the hippocampus and the tangential section of the caudal end of the hippocampus (this is not shown in the low-power series of photomicrographs, but it can be appreciated in Fig. 3.9d).

Other than an increase in size, the infant brain at five years shows little difference from the brain at one year of age. Figure 3.6 shows a series of sections of this brain through the medial temporal lobe in which the growth in the hippocampal structures is evident. The EC shows lamination similar to that of the one year old (compare Figs. 3.5a–c, 3.6a–c) and the adult, and the same holds true for the amygdaloid complex (Figs. 3.5a, 3.6a), the hippocampal head (Figs. 3.5b, 3.6b), and the uncal portion of the hippocampus (Figs. 3.5c, 3.6c), while the hippocampal body remains unchanged (Figs. 3.5d, 3.6d).

The HF and MTL in the 14 year old case presented in Fig. 3.7 show no evident differences from the five year old case in either size compared to the neocortex or the organization of the HF. The four levels presented in the coronal sections in Fig. 3.7 show the rostral EC at the level of the amygdaloid complex (Fig. 3.7a), the

hippocampal head (Fig. 3.7b), the uncus (Fig. 3.7c), and the body of the hippocampus (Fig. 3.7d). All of these indicate that little growth has occurred relative to the five year old case.

In summary, although still limited in size and immature, the HF at birth presents all of the gross anatomic features present in the adult. The hippocampus grows in size during the first postnatal year, albeit comparatively less than the temporal neocortex. This fact explains why the position of the cortex at the ventral surface of the brain expands medially, thus obscuring the view of the ventral thalamus at the ventral surface of the brain (Figs. 3.1, 3.2 compared to Fig. 3.3c, d). A gross examination of the medial temporal lobe indicates that it is mainly the body and tail of the hippocampus that present the greatest increases in length during the first postnatal year. Moreover, an overall microscopic examination reveals that the rostrocaudal sequence of the different components of the MTL (HF and PHR) maintain their relative positions along the rostrocaudal axis during postnatal development.

Although we will consider this in more depth later, the set of low-power photomicrographs shown in Figs. 3.4–3.7, which represent different ages, show that the structural differentiation of the HF components progressively improves. In particular, the lamination of the EC, the cellular components of the DG, and the ammonic fields CA3, CA2 and CA1, as well as the subiculum, presubiculum and parasubiculum are almost adult-like from the first postnatal year on. Therefore, the relative posfitions adopted by the different components of the HF—which are useful as identifiable gross anatomic and MRI landmarks—are comparable across all ages, from the newborn to the adult human brain.

Chapter 4
Microscopic Anatomy of HF Fields

In this section, rather than provide a detailed description of the cellular characteristics of the different fields of the HF, since they have been already extensively reviewed elsewhere (Insausti and Amaral 2004; Amaral and Lavenex 2007), we will focus on the lamination and the global microscopic appearance of the fields, although some superficial notes about the neuronal profiles will be provided as necessary (see Fig. 4.12).

4.1
Dentate Gyrus

The microscopic appearance of the DG at birth is presented at four different rostrocaudal levels in Fig. 4.1. The rostral pole of the DG appears at the uncal portion of the hippocampus as a circular structure that corresponds to the rostralmost extreme of the DG, tangentially cut so that it acquires a closed cul-de-sac appearance (Fig. 4.1a). The medial bend of the DG ends at the band of Giacomini (asterisk in Fig. 4.1–4.4b) near the gyrus intralimbicus, immediately caudal to the band of Giacomini.

The most common appearance of the DG as a U-shaped structure is visible in the body of the hippocampus (Fig. 4.1c). The DG increases in complexity towards its caudal end, mostly due to the tilt of the hippocampal tail and thus the obliquity of the plane of section. As tail of the hippocampus and the fimbria decrease in volume towards the beginning of the fornix underneath the corpus callosum, the long axis of the hippocampus tilts concomitantly in a dorsal (upward) direction. This gives the hippocampus an elongated shape, while the DG acquires a highly irregular profile that presents several points of section that resemble "pouches" at the tail of the hippocampus (Figs. 4.1d, 4.2d, 4.4d). Those "pouches" correspond to tangential sections of the irregularities in the DG, which, although present all along the DG, and more evident in parasagittal sections (from where the term "dentate"—or "teeth"—in DG is derived; Klingler

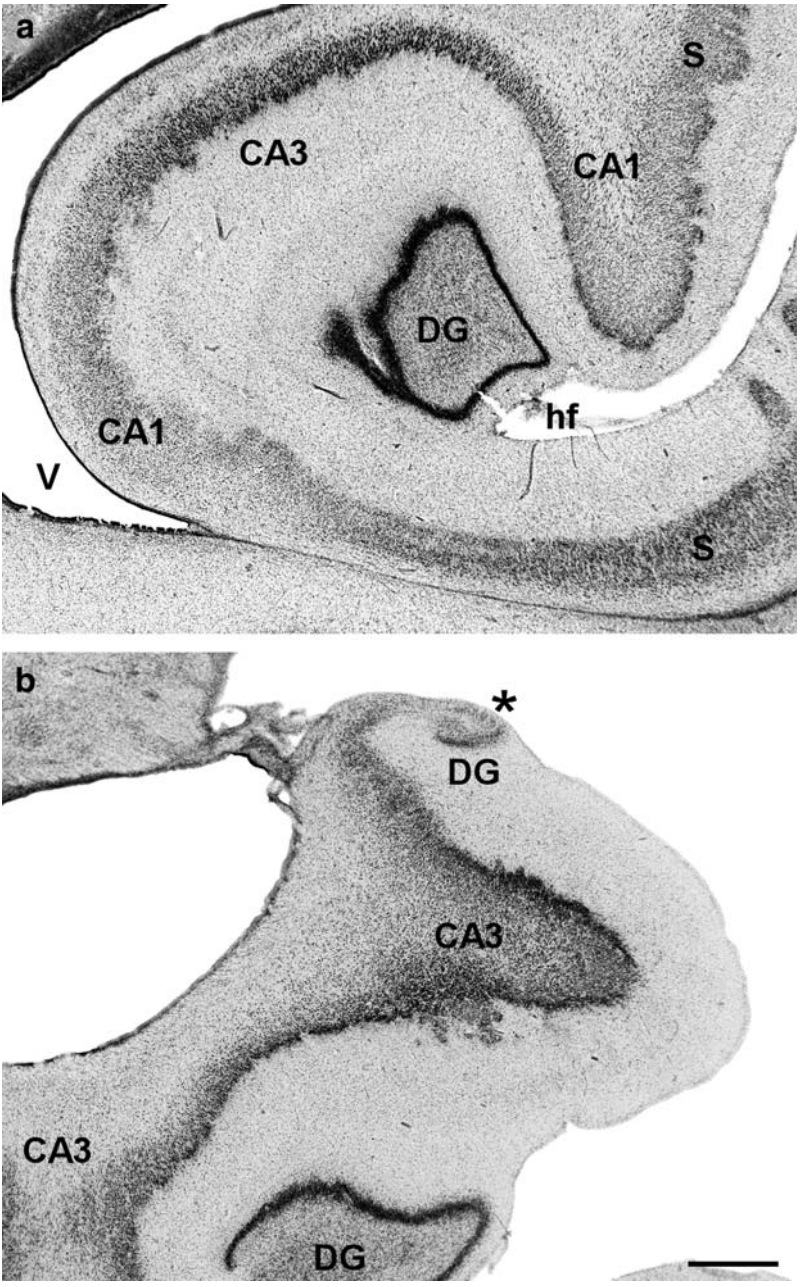

Fig. 4.1 (continued)

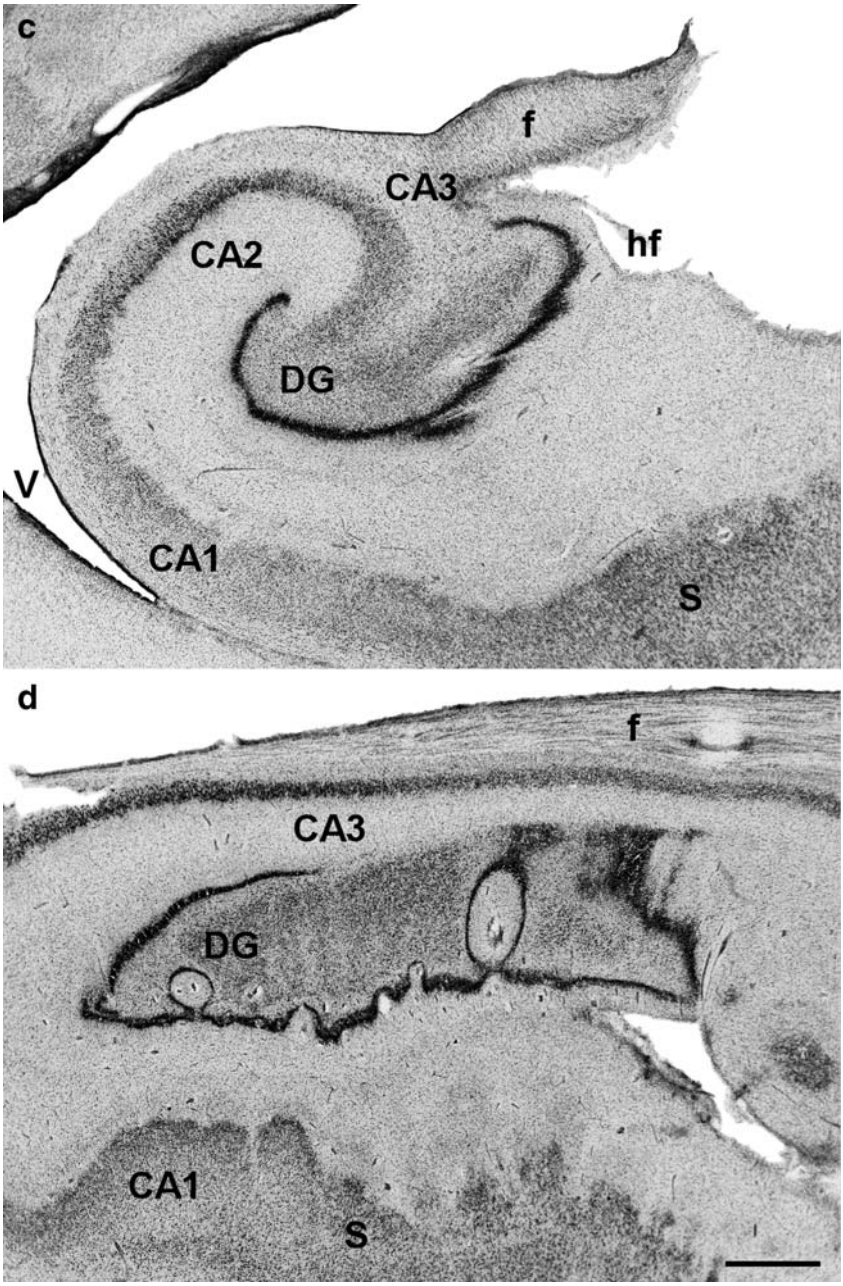

Fig. 4.1 High-power microphotographs of the DG, from rostral (**a**) to caudal (**d**) levels, in the newborn brain. The three layers of the DG are easily visible, but the lamination is not very evident at this age. At the rostral level (**a**), the granular cell layer of the DG shows a more or less circular shape, and is surrounded dorsally and laterally by CA1 due to the

1948), are also evident in the hippocampal tail. At the rear end of the hippocampus, the fasciola cinerea occurs as a small bump on the external surface of the hippocampus, and this corresponds to the caudalmost extreme of the DG (not shown). The fimbria exhibits a thick bundle of fibers when it is cut tangentially in the coronal (almost frontal) plane. These characteristics are also clearly visible in the brains of one year, five year and 14 year old brains (Fig. 4.2c, d, 4.3c, d, 4.4c).

The three layers of the DG are easily discernible at all levels: the outermost is the molecular layer, limited by the obliterated hippocampal fissure, which contains mainly dendrites of the granule cell layer. The small nuclei and densely packed cell bodies form the granule cell layer, while the polymorphic layer or hilar region occupies the innermost position in the DG. The outer border of the molecular layer of the DG is clearly delimited by the obliterated hippocampal fissure (Figs. 4.1a, c, 4.2a, c, d, 4.3a, c, d, 4.4a, c).

Although we did not undertake specific studies to demonstrate maturation indicators at the cellular level, we have considered the overall aspect of individual neurons based on the definition of the soma and proximal dendrites in the thionin-stained material. It was not possible to distinguish between neurons and glial cells based on the present material, and so both neurons and glial cells together are considered to indicate the cellularity of the different components of the HF in the present study. However, it has been described that the most abundant cells in the DG at birth are glial cells, which typically exhibit an oval nucleus dotted with dense clumps of chromatin at the periphery and no apparent nucleolus in thionin-stained sections. We observed cells with this morphology (presumably glial cells) in the molecular layer of the DG, which contains few neurons. As they can also be found in other parts of the central nervous system, such as the white matter, we feel inclined to include them as glial cells, in agreement with Seress (Seress 2001; Seress et al. 2001).

Overall, in Nissl-stained preparations, the most noticeable layer in the DG is the granule cell layer (Amaral et al. 2007). The granule cell layer is approximately 6–10 cells thick (counted by their nuclei), with oval nuclei. In the newborn, the granule cell layer (Fig. 4.1) lacks the sharpness seen at a more advanced ages (Figs. 4.2–4.4) and in the adult. Although at times the granule cell layer shows contour irregularities, we did not observe duplication in the granule cell layer (Figs. 4.1–4.4), a characteristic neuropathological finding in epilepsy cases (Houser 1990; Babb et al. 1991; Mouritzen-Dam et al. 1992). Experimental data

Fig. 4.1 (continued) special organization of these areas. The hf is also visible at this level. More caudally (**b**), the DG is presented at the level of the band of Giacomini (*asterisk*), reflecting the flexures of the DG at the hippocampal head. The DG is surrounded by the CA3 field. Further caudally (**c**), the DG shows its typical appearance, with a darker band corresponding to the granular cell layer, as well as the molecular (external) and polymorphic (or hilar) layers. At the most caudal level (**d**), the DG assumes an irregular shape, as the plane of section is oblique due to the upward inflexion of the hippocampal tail (see text for further details). *Scale bar* is 1 mm

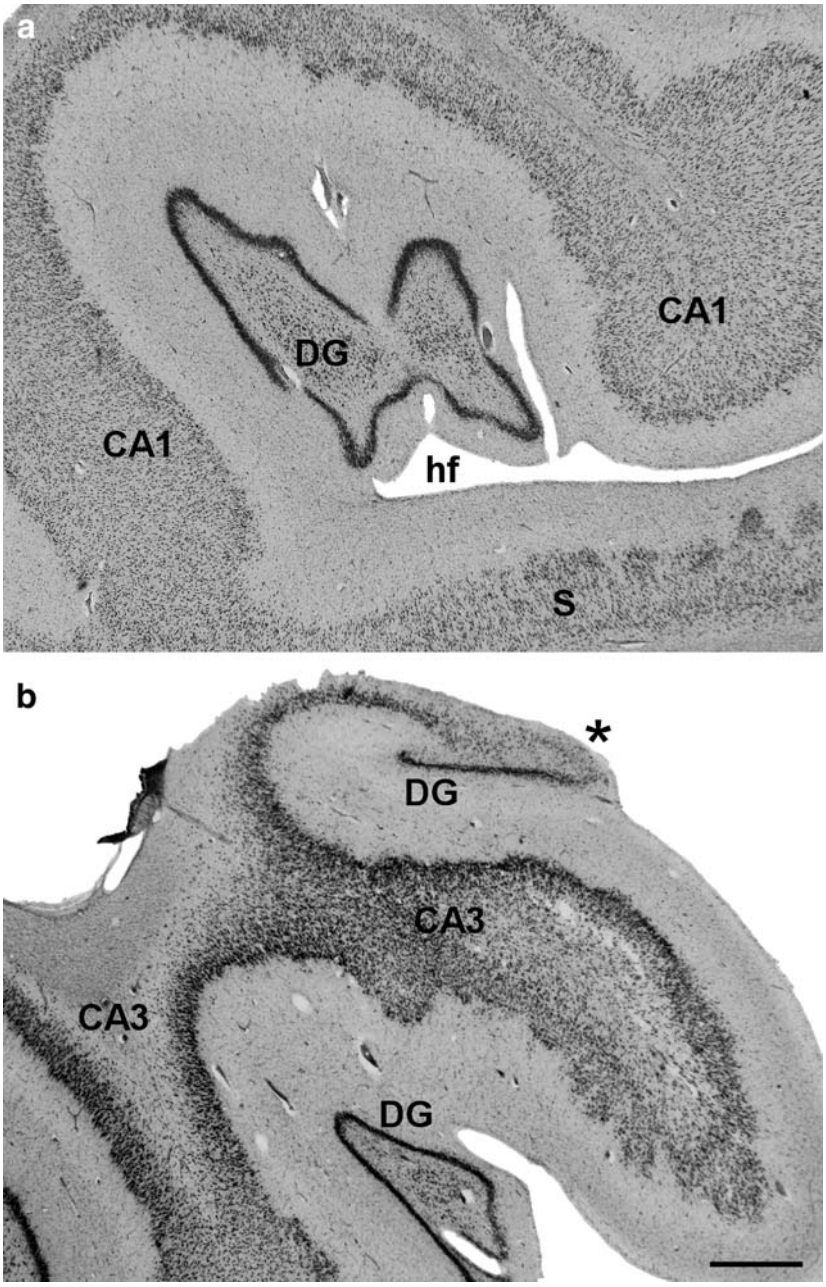

Fig. 4.2 (continued)

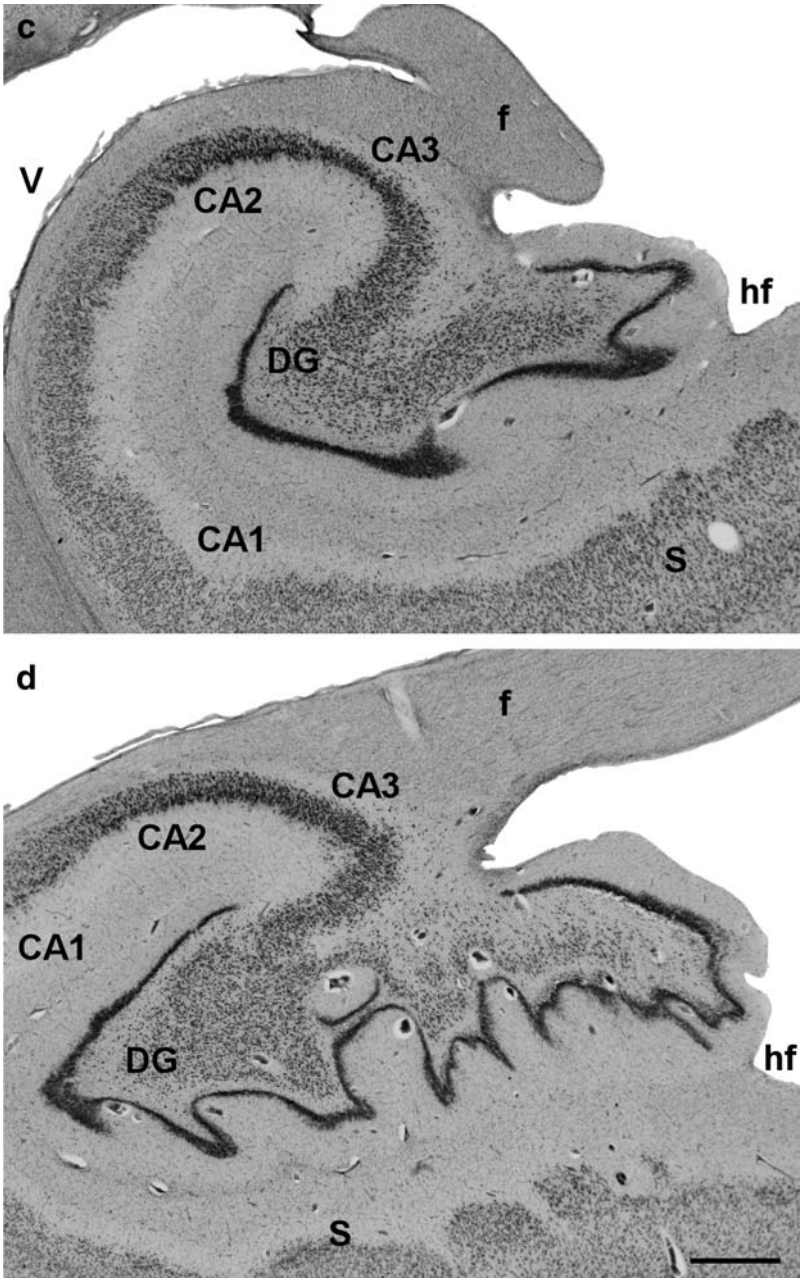

Fig. 4.2 High-power pictures of the DG from rostral (**a**) to caudal (**d**) levels of the DG in the case of a one year old. The levels are approximately equivalent to those shown in Fig. 4.1. The definition of the three layers of DG is more evident at one year than in the newborn (**a**). The band of Giacomini (*asterisk in* **b**) is also visible in the hippocampal head, and greater cellular definition can be observed, mainly in the pyramidal layer (**c**). At the most caudal level (**d**), the shape of DG is irregular due to the plane of the cut. *Scale bar* is 1 mm

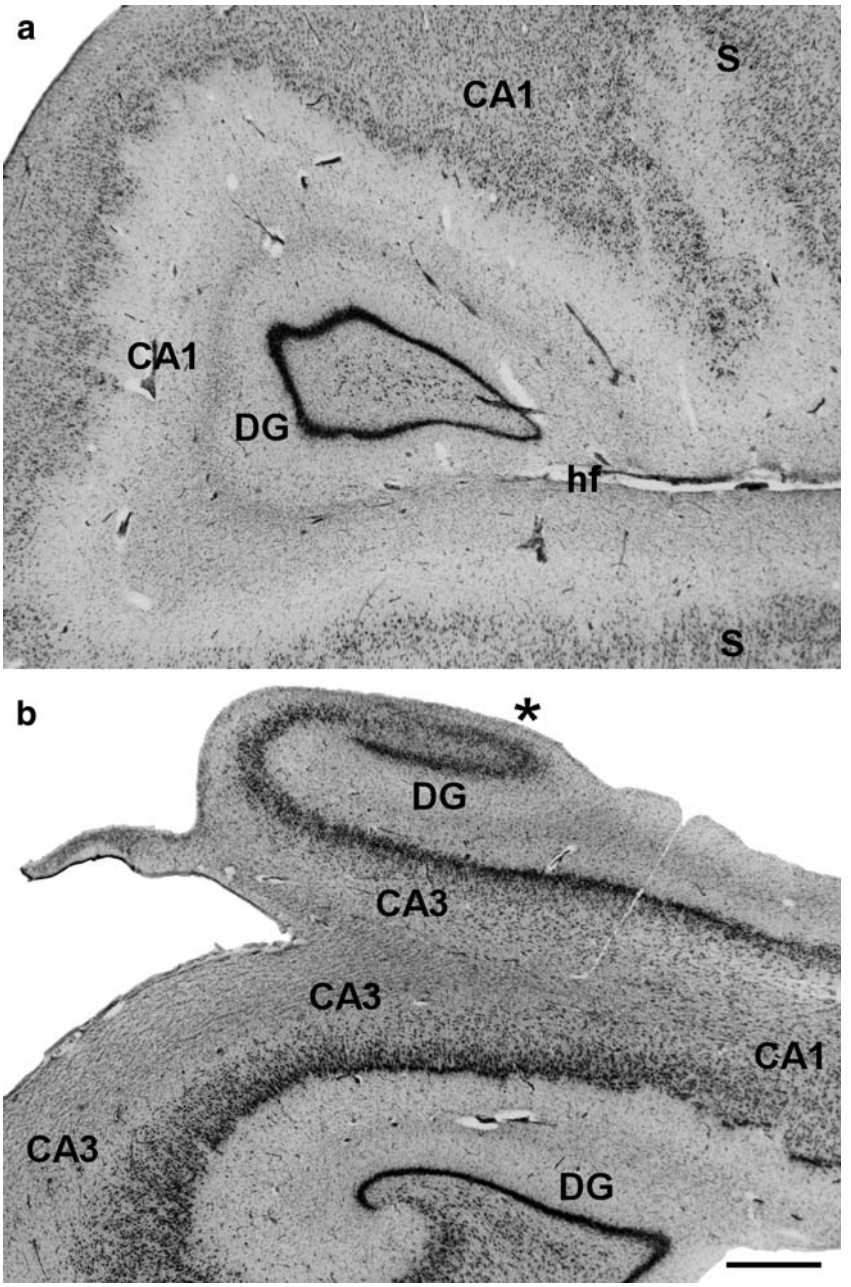

Fig. 4.3 (continued)

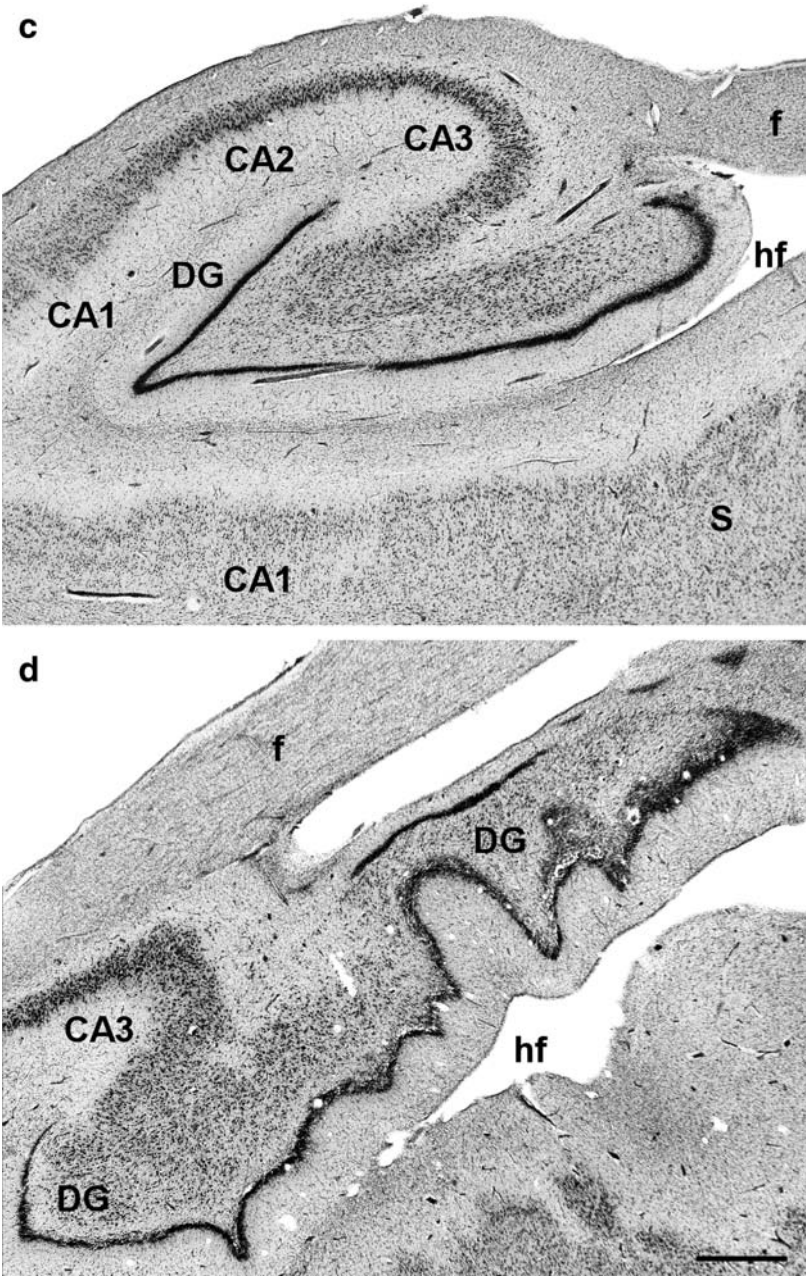

Fig. 4.3 Photomicrographs taken from rostral (**a**) to caudal (**d**) levels of DG in a five year old. The same areas as those apparent at previous ages are distinguishable here (for example, the *asterisk in* **b** corresponds to the band of Giacomini), but the layers show a more adult-like appearance. *Scale bar* is 1 mm

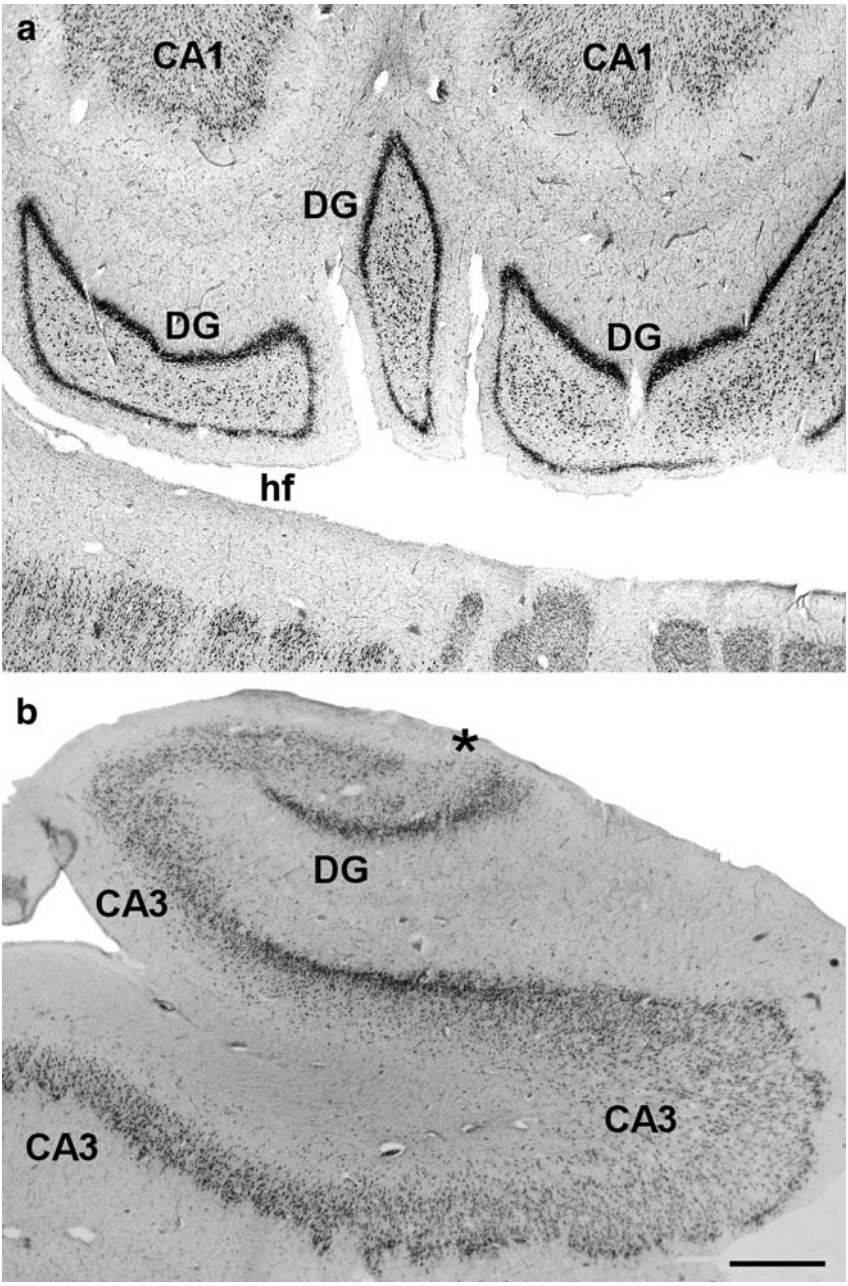

Fig. 4.4 (continued)

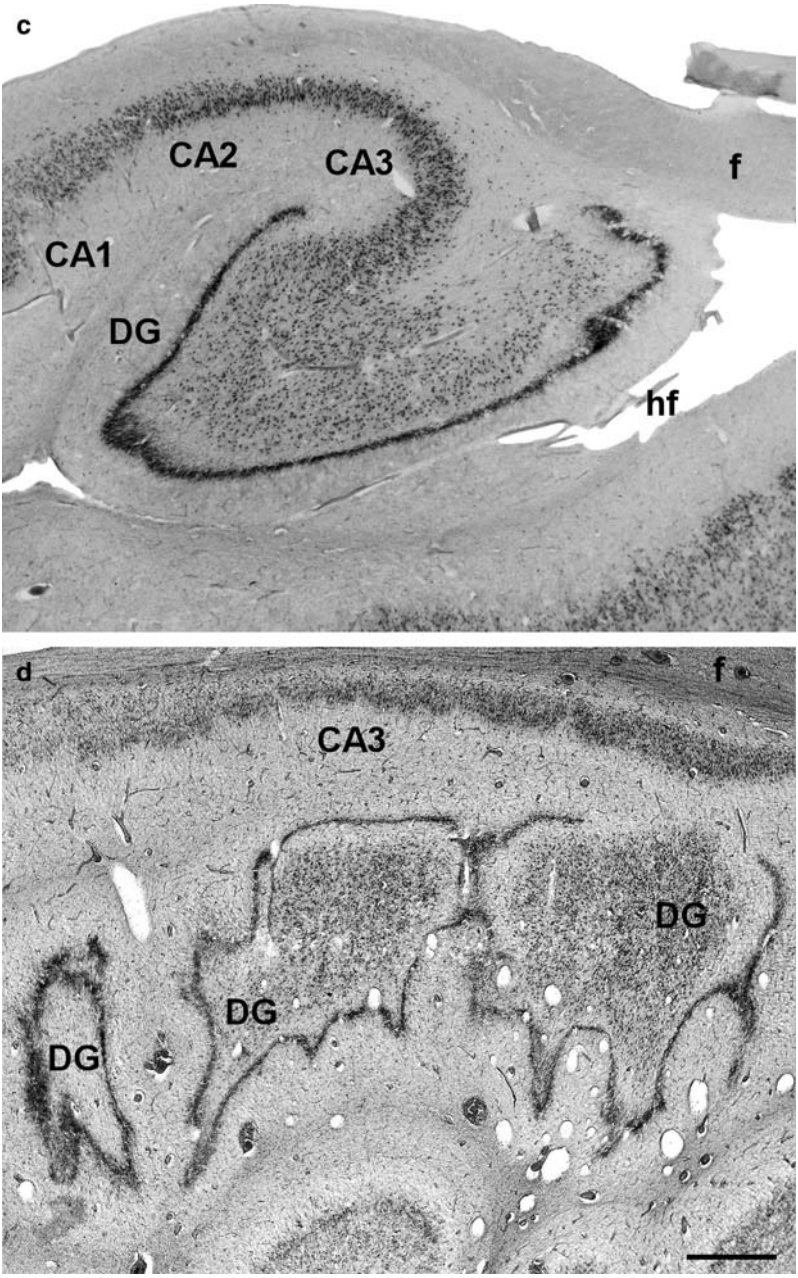

Fig. 4.4 Rostral (**a**) to caudal (**d**) sequence of pictures of DG in a 14 year old. Levels are approximately equivalent to those for previous ages (compare with Figs. 4.1–4.3). The layer definition and the general structural overview closely resemble those found in the adult. *Scale bar* is 1 mm

in monkeys reveal that most of the neurons in the DG form prenatally (Rakic and Nowakowski 1981), and observations in humans suggest that some neurons in the DG might be produced postnatally (Eriksson et al. 1998), although many of these cells may be glial cells (Seress 2001). Likewise, the question of cell death associated with postnatal development is still open, although no significant postnatal neuronal death in humans has been reported (Seress 2001).

The polymorphic cell layer is also distinguishable at birth (Fig. 4.1c). However, the cell population is predominantly small, and despite the fact that the degree of neuron maturity (defined by the histological appearance upon Nissl staining of individual neurons with well-defined somas, as well as the beginning of the principal processes present—mainly dendrites) varies widely, most of the cellular elements present in the polymorphic layer consist of small, rounded cells.

The gross morphological appearance and the overall topography and organization of the DG during the first and subsequent postnatal years show little variation (one year old: Fig. 4.2; five years old: Fig. 4.3; 14 years old: Fig. 4.4). However, particularly by the end of the first postnatal year, the aspect of the neuronal elements assumes a much more adult-like appearance with respect to the cellular and fiber strata of the DG (compare Figs. 4.1c, 4.2c). At the end of the first year (Fig. 4.2), the granular cell layer is much better defined compared to the full-term newborn, with a sharper appearance for the granule cell layer. The constituents of the DG do not change, although the DG increases in size. This is likely due to the growth in neuron size (in particular dendritic trees) and synaptogenesis, which increase the number of synapses, as suggested in the nonhuman primate (Lavenex et al. 2007). However, the same authors have shown with unbiased stereological methods that a comparison of the number of DG granule cells between three week and three month old monkeys indicated that more than 30% of the granule neurons were added postnatally. At three months, the number of DG granule neurons appears to be similar to that found for adult monkeys (Lavenex et al. 2007). In contrast, unbiased estimates of the DG volume with the Cavalieri method show that the volume of the DG in the monkey increases slightly between three weeks and three months postnatally, but the volume more than doubles between three months and 7–13 years (Lavenex et al. 2007).

A clear example can be observed, for instance, in the subgranular portion of the DG, which is better defined in subsequent postnatal ages than in the newborn. While in the newborn the subgranular space contains many neurons (Figs. 4.1a, 4.2a), at one year the situation has changed dramatically (Fig. 4.2a). This is in agreement with previous observations that indicate that most of the cell proliferation has taken place by 24 gestational weeks, with the exception of the polymorphic cell layer of the DG, which continues accumulating immature cells until the eighth postnatal month (Seress et al. 2001). An additional possibility is that the growth and ramification of the granule cell dendritic tree contributes significantly to the subgranular space brought about by the basal dendrites of granule cells, a specific trait of human and nonhuman primates (Seress and Mrzljak 1987).

Studies in the monkey indicate that the arborization of the dendritic tree of granule cells (Seress 2001; Seress and Ribak 1995a, b), an external indicator of maturation, takes place during the first six postnatal months, a time when the dendritic tree is comparable in appearance and length to one and three year old monkeys (Duffy and Rakic 1983). Some of these granular layer neurons correspond to basket cells and other presumably inhibitory interneurons that must undergo a process of maturation that appears to finish by the end of the first year of life (for a more detailed review in the rodent, see Amaral and Lavenex 2007).

Another of the principal cell constituents of the DG is the mossy cell that links granule cells located at different levels along the longitudinal axis of the hippocampus (Amaral and Lavenex 2007), and which presents the postnatal maturation of thorny excrescences that seem to be complete at three months of age, while other processes such as pedunculate spines increase in number until the ninth postnatal month (Seress and Ribak 1995a). A similar process has been described in the monkey DG, where the number of neurons remains stable between 3 months and 7–23 years while the number of DG granule cells increases between three postnatal weeks and three months (Lavenex et al. 2007).

Although comparable quantitative data do not exist in humans, the overall morphologic features described above suggest that similar processes may also take place in humans, as studies with proliferation markers indicate that cell division affects glial or endothelial cells rather than neurons (Seress et al. 2001).

The characteristic projection of the granule cell layer, the mossy fibers that establish synaptic contact with CA3 dendrites at the stratum lucidum, will be considered with the CA3 neurons of the hippocampus.

4.2 CA3

Along the transverse axis of the hippocampus alluded to above, the DG is followed by field CA3 of the hippocampus. CA3 occurs in the space delimited by both extremes of the DG, and fills much of it, coming into close contact with cells at the polymorphic cell layer of the DG (Fig. 4.5). Some controversy has resulted from the fact that different authors, including Lorente de Nó (1934) in his original description of CA fields (cornu ammonis or Ammon's horn), have given the CA3 segment that is inserted between the opened arms of the DG the name CA4. However, mainly due to the fact that cells of the polymorphic cell layer can be separated from CA3 through their distinct connectivities, we follow previous reports that have dropped the term CA4 (Insausti and Amaral 2004).

At birth, CA3 displays the same layer (strata) organization as seen in the adult. CA3 is readily distinguishable from the remaining hippocampal fields as it is characterized by large, darkly stained pyramidal cells. Even at low-power magnification, the continuation of CA3 into the space opened by the extremes of the

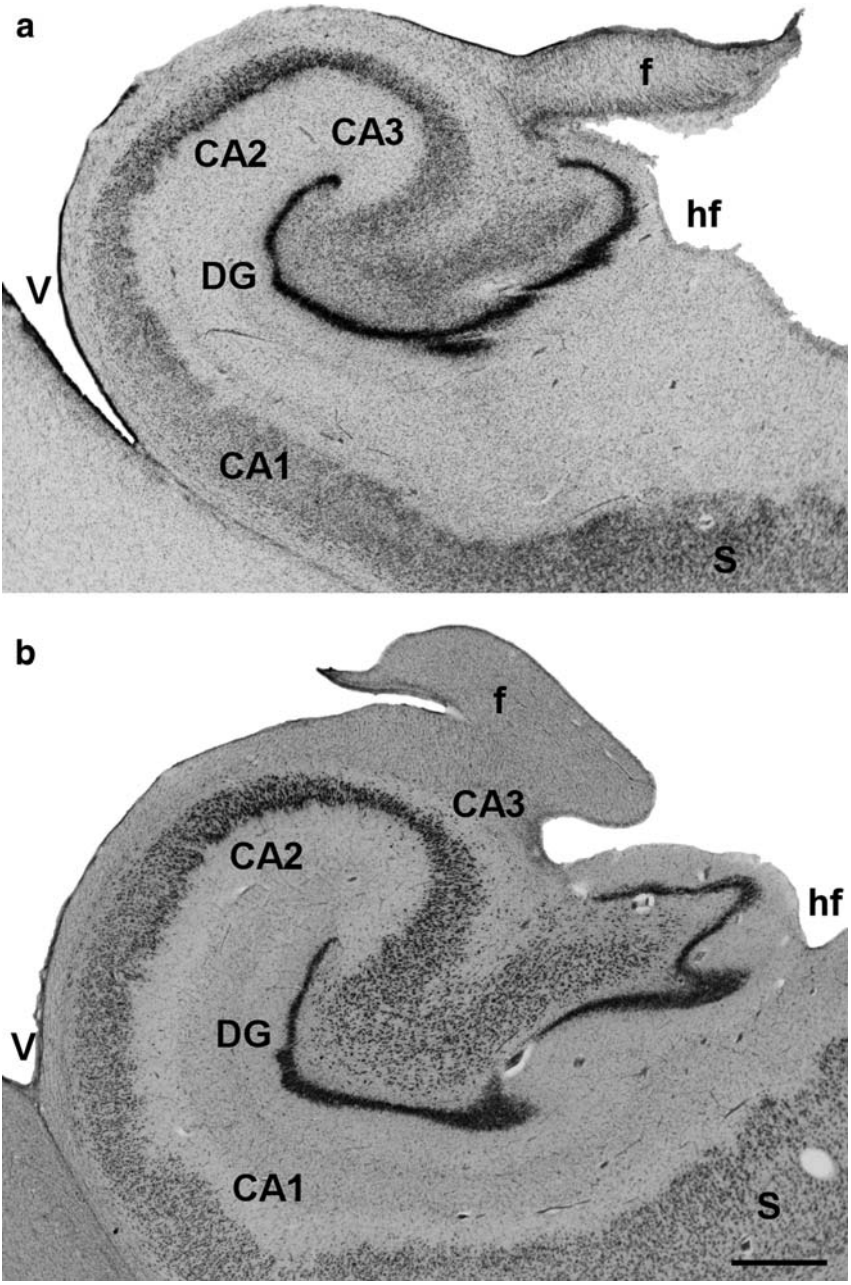

Fig. 4.5 (continued)

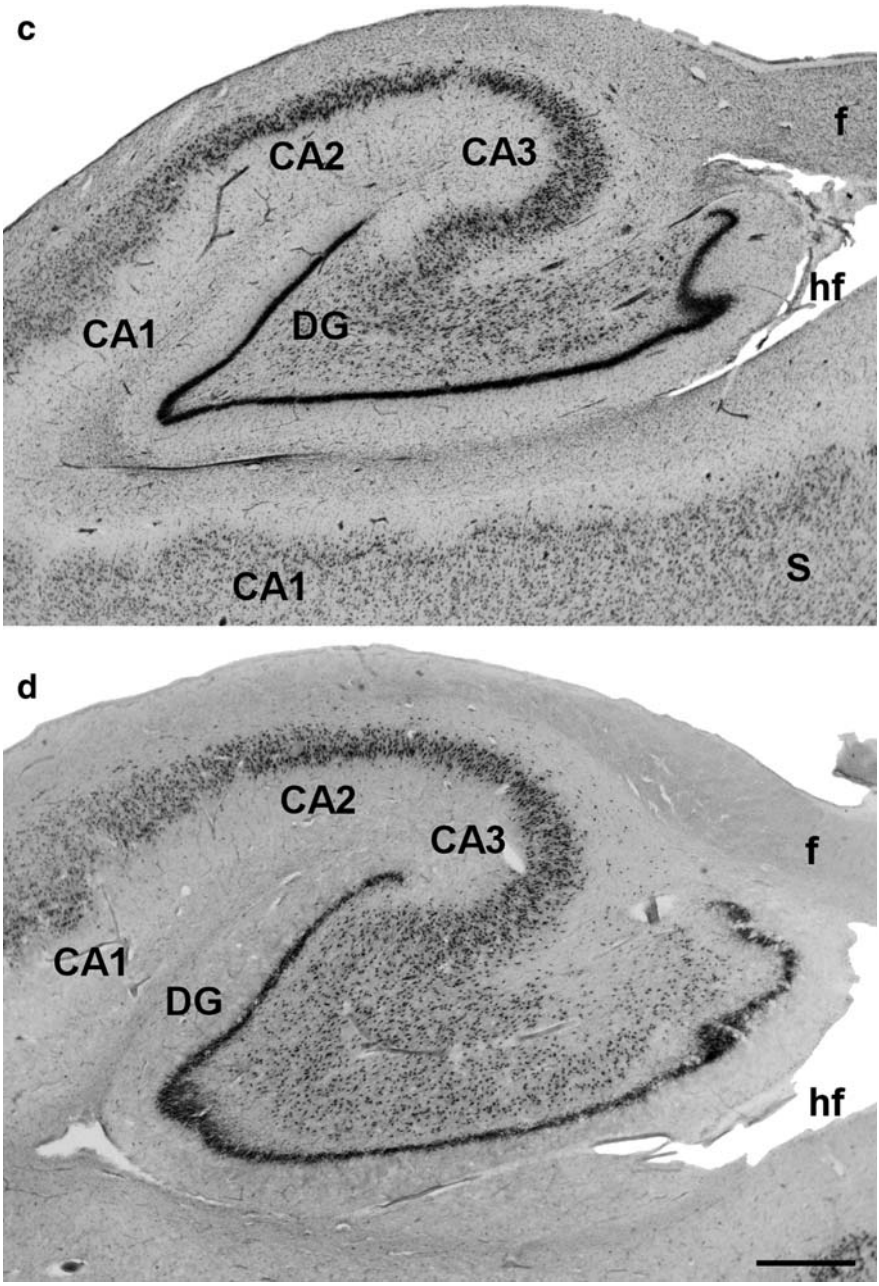

Fig. 4.5 Series of photomicrographs of the hippocampal fields CA3 and CA2 at different ages: newborn (**a**), 1 year (**b**), 5 years (**c**), and 14 years (**d**) old. Already in the newborn (**a**), the overall appearance and lamination pattern of these hippocampal fields is well established. However, although is more clearly visible in older ages, from 1 year (**b**) on, as in (**c**) (5 years old), and (d) (14 years old), very similar to that observed in the adult. *Scale bar* 1 mm

granule cell layer of the DG is apparent at birth and at subsequent postnatal ages (Fig. 4.5: a, newborn; b, 1 year; c, 5 years; d, 14 years).

At birth (Fig. 4.5a), the CA3 field presents a mixture of cells consisting of apparently less mature neurons as well as probably glial cells, although all of the strata are well organized. Moving from the point closest to the ventricular surface, we find that the outermost stratum corresponds to the alveus, which lines the ventricular surface of the floor of the temporal horn in the lateral ventricle. The alveus contains axons of pyramidal cells of the hippocampus, in continuation with the fimbria (Fig. 4.5) and ultimately the fornix, the main subcortical output fiber system of the hippocampus that is directed towards subcortical structures and is present at all levels of the hippocampus. Immediately below the alveus is the stratum oriens, which contains basal dendrites of the pyramidal cells. The stratum oriens is sparsely populated by neurons that stain positively for different peptides (Cebada-Sánchez et al., in preparation) and are likely correspond to interneurons. Therefore, both the alveus and the stratum oriens are cell-sparse strata, and at low-power magnification they look like white matter.

Underneath the stratum oriens lays the stratum pyramidale or pyramidal cell layer, which is the most characteristic of the hippocampal strata. At birth, the stratum pyramidale consists of large stained neurons 8–10 cells thick. Next to the stratum pyramidale is the termination of the projection from the mossy fibers originating from the granule cells of the DG, known as the stratum lucidum. This stratum is only present in CA3, as neither CA2 nor CA1 receive mossy fiber projections. The stratum lucidum is much more difficult to appreciate in Nissl-stained preparations in humans compared to rodent or nonhuman primate brains, as it does not exhibit a clear decrease in glial cells as seen in other species, and because part of the mossy fiber projection travels within the stratum pyramidale (Insausti and Amaral 2004). Immediately adjacent to the pyramidal cell layer is the stratum radiatum, consisting of apical dendrites of pyramids in the stratum pyramidale. The stratum radiatum is continued by the stratum lacunosum-moleculare, which in turn abuts the hippocampal fissure and thus faces the outermost part of the molecular layer of the DG. The stratum radiatum and the stratum lacunosum-moleculare largely consist of the main dendrites and distal ramifications of CA3 pyramids, and so they look cell sparse like white matter at low magnification.

CA3 increases in size significantly during postnatal development. Figure 4.5 shows low-power photomicrographs of cases at birth (a), one year (b) five years (c), and 14 (d) years, all taken at the same magnification and at the same level, which illustrate this fact. Again, the greatest change takes place during the first postnatal year (Fig. 4.5a, b), probably due to the dendritic growth and elongation as well as the establishment of the sets of intrinsic and extrinsic connections for CA3. Information on the postnatal development of CA3, in particular the characteristic mossy fiber projection, which is readily demonstrated by the Timm method, is scarce. Seress and Ribak (1995b) reported that Timm staining exists at birth in rhesus monkeys, although the staining increases in density by the third

postnatal month and even more in adult rhesus monkeys. It is very likely that the same phenomenon occurs in humans, and that the growth observed at postnatal ages in CA3 is accompanied by an increase in the size and number of synaptic specializations known as thorny excrescences. In this regard, although mossy fibers present a mature appearance at birth, and the thorny excrescences of CA3 neurons also appear mature, the width of the stratum lucidum increases at six months in the rhesus monkey (Seress and Ribak 1995b). Likewise, the density of spines in the stratum lacunosum-moleculare and the stratum oriens (basal dendrites) shows a protracted maturation in the rhesus monkey (Seress and Ribak 1995b).

4.3 CA2

CA2 is the hippocampal field that follows CA3 in the mediolateral direction. CA2 is usually difficult to delimit in Nissl-stained preparations, although its hallmark is probably an increased cell packing density relative to CA3. CA2 overlaps to a certain extent with CA3 (Fig. 4.12b), and its larger pyramids compared to those of CA1 are useful for separating these fields. The lack of a stratum lucidum, another major feature used to distinguish CA2, is perhaps less noticeable in Nissl-stained sections in humans (see above). However, the other CA2 characteristics and the lamination are all similar to those of CA3.

Figure 4.5a–d shows panoramic views of CA3 and CA2 at birth and in one, five and 14 year old children. At birth (Fig. 4.5a), the border between CA3 and CA2 is inconspicuous because the pyramids of CA3 extend under CA2. Thus, CA2 is limited to a cell layer that is closer to the stratum radiatum that presents a higher cell packing density (Fig. 4.12b). In contrast, the border between CA2 and CA1 is easily noticeable because of both the larger CA2 neurons and the stronger staining density they present compared to CA1 pyramidal neurons. At birth, there is a band of more closely packed neurons at the border with the stratum radiatum (Fig. 4.12b) that is also present at later ages. While the definition of the border between CA3 and CA2 hardly improves, the limit with CA1 becomes progressively better defined (Fig. 4.5a–d) at all postnatal ages (Arnold and Trojanowski 1996). The overall increase in the size of the hippocampus and the maturation of the stratum pyramidale means that it becomes easier to identify the limits of CA2 as the age of the brain increases.

4.4 CA1

On the one hand, the CA1 hippocampal field mainly covers the part of the hippocampus directly underneath the DG; on the other, it lies above the more or less extended obliterated line of the lateral ventricle cavity plus a small portion of the

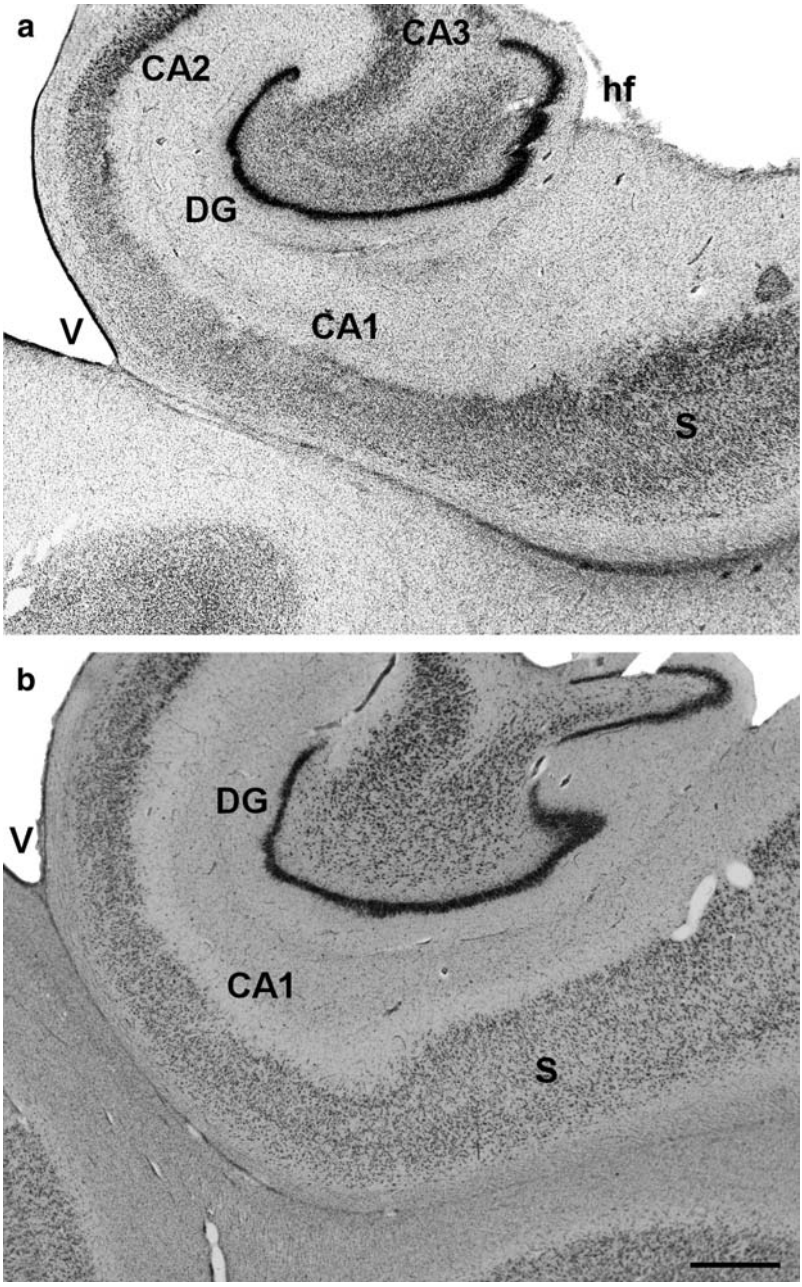

Fig. 4.6 (continued)

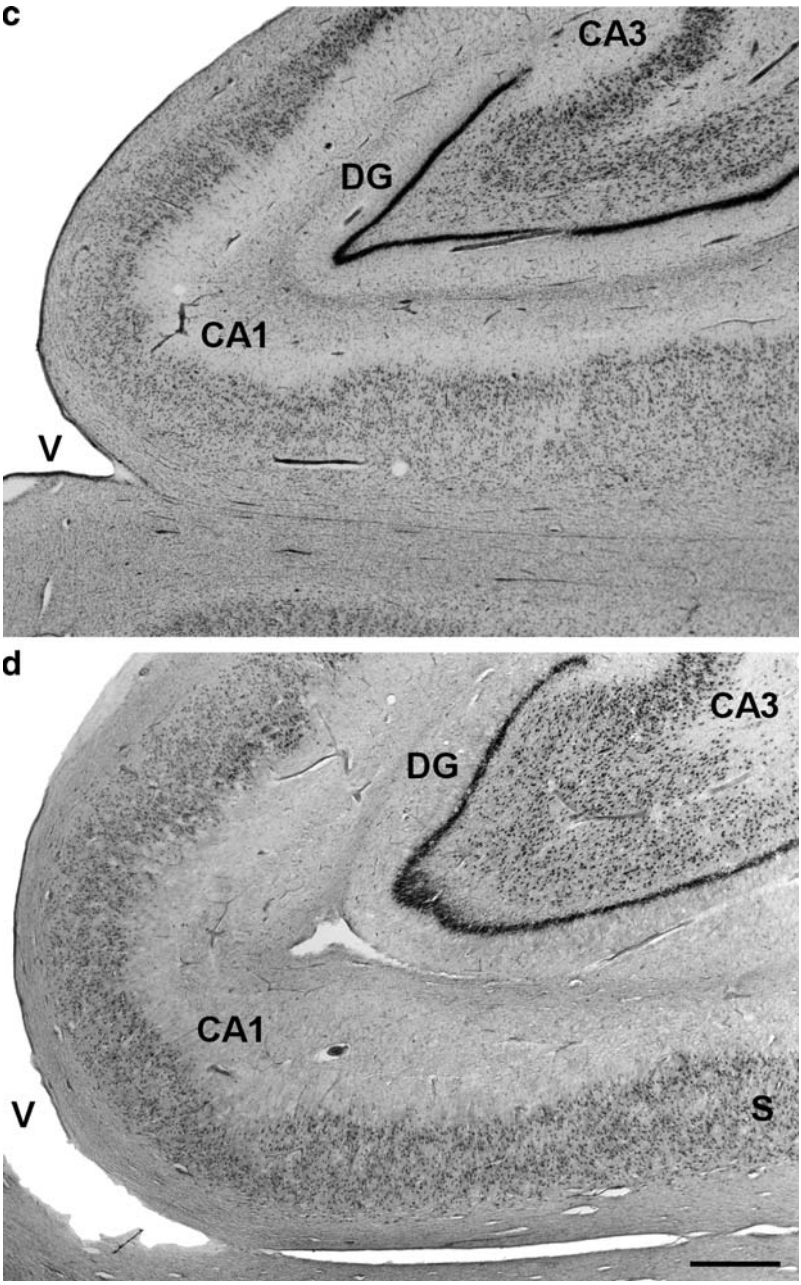

Fig. 4.6 (continued)

ventralmost part of the lateral ventricle (Figs. 3.4–3.7 and Fig. 4.6a–d). From birth, CA1 contains small pyramidal cells stacked to a thickness of 15–20 cell bodies, unlike CA3 and CA2. Although many of the cells present in CA1 at birth exhibit features that are described in Arnold and Trojanowski (1996) as being suggestive of immaturity, the overall disposition of the layers is already present (Fig. 4.6a).

CA1 grows along with the remainder of the hippocampal fields and the DG. The largest variation takes place in the first postnatal year, with a notable increase in size, both as a field and as individual neurons (compare Figs. 4.6a, b). By one year of age (Fig. 4.6b), the cells acquire better-defined soma borders and processes that suggest increased maturity, the stratum pyramidale becomes better organized, and the stratum radiatum becomes clearly visible. The presence of the stratum radiatum is a distinguishing feature that aids in the delineation of the border with the adjacent subiculum (Rosene and van Hoesen 1987).

The microscopic appearance of CA1 hardly changes aside from an apparent increase in the neuropil, which likely suggests the growth of CA1 axonal and dendritic branching, as well as connectivity with other hippocampal fields, notably the Schaffer collaterals. The cells in CA1 also show further maturation with respect to the cytoskeleton (Arnold and Trojanowski 1996) and other immunocytochemical features (Lavenex et al. 2007).

This variation, although subtle, can be appreciated at subsequent ages, as shown in Fig. 4.6c (five years old) and d (14 years old). Reports in the literature (Hevner and Kinney 1996) indicate that some of the EC projections to CA1 are already present by the sixth month of gestation, and that this connectivity continues after birth and probably beyond the first year of age, as the perforant path grows postnatally (Benes 1989).

4.5 Subiculum

The subiculum is a continuation of CA1 along the mediolateral axis of the hippocampus, and is already clearly present at the time of birth. It abuts the presubiculum distally (farther from CA1). As seen in the adult, the subiculum displays a number of pyramidal cells that are stacked unevenly on top of each other to a thickness of 30 or more pyramidal cells (see Fig. 4.7). In contrast to CA1, the subiculum lacks the orderly disposition of layers seen in CA fields of the

Fig. 4.6 Series of photomicrographs of field CA1 in the newborn (**a**), one year old (**b**), five year old (**c**) and 14 year old (**d**). As in the other ammonic fields, the strata are well defined at the time of birth (**a**), but they become more clearly defined with age. However, the pyramidal cell layers in CA1 and the subiculum (S) look very similar, especially up to one year of age. At five years old (**c**) and 14 years (**d**) old, the neuronal profiles in the pyramidal cell layer are better defined, so the separation between CA1 and the subiculum is somewhat more evident. *Scale bar* is 1 mm

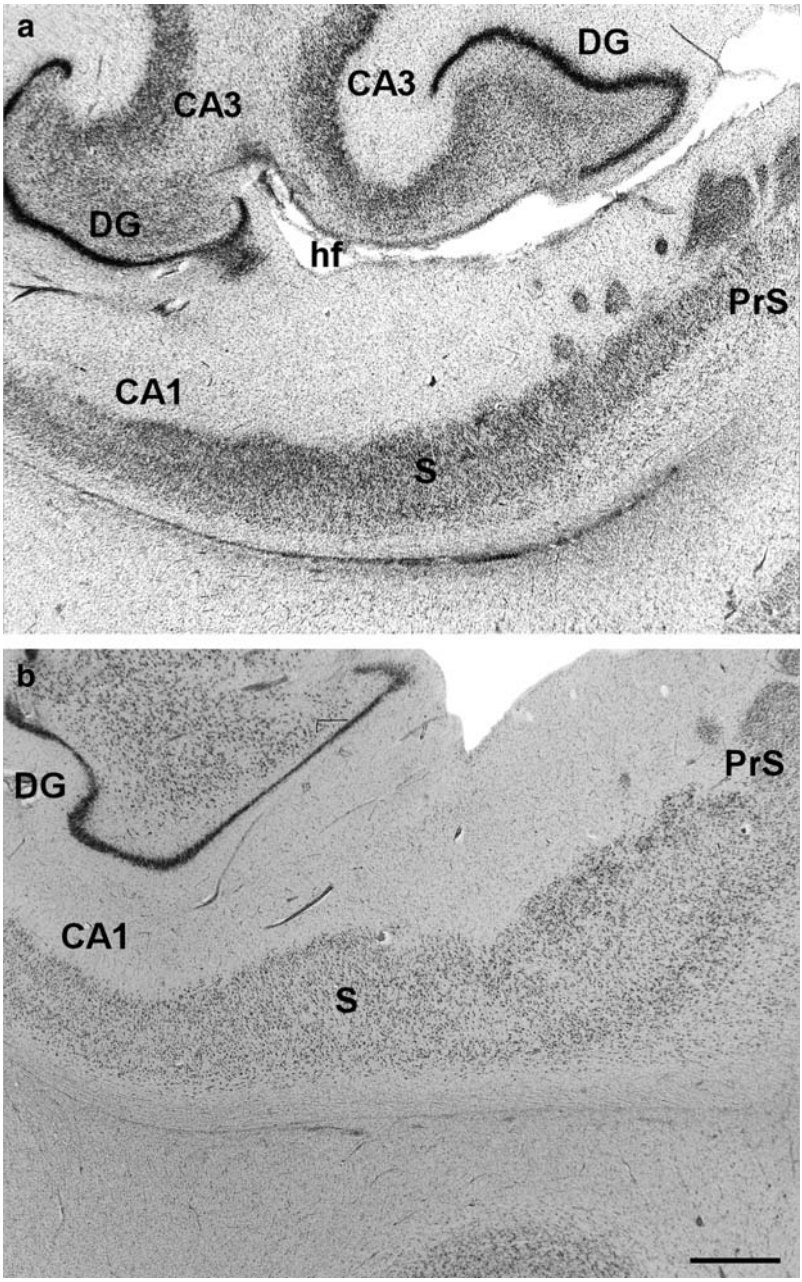

Fig. 4.7 (continued)

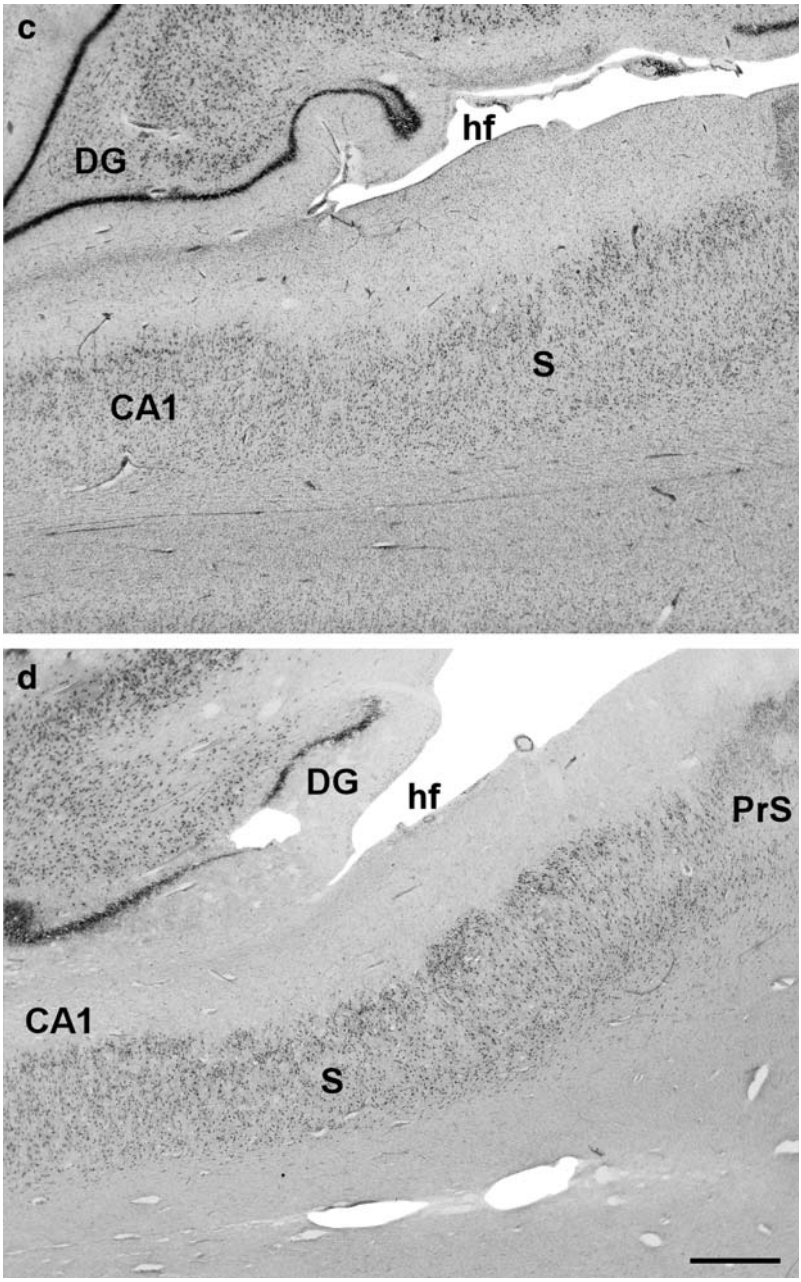

Fig. 4.7 Series of photomicrographs of the subiculum (S) in the newborn (**a**), one year old (**b**), five year old (**c**), and 14 year old (**d**) cases. The molecular layer of the subiculum (the most superficial) is thicker than that of CA1 at all ages, and is clearly distinguishable from

hippocampus, and so the dendrites of pyramidal neurons form a rather thick molecular layer that is already very wide at the time of birth (Fig. 4.7a). The portion of the subiculum that neighbors CA1 is defined by the presence of subicular neurons under a progressively thinner layer of CA1 pyramids, such that an oblique border is defined between both CA1 and the subiculum (for further details, see Insausti and Amaral 2004). This oblique border is inconspicuous at birth (Fig. 4.7a), but becomes much more visible from the first postnatal year on (Fig. 4.7b–d). The other extreme of the subiculum abuts the presubiculum, and it is often the case that clumps of small cells belonging to the presubiculum lie in the molecular layer of the subiculum, thus forming an overlap zone due to the tangential section of the external principal layer of the presubiculum (see below). The distal end of the subiculum usually presents a rounded shape in the transition with the proximal extreme of the presubiculum, very much like that formed by the distal tip of the subiculum in monkey species.

Apart from the molecular layer, the pyramidal cell layer of the subiculum is not homogeneous and it often presents clumps of darkly stained neurons that become noticeable at the end of the first postnatal year and continue at subsequent ages (Fig. 4.7b–d). Finally, a polymorphic layer made up of smaller neurons occupies the deepest cell layer of the subiculum. The polymorphic cell layer is already present at birth, and seems to change little during the postnatal years (Fig 4.12c).

As in other hippocampal fields, growth occurs most rapidly during the first postnatal year (compare Fig. 4.7a, b), when the changes alluded to above take place. However, the overall appearance of the subiculum changes little during the postnatal development of the HF (Figs. 4.7b–d).

4.6 Presubiculum

The presubiculum follows the subiculum along the mediolateral axis of the hippocampus. The prefix “pre-” suggests that it precedes the subiculum if we consider the series of hippocampal fields beginning with the EC and ending with the DG. However, the phylogenetic considerations of early human neuroanatomists (Filiminoff 1947) and the divisions proposed for the cortical mantle (Stephan and Andy 1970) lead to the exact opposite sequence of fields. In this proposal, the HF contains the so-called archicortex (also termed the allocortex), which presents a single cellular layer; the elements of the HF mentioned so far (DG, CA3, CA2,

Fig. 4.7 (continued) the underlying pyramidal layer. The transition between CA1 and the subiculum forms an oblique border that is hardly seen at birth (**a**) but becomes progressively more apparent at one year old (**b**), five years old (**c**), and 14 years old (**d**). The deepest layer of the subiculum, the polymorphic layer, is inconspicuous at this magnification. *Scale bar* is 1 mm

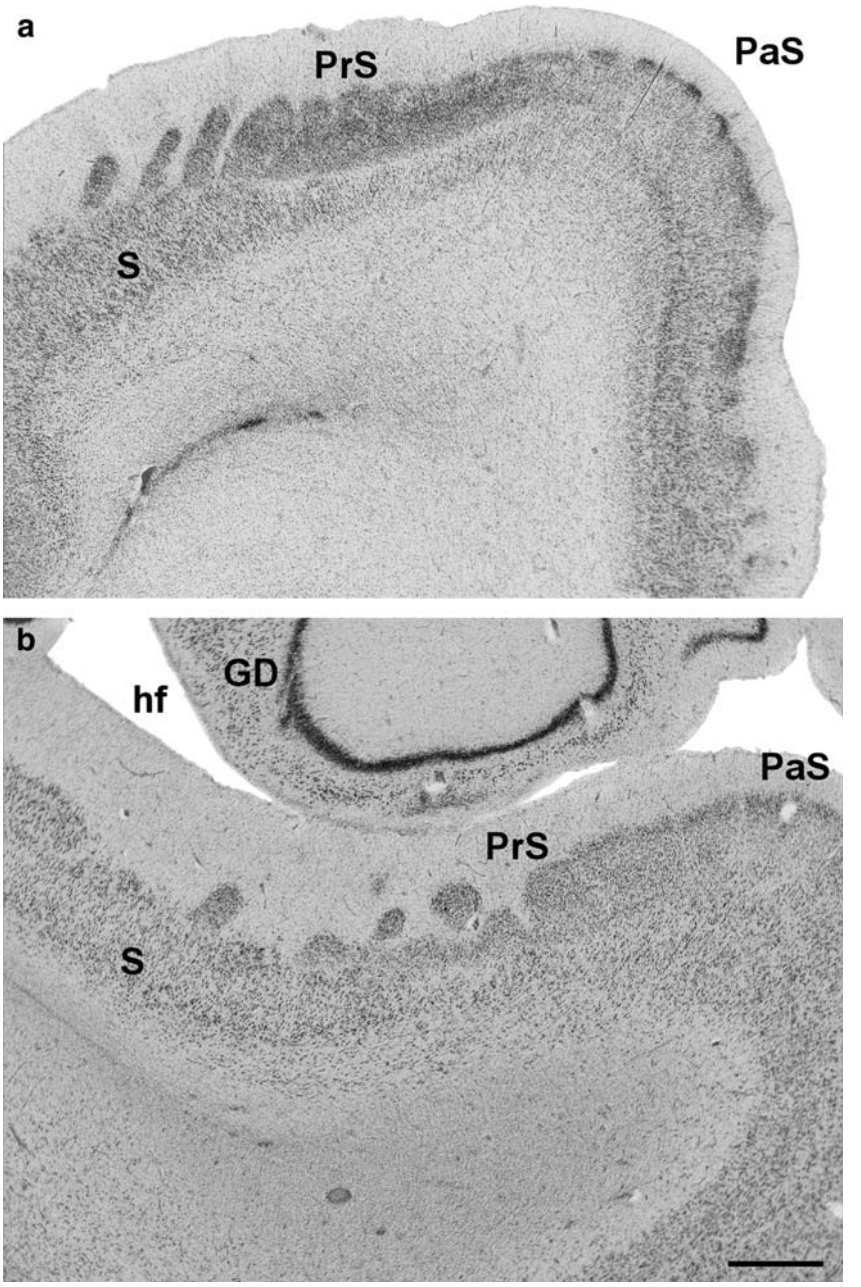

Fig. 4.8 (continued)

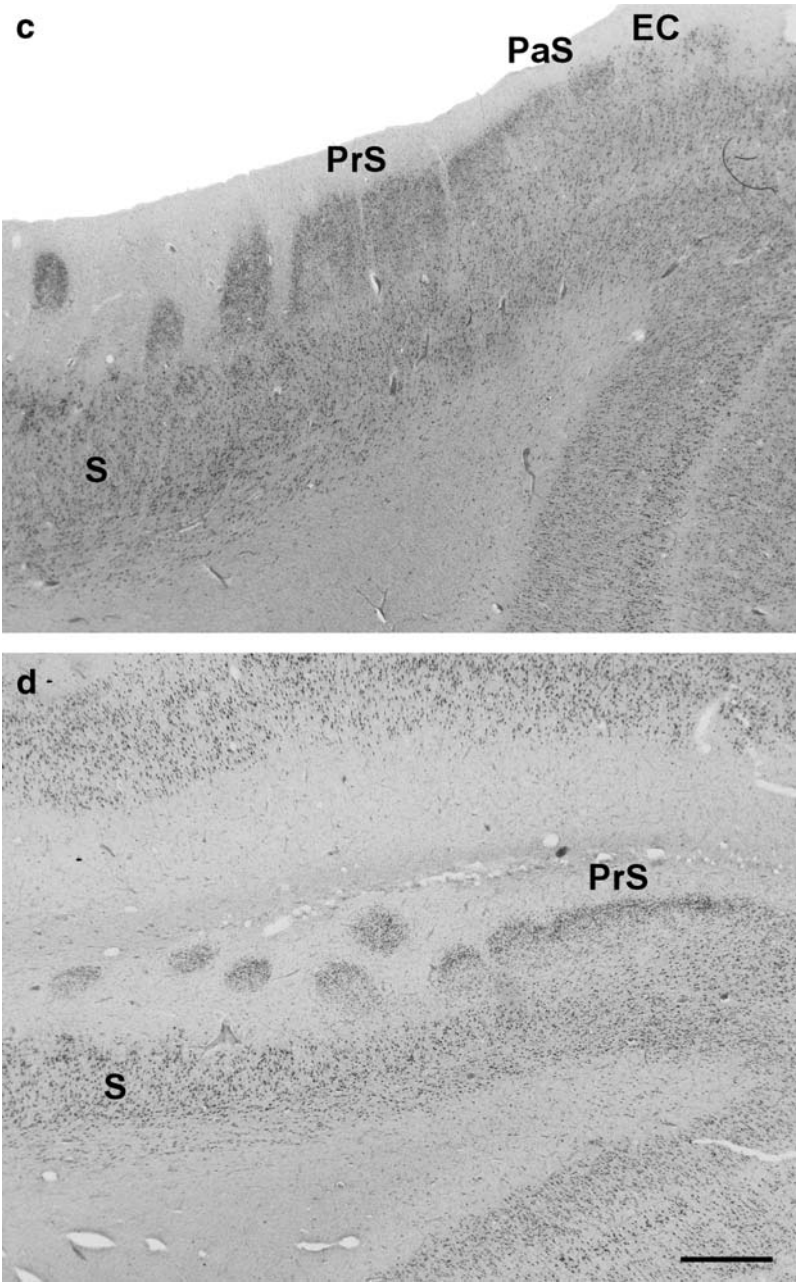

Fig. 4.8 Series of photomicrographs of the presubiculum in the newborn (**a**), one year old (**b**), five year old (**c**), and 14 year old (**d**) cases. At all ages, the lamina principalis interna and externa (the external and internal principal laminae) are separated by a lamina dissecans and are clearly distinguishable (see text for further explanation). The lamina principalis externa form the typical "islands" of the presubiculum. *Scale bar* is 1 mm

CA1, and the subiculum) would fall into this category. On the other hand, the remaining elements, namely the presubiculum, parasubiculum and the EC, would then be located in the so-called periarchicortex (also termed periallocortex), and these regions are characterized by a reduced number of layers compared to the typically six-layered cortical regions, better known as the neocortex (or the isocortex).

The presubiculum presents two main layers, the lamina principalis externa, consisting of small cells, and the lamina principalis interna, comprising somewhat larger cells (Braak 1980). Both cellular layers are separated by a cell-sparse layer termed lamina dissecans. The presence of this lamina dissecans characterizes certain parts of the periarchicortex, including the presubiculum, the parasubiculum, and the EC (Rose 1927), as these components of the HF present lamina dissecans at some point along their rostrocaudal dimension.

The presubiculum presents a mature appearance at birth (Fig. 4.8a). Both the lamina principalis externa and the lamina principalis interna are patent, separated by the lamina dissecans. The lamina principalis externa of the presubiculum closest to the subiculum is always broken into clumps of small cells, the most medial of which are usually located in the thick molecular layer of the subiculum (see above). The lamina principalis interna is much more homogeneous, and although it contains many immature-looking neurons, it is clearly demarcated from the rounded distal extreme of the subiculum (see Fig. 4.8a).

The presubiculum grows in size during postnatal development, similar to other HF fields (Figs. 4.8a–d). However, other than the progressive neuronal definition of the neurons, no changes are observed, and so the presubiculum can be considered an HF field that shows few changes during postnatal development. As presented in Fig. 4.8, the only noticeable change is the relative blurring of the lamina dissecans due to the presence of scattered neurons.

4.7 Parasubiculum

The parasubiculum is probably the least known of all HF components. It starts at the level of the hippocampal fissure, and, at least in the monkey brain, is somewhat less extensive than the presubiculum (Insausti and Muñoz 2001). The level at which it is best developed corresponds to the rostral portion, while caudally it becomes progressively less distinct and merges with area TH of the PPH (Bailey and von Bonin, 1951).

The parasubiculum consists of an external and an internal principal layer that are separated by a small but distinct lamina dissecans (see Fig. 4.9). The external principal layer contains larger cells than the lamina principalis externa of the presubiculum, while the internal principal layer contains neurons with dispositions that resemble those of the caudal and caudal limiting

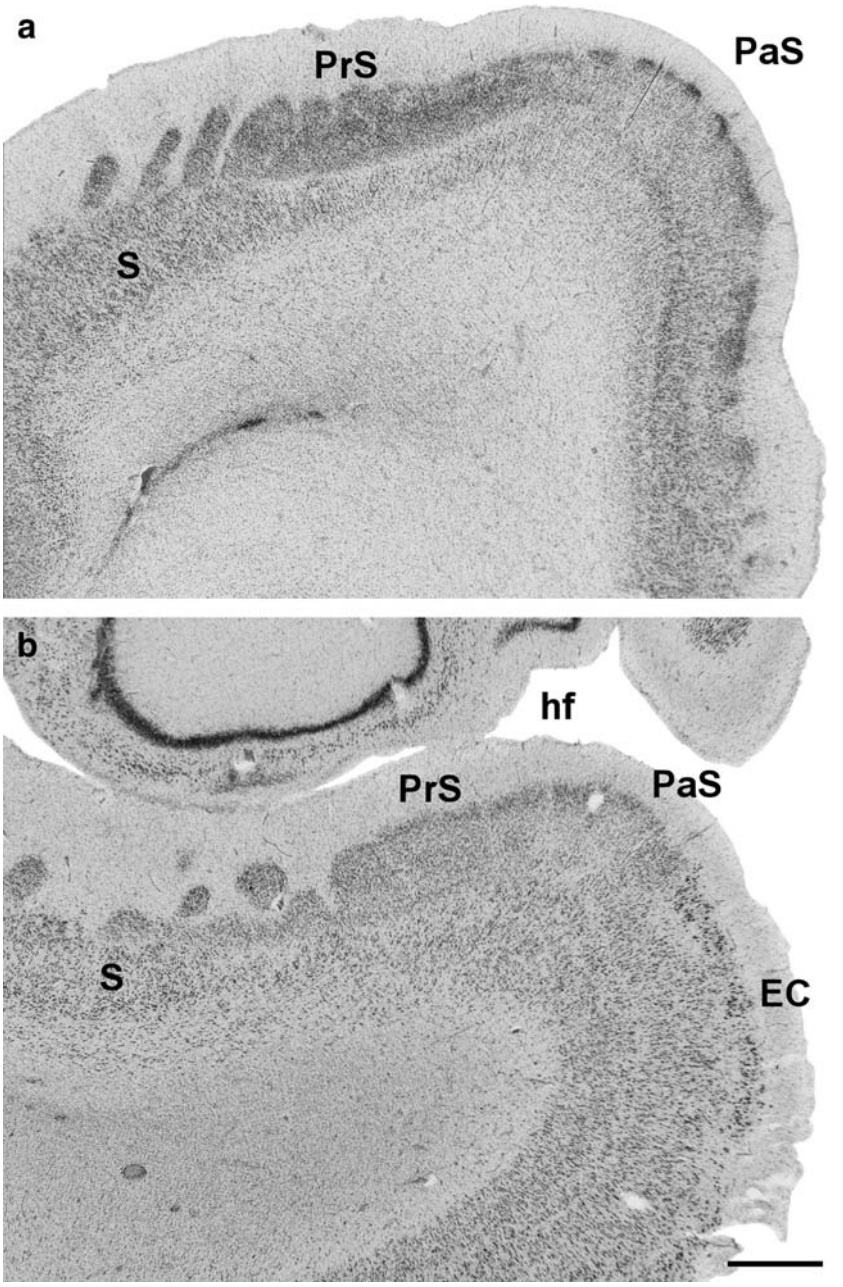

Fig. 4.9 (continued)

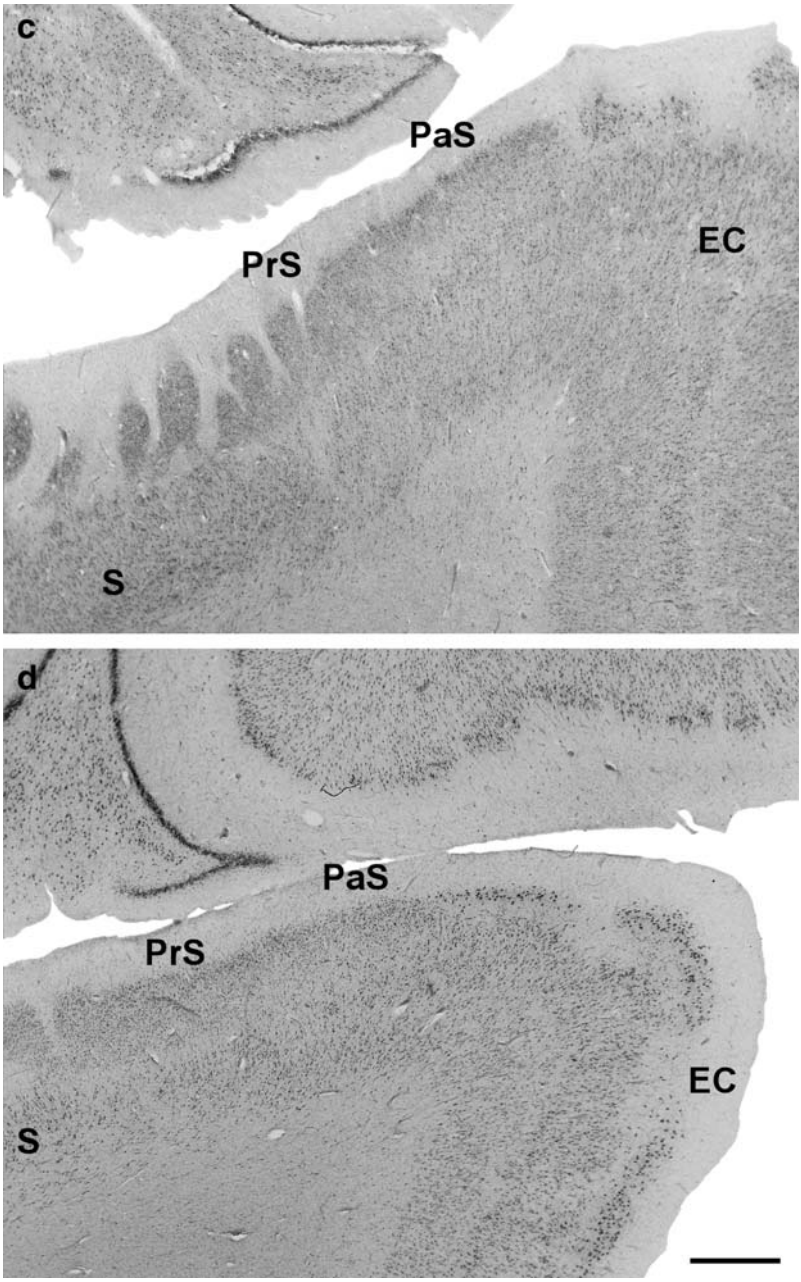

Fig. 4.9 Series of photomicrographs of the parasubiculum in the newborn (**a**), one year old (**b**), five year old (**c**), and 14 year old (**d**) cases. Note the contrast with the presubiculum in the lack of characteristic "islands," and also with the neighboring EC in the absence of lamination of the EC. The three layers of the parasubiculum are already present in the newborn (**a**), and show few changes with age (**b**–**d**). *Scale bar* is 1 mm

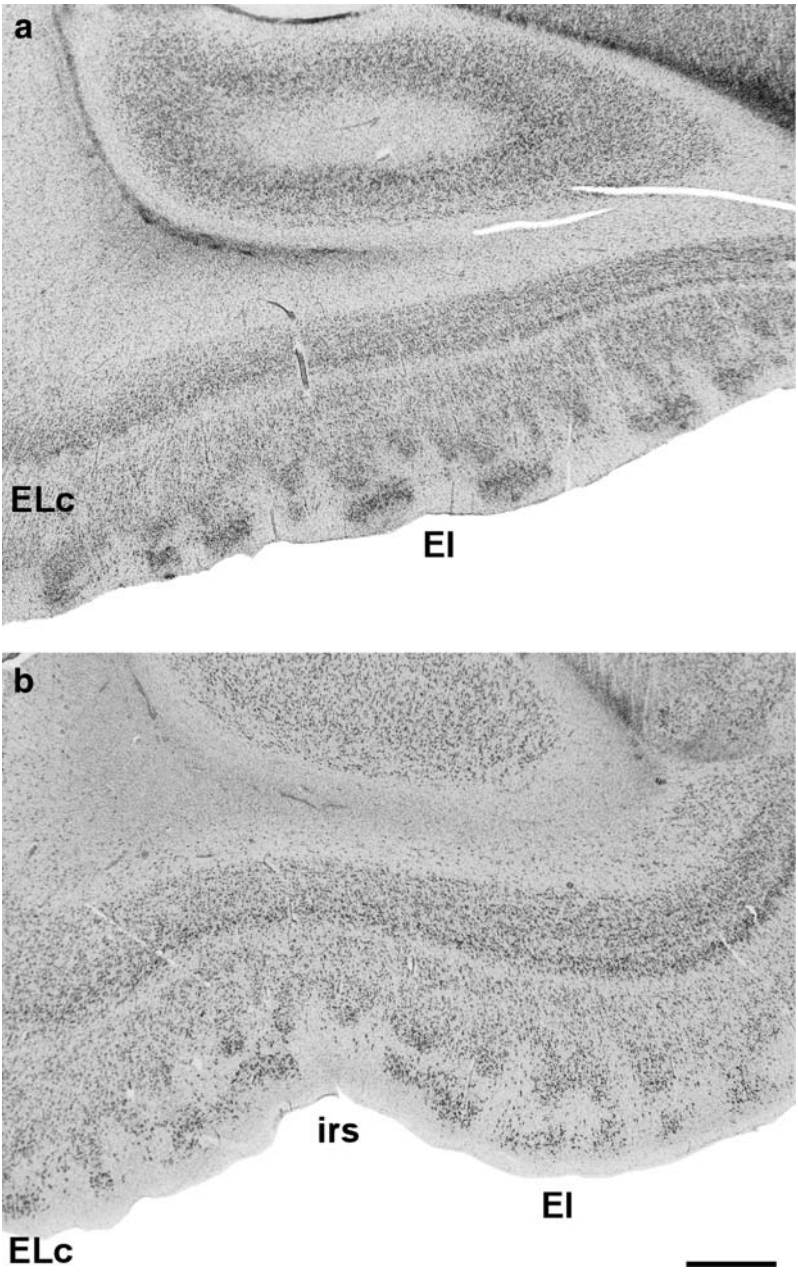

Fig. 4.10 (continued)

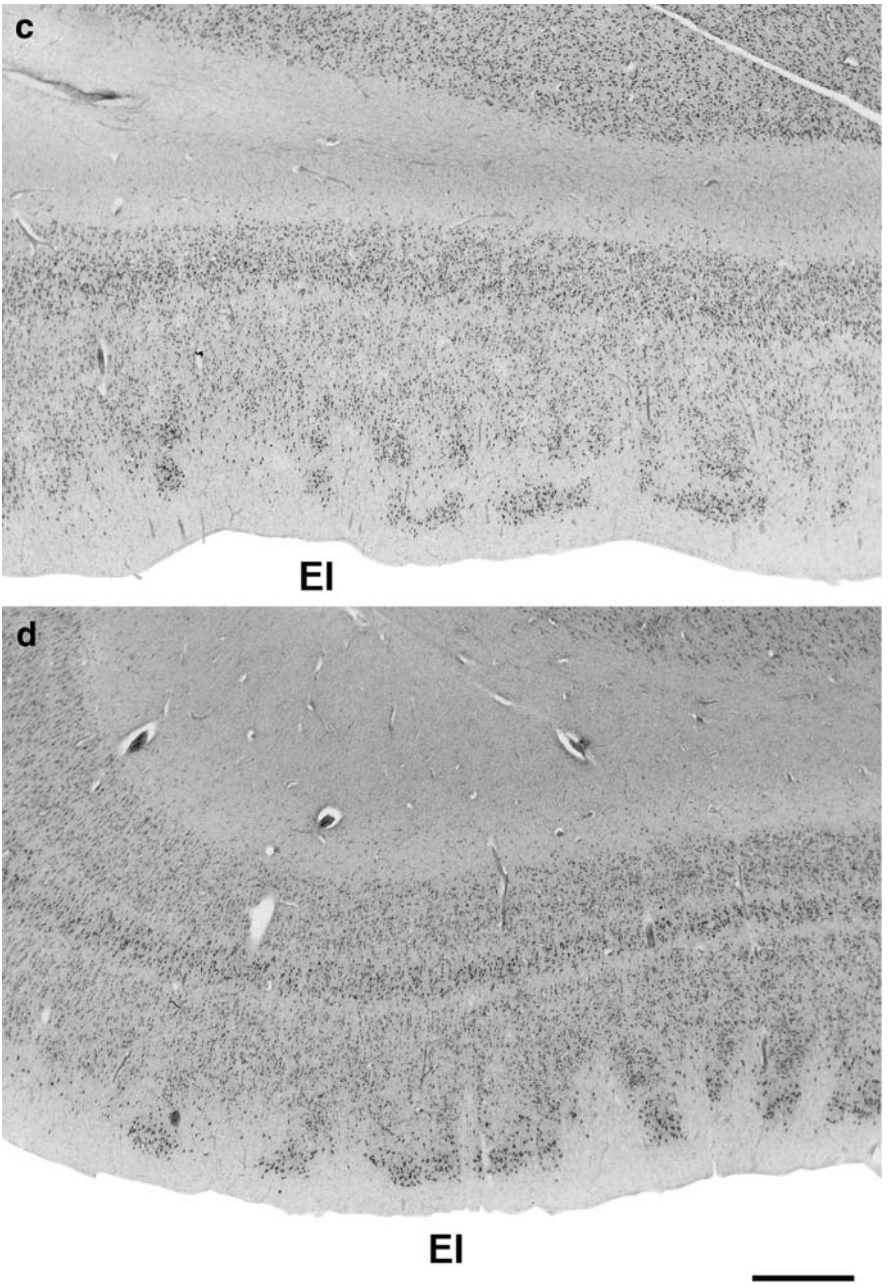

Fig. 4.10 High-power photographs of the EC at the intermediate level in the newborn (**a**), one year old (**b**), five year old (**c**), and 14 year old (**d**) cases. The lamination pattern of the EC is very characteristic and is distinguishable from surrounding areas. This pattern is already present at birth (see picture **a**), although the neurons appear immature compared to older ages (see pictures **c**, **d** and **e**). *Scale bar* is 1 mm

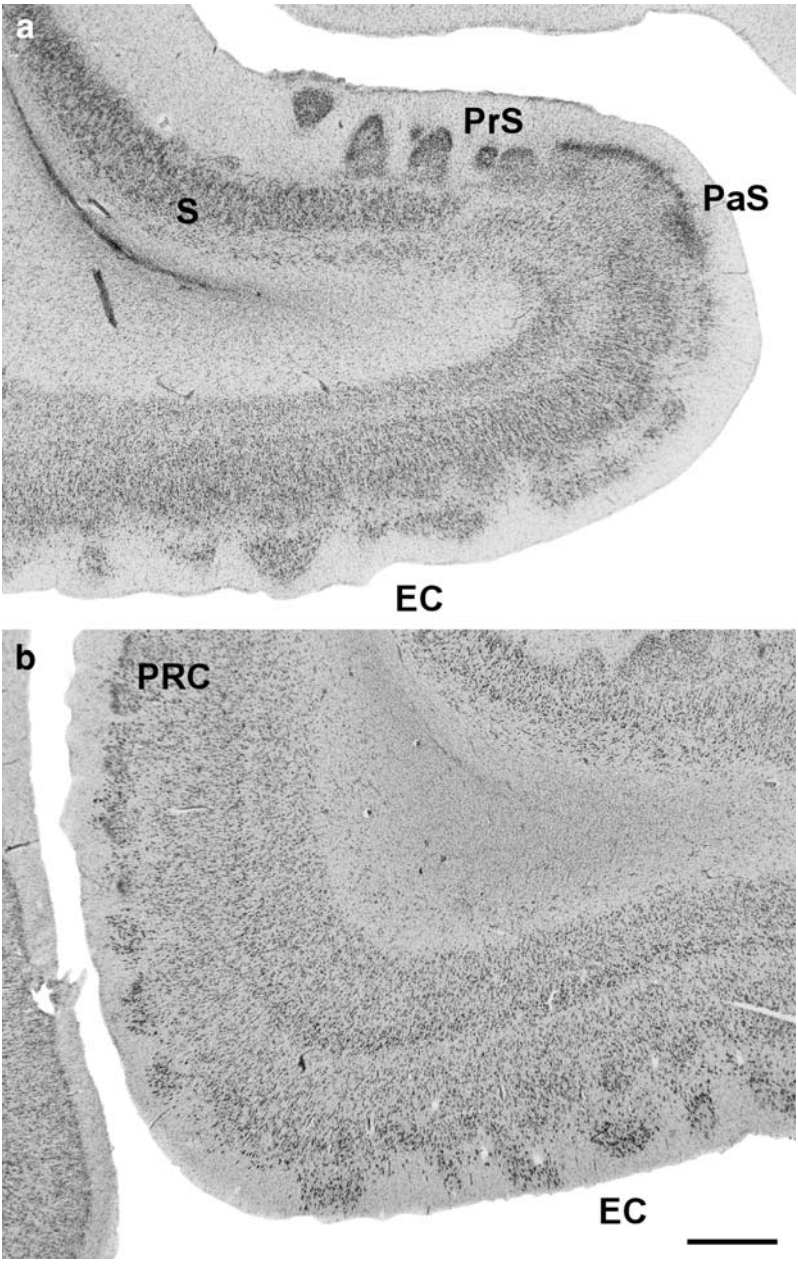

Fig. 4.11 (continued)

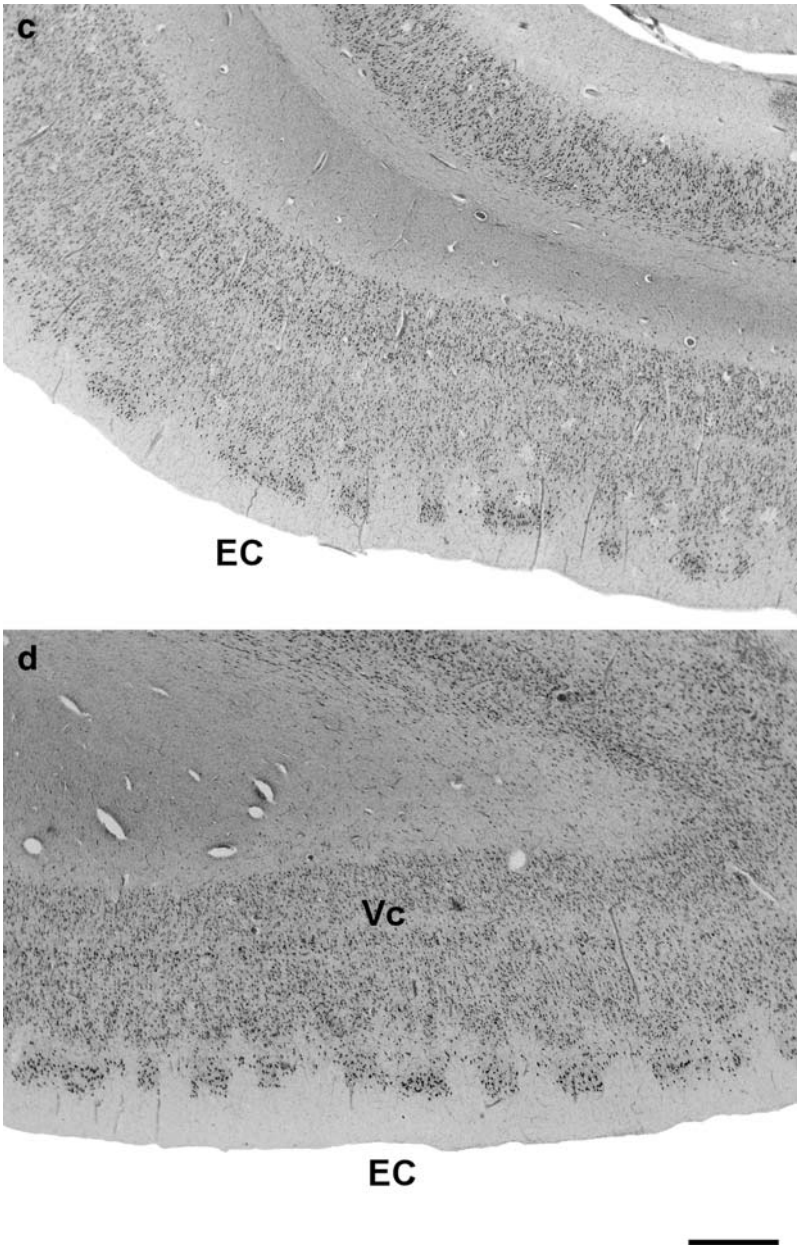

Fig. 4.11 High-power photographs of the EC at the caudal level in the newborn (**a**), one year old (**b**), five year old (**c**), and 14 year old (**d**) cases. The lamination pattern of the EC is very characteristic and is distinguishable from surrounding areas. This pattern is already present at birth (see picture **a**), although the neurons appear immature compared to older ages (see pictures **c**, **d** and **e**). *Scale bar* is 1 mm

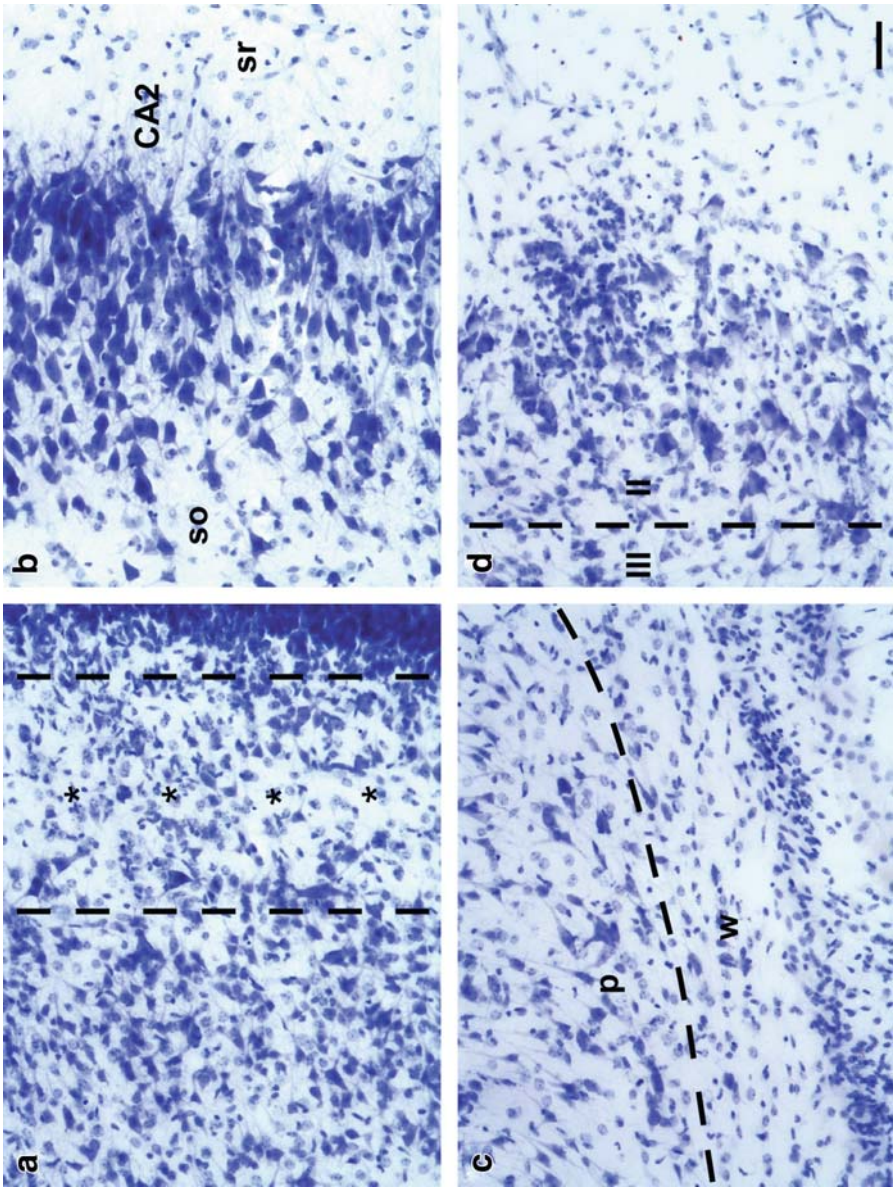
a
b
CA2
sr
so
c
p
w
d
II
III

subfields of the EC rostrally, and the deep layers of area TH of the PPH further caudally.

With these considerations in mind, at birth the parasubiculum is poorly defined and very narrow, and is located at the distal extreme of the presubiculum (Fig. 4.9a). Both the external and the internal principal layers are relatively similar, and they mainly consist of small neurons that appear to be rather undifferentiated. During the first postnatal year, a dramatic change takes place (compare Fig. 4.9a and b): while the small cellular type is predominant in the external principal cellular layer, the internal layer contains larger neurons, although its disposition is still disorganized, and the lamina dissecans is populated by medium-sized neurons, which gives a blurred appearance to this layer. Nonetheless, by the fifth postnatal year of age (Fig. 4.9c), the neurons in the internal principal layer adopt a rather more columnar disposition, as can be seen in Fig. 4.9c. From this time point on, the parasubiculum barely changes, as illustrated by the 14 year old case presented in Fig. 4.9d.

4.8 Entorhinal Cortex

The EC can already be recognized in an embryo at ten weeks postgestation (Kostovic et al. 1993). Connectional studies carried out in a fetus at six months postgestation by means of the lipophilic dye DiI show that, at this age, projections from the EC to the subiculum and CA1 fields are already established (Hevner and Kinney 1996). Therefore, the EC not only appears as a distinct field early during development, but some of its most important connections start to develop at prenatal ages.

The EC is present at birth and displays both mediolateral and rostrocaudal gradients of lamination (Graterón et al. 2002). In some respects such as the laminar organization of the EC, the newborn is similar to the adult. Figure 4.10a shows the intermediate portion of the EC, where all of the layers present in adults are clearly present. Conspicuous cell islands can be seen in layer II; however, these

Fig. 4.12 High-power photomicrographs showing details of the cellular population in the subgranular layer of the DG at birth (**a**, *asterisks*). The *broken lines* indicate the inner border of the granular cell layer (at *right*) and the polymorphic layer of the DG. **b** shows a detailed view of the hippocampal field CA2 in a newborn. Note the stratum radiatum (*sr*) to the *right* and the stratum oriens (*so*) and alveus to the *left*. Some pyramidal neurons of CA3 can be seen below the stratum pyramidale of CA2. **c** depicts the polymorphic cell layer (*p*) of the subiculum above the white matter (*w*) of the angular bundle and the fused hippocampal fissure in one newborn. **d** shows a detailed view of the superficial layers of the intermediate portion of the EC at birth. Note the coexistence of clumps of small, immature-looking neurons intermingled with larger stellate cells in layer II. The separation between layers III and II is indicated by the *dashed line*. *Scale bars* in all panels are 50 μm

are linked to columns of neurons that belong to layer III. A clear lamina dissecans is evident at this level; the deep layers exhibit larger pyramids in layer V, while layer VI consists of neurons of various sizes and shapes. Therefore, the lamination pattern seen in the adult (Insausti et al. 1995) is already developed by the time of birth. The cases at subsequent ages presented in Fig. 4.10 (b, one year old; c, five years old; d, 14 years old) show no variation in the laminar organization of the EC, although the cell islands in layer II become more and more independent of the columns of layer III neurons. Moreover, layer III adopts a rather uniform appearance, except at the rostral portions of the EC, where it shows some clustering. However, the size of the EC increases, most likely due to the development of cortical and subcortical connections that have been demonstrated in the nonhuman primate brain (Insausti et al. 1987; Insausti and Amaral 2008). The EC portion situated caudal to the opening of the choroidal fissure corresponds to the caudal and caudal limiting subfields described in the adult EC (Insausti et al. 1995).

Consistent with the rostrocaudal and mediolateral gradients of lamination in the adult, the newborn EC also shows similar rostrocaudal and mediolateral gradients of maturation (Fig. 4.11a). In this figure, the laminar pattern is similar to the adult, and a cell-sparse band under layer V (sublayer Vc, in the nonhuman primate: Amaral et al. 1987; in the adult human brain: Insausti et al. 1995) is clearly noticeable at this level. Likewise, a more columnar type of organization is also visible, as is the case in the adult counterpart. The cases with different ages presented in Fig. 4.11b–d (b, one year old; c, 5 years old; d, 14 years old) show an increase in size and neuronal definition on thionin-stained material but exactly the same cytoarchitectural organization (Fig. 4.12d).

Chapter 5
Correlation Between Anatomy and MRI

This section describes the appearance of the HF as it grows postnatally, relating gross anatomical and microscopic features of the HF to its appearance in MRI images.

One of the main goals of this part of the study was to compare the MRI appearances of the HF structures with neuroanatomical section series, and to ascertain which specific components of the HF correspond to precise and recognizable landmarks in MRI images. In this way, the landmarks described in the gross anatomical chapter can be applied to the images to facilitate their interpretation in terms of specific components of the HF whenever possible. A secondary objective was to verify whether this comparison would allow the calculation of relative distances of landmarks along the medial temporal lobe, and particularly those related to the HF in the MRI series. Our aim was that this correlation should provide a guide for clinical MRI studies in the postnatal period of development of the human HF. To assess the longitudinal distances at which relevant structures of the HF were located, we chose to use the limen insulae or frontotemporal junction as a fixed starting point, as the temporal poles were not always available. Distances to the limen insulae of anatomical structures that are capable establishing the location and extent of the HF, amygdala and surrounding cortex (PHR) were calculated. Only those pertaining strictly to the HF are presented. For the MRI segmentation we applied our own previously described criteria and segmentation procedure to volumetric evaluation of the temporal pole, EC and PRC in MRI images in adults (Insausti et al. 1998b).

The data presented here, although preliminary, are based on a series of 12 cases that are useful for MRI among the 21 cases included in our series (see Table 2.1). As stated before, the brains came from routine autopsies, and none of them had been diagnosed with neurologically related diseases; they were all considered normal after being examined by an experienced neuropathologist.

MRI images were obtained for 12 brains (Table 2.1; one brain at 30 gestational weeks, one at 38 gestational weeks, four newborns, one two week old brain, one three weeks old, one 1.5 years old, two five year old brains, and one from a 14 year old). The procedure applied before the acquisition of MRI images was as follows. Brains were retrieved from the formalin storage solution and were washed

throughout in distilled water to remove excess fixative. They were then placed in 4% paraformaldehyde and briefly rinsed in distilled water before MRI. Image acquisition was performed in one of two different ways:

1. The brains were first encased in 1.5% agar in lukewarm distilled water, which facilitated handling of the brain (agar held the blocks together during MRI acquisition), as the brains were usually previously blocked for neuropathologic examination. In addition, the agar maintained the humidity of the brain and its anatomical orientation, and did not produce a signal at the agar/brain interface, thus avoiding signal problems resulting from placing the brain in water (Schumann et al. 2001).
2. MRI images were directly obtained after removing excess fluid and carefully soaking the surfaces; the brains were then held in a plastic container that acted as in the procedure described by Schumann et al. (2001) for MRI image acquisition. The reason that we simplified our procedure was that brains encased in agar were used for further histological processing and neuroanatomical evaluation, and sometimes the removal of the agar encasing damaged the structures being studied and the further processing of the brain, especially in very young cases and in cases with less than optimal fixation.

MRI images were obtained with a 1.5 T Philips Intera MRI scanner at the Department of Radiology of the Albacete University Hospital, with a 12.7 cm (5 in.) general purpose receive-only surface coil. Either a wrist or an elbow antenna was placed near the surface of the brain. T1-weighted MR images were obtained in the coronal plane. Whenever possible, the coronal plane was placed orthogonal to the AC–PC line, although it was not always possible to clearly identify the AC–PC line, especially in stillborns and newborns. In such cases, an approximation was used. Images were acquired in the coronal plane, and complementary axial and parasagittal planes were also obtained using a TIR or SE-HR spin-echo sequence (matrix 512 $\times$ 512, thickness = 2 mm) with no interval between adjacent sections. These were the typical acquisition parameters, although in each exploration series of images at other thicknesses and intervals were also acquired to obtain the best definition of the HF structures for each individual case.

When calculating the relative distances in the neuroanatomical and MRI series, we counted the number of sections away from the limen insulae taking into account the thickness at which the MRI was obtained and the interval between sections. The same procedure was also applied to the neuroanatomical series, where the nominal thickness of the sections (typically 50 μm) and the interval at which sections in the series were mounted (typically every 250 μm) were considered. The number of sections multiplied by the thickness and the interval gave a number that was represented on a vertical bar, where the anatomical and MRI distances to the limen insulae were indicated (Fig. 5.4), an approach used previously (Insausti and Amaral 2004; Gonçalves-Pereira et al. 2005).

The fact that the brains were fixed before the MRI scans facilitated the comparison between both series, and no correction factors were needed (Bobinski

et al. 2000). However, shrinkage of the tissue due to fixation must be taken into account when extrapolating to the living subject. Formalin fixation has been reported to cause a 33% reduction in volume (Mouritzen-Dam 1979; Quester and Schröder 1997), and therefore control measurements of brain shrinkage should be taken into account before our results can be applied to in vivo MRI examinations in children.

As an additional objective, we present our preliminary findings on the spatial relationship of the medial temporal lobe (HF, amygdala, PHR) to extrahippocampal nervous structures, mainly diencephalic structures, that could be used as reliable external landmarks to determine variations in the size of the hippocampus in children, particularly those with developmental amnesia in which an atrophy of the hippocampus has been described (Vargha-Khadem et al. 1997; Vargha-Khadem et al. 1994), with the aid of a reference point outside the medial temporal lobe.

The spatial arrangement of these HF structures closely matches our own and other reports on the correspondence between the caudal limit of the uncus and the end of the EC (Insausti et al. 1998b; Bonilha et al 2004; Pruessner et al. 2000, 2002; Insausti and Amaral 2004). This kind of gross anatomical and neuroanatomical correlation has been employed throughout the analysis.

An example of how the topography of the HF relates to extrahippocampal landmarks is the example of the LGN and the gyrus intralimbicus shown in the ventral aspect of the brain in a newborn indicated in Fig. 3.1. The location of the LGN as a bulging eminence on the ventral aspect of the diencephalon and medial to the cortex of the PHR is indicated. Moreover, the bulge of the LGN is, in this view, right behind the end of the uncus formed by the gyrus intralimbicus. The EC ends slightly behind the end of the uncus (1.5–2 mm), and so the presence of the gyrus intralimbicus as an intrahippocampal landmark and the LGN as an extrahippocampal landmark can be used as orientation points for the anterior hippocampus and EC on MRI images in human infants.

Measurements with a comparison of the calculations from the MRI and the neuroanatomical series are presented in Fig. 5.4, and this shows the overall concordance between the neuroanatomical and the MRI series lengths once the histological processing shrinkage has been taken into account. It should be kept in mind that reductions in brain tissue due mainly to fixation, section thickness and other unknown factors can account for a shortening of between 4% and 14% (Kraus 1962, cited by Quester and Schöder 1997). We did not perform specific calculations of the amount of volume reduction due to fixation and processing because of the heterogeneity of our cases. Some additional mismatch can be explained by the definition of MRI images, which can show in a less detailed way the rostral or caudal limits of the structures of the HF and the orientations of blocks that may not have strictly "parallel" planes of section. Blocks were usually obtained at the time of neuropathological examination, where the first section was routinely made at the level of the mammillary bodies, more or less perpendicular to the long axis of the brain; that is, between the frontal and occipital lobes,

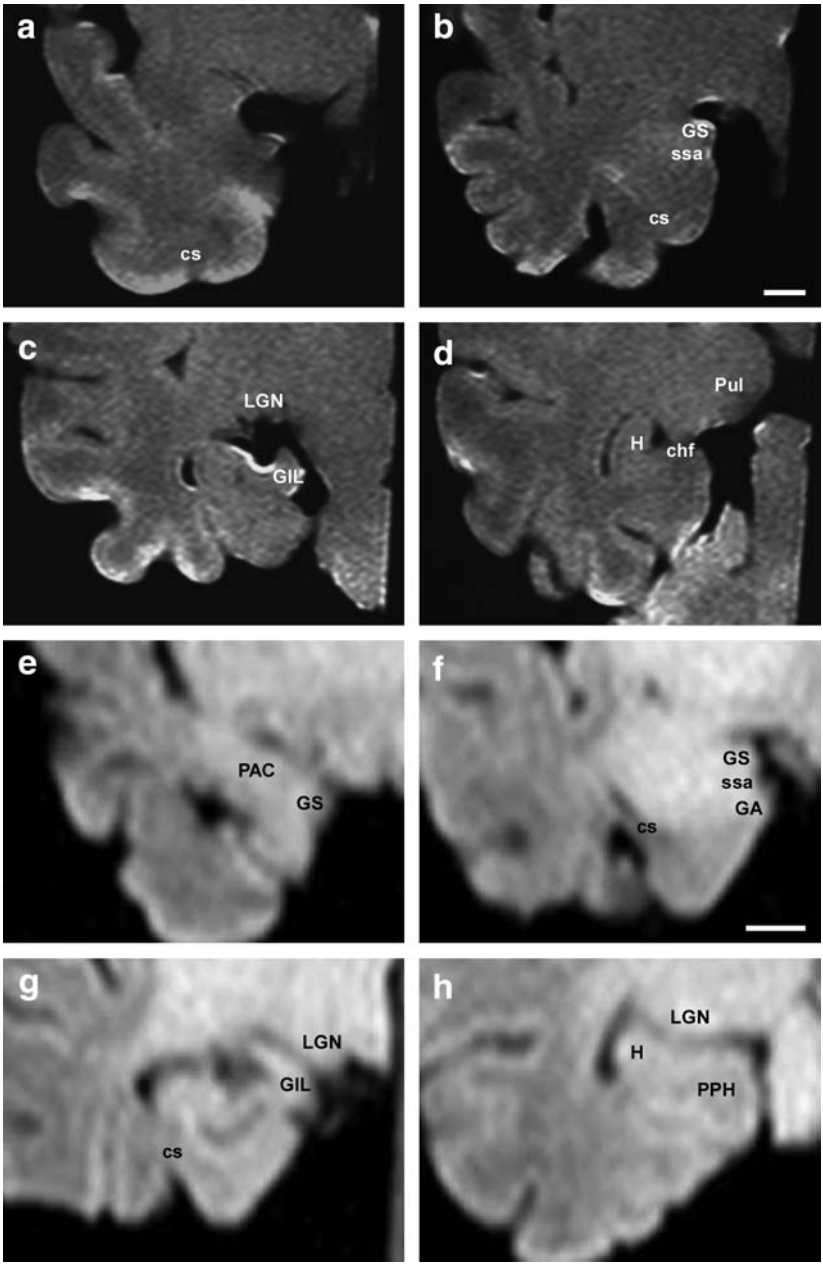

Fig. 5.1 Series of coronal MRI images at birth in two different newborn brains. **a–d** show some of the morphological features seen in Fig. 3.4, (although this is a different case with the same age) such as the gyrus semilunaris (GS), the sulcus semiannularis (*ssa*), or the collateral sulcus (*cs*). **c** is at the level of the gyrus intralimbicus (GIL), and the beginning

slightly off the AC–PC line. This fact can explain some of the mismatch that has already been described. However, the neuroanatomical identification and the correspondence between both series can still be appreciated. Obviously, those measurements need to be adjusted with in vivo MRI series, as retraction occurs due to fixation (Mouritzen-Dam 1979; Quester and Schröder 1997), so that in vivo distances among structures in the medial temporal lobe should be larger. The heterogeneity of our material and the fact that we received it pre-fixed precluded calculating the volume retraction. The lines in Fig. 5.4 indicate the growth of the HF from the time of birth until 14 years, and can be compared with its size in the typical adult brain shown in Fig. 23.4 of Insausti and Amaral (2004), where it is a little more than 1 cm longer than at 14 years.

Figures 5.1–5.3 (except Fig. 5.2a–d) are from the cases studied and illustrated in the previous chapters on macroscopic and microscopic anatomy.

Figure 5.1 presents a series of MRI images along the temporal lobe of two newborn cases. Panels e–h correspond to the series of low-power photomicrographs shown in Fig. 3.4. In both Fig. 5.1a and e, the level of the limen insulae is evident; b and f correspond to the amygdala and rostral part of the EC; c and g show the level of the gyrus intralimbicus and the caudal part of the EC under the hippocampal fissure; in addition, the bulge of the LGN on the ventrolateral surface of the diencephalon can be seen; d and h show the midbody of the hippocampus at the level of the rostral pulvinar. Even at this early age, and despite the low detail present in the images, most of the prominent features of the medial temporal lobe can be visualized. The neuroanatomical analysis in this particular case confirmed the structures that are identifiable on the MRI images.

Figures 5.2 and 5.3 show MRI images at subsequent ages. Figure 5.2a–d are from one 1.5 year old case that is not represented microscopically. In this case, b shows the beginning of the lateral ventricle, while the rest of the panels are at the same level as indicated in Fig. 5.1. Figure 5.2e–h are from a five year old case shown previously in Fig. 3.6. Panel e is at the level of the amygdala and rostral EC, where the sulcus semiannularis and the gyrus semilunaris and gyrus ambiens can be seen. Panel f insinuates the digitationes hippocampi at the rostral part of the uncus. This level would correspond to the intermediate portion of the EC. Panel g shows the level of the gyrus intralimbicus at the level of the caudal part of the EC. Finally, panel h shows the rostral portion of the hippocampal body and the bulging of the LGN. Figure 5.3 is from a 14 year old (also shown in Fig. 3.7). Here, panel a is at the beginning of the amygdala and the rostral part of the EC

Fig. 5.1 (continued) of the LGN is noticeable on the same section (see text for further details). **d** shows the hippocampal tail (H), the choroidal fissure, and the prominence of the pulvinar (*pul*). **e–h** are other examples of coronal MRI images that, in this case, correspond to the same brain whose neuroanatomical sections are presented in Fig. 3.4. Those images, although of a lower quality, can be compared with **a–d** in Fig. 3.4. Structures such as the gyrus semilunaris (GS), sulcus semiannularis (*ssa*) and gyrus ambiens (GA) are easily observed in both the MRI and low-power photomicrographs. Note the presence of the LGN too. *Scale bar* is 0.5 cm

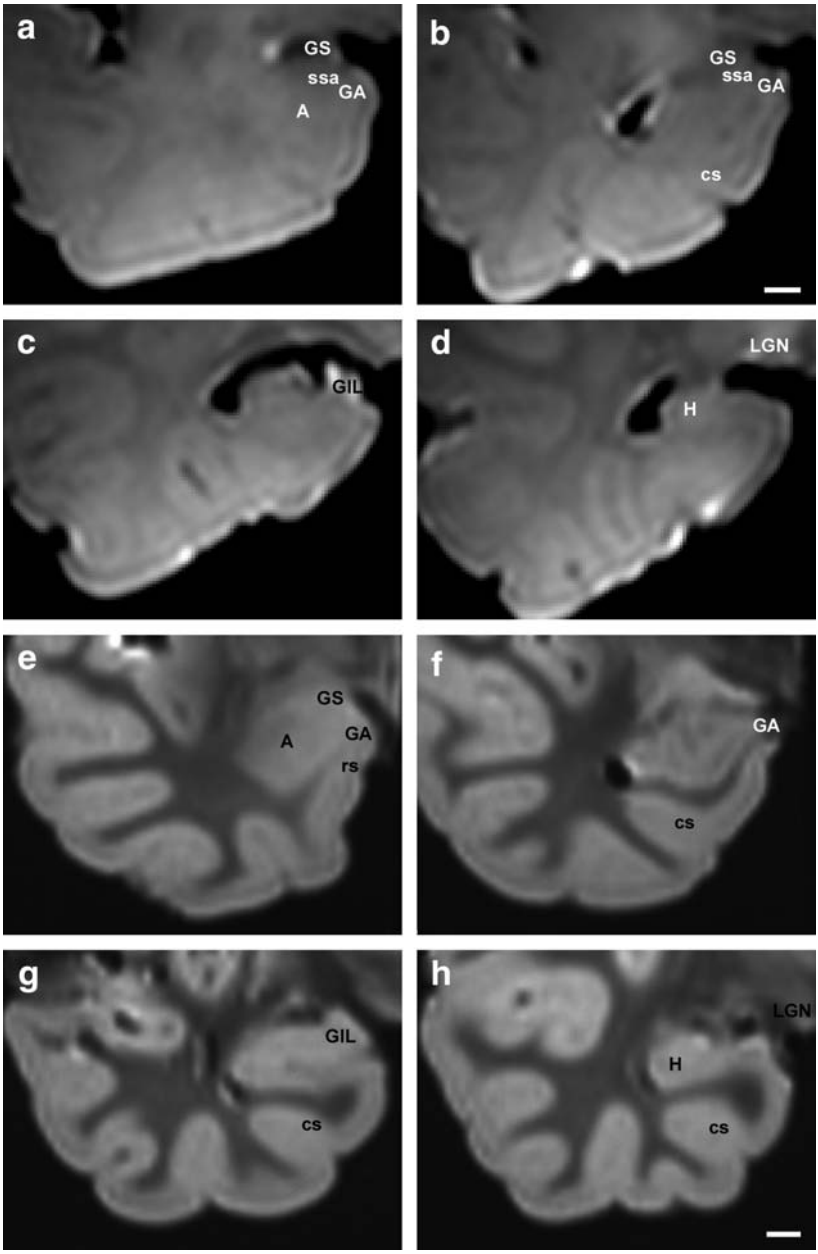

Fig. 5.2 Series of coronal MRI images for one 18 month old case (**a**–**d**). Although no neuroanatomical series was available in this case, note that the same set of structural landmarks can used as in the newborn. **e**–**h** are from a five year old case whose neuroanatomical sections are presented in Fig. 3.6. Note the better definition of the amygdaloid complex, as well as the outline of the EC (**e**) rostrally. The beginning of the hippocampus, as well as the gyrus ambiens (GA), can be seen in **f**, while **g** and **h** show the gyrus intralimbicus (GIL) level and the mid-body hippocampus, respectively. *Scale bar* is 0.5 cm

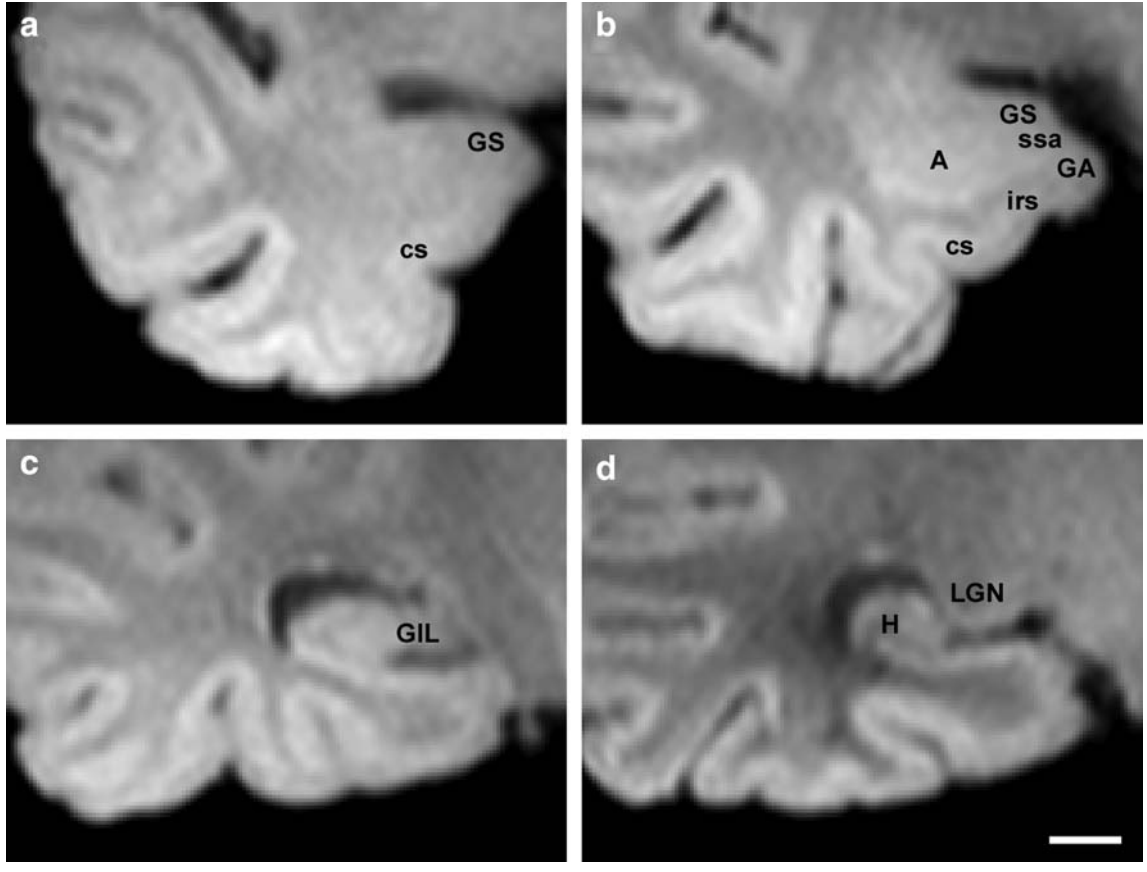

Fig. 5.3 Series of coronal MRI sections in one case (a 14 year old) whose neuroanatomical sections are also presented in Fig. 3.7. The structural similarity between both series is much closer than at other ages, particularly in **b**, where the location of the intrarhinal sulcus (*irs*) is readily apparent. *Scale bar* is 0.5 cm

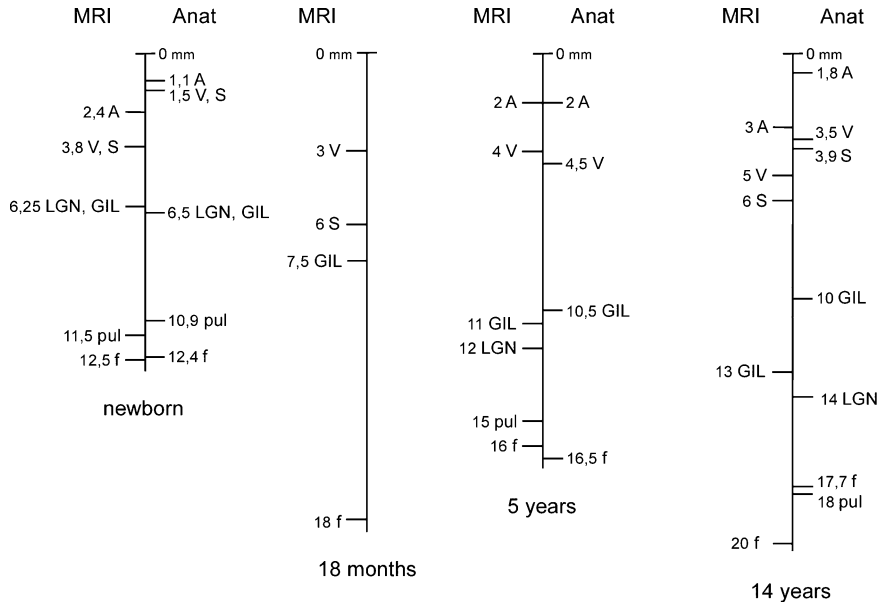

Fig. 5.4 Schematic representation of the lengths of different anatomical landmarks relative to a common starting point (limen insulae)

with the collateral sulcus. Panel b shows the amygdala at midlevel and the rostral EC. Both the gyrus ambiens (limited by the intrarhinal sulcus ventrally) and the gyrus semilunaris (dorsal to the sulcus semiannularis) can be seen. Panel c is at the level of the gyrus intralimbicus and the caudal part of the EC. Panel d is at the midlevel of the body of the hippocampus, and the prominence of the caudal part of the LGN can be also seen.

As expected from samples of pre-fixed tissue, the neuroanatomical series matched the MRI series of images rather well, although in the cases shown in Fig. 5.4 the distances at which the medial temporal lobe structures progressively appeared were not corrected for shrinkage.

However, and in agreement with previous studies, the MRI of fixed tissue offers an opportunity to compare neuroanatomical preparations and in vitro morphology for developmental studies in humans (Brisse et al. 1997; Kostovic et al. 2002; Judas et al. 2005; Rados et al. 2006). Interestingly, Rados et al. (2006) also show the LGN in a full-term newborn, likely at the beginning of the body of the hippocampus.

An example of the utility of structural MRI explorations in children is provided by autism, which has been assessed in post mortem MRI examinations of the brain (Bailey et al. 1998; Schumann et al. 2001), and has produced interesting

findings that are discussed later. Likewise, Bobinski et al. (2000) have shown that the hippocampus presents a strong correlation between volumetric determination and atrophy due to reduced neuronal number (as determined by an unbiased neuronal count), and so volumetric measurements of the HF for different pathological conditions are reliable indicators of pathological phenomena.

Chapter 6
Functional and Pathological Aspects of the Maturation of the Human Hippocampal Formation

6.1
Human and Nonhuman Primate Memory Maturation, and Effect of HF Lesions

Experimental data in nonhuman primates are scarce. However, it has been shown that the fetal hippocampus displays maturation of the dendritic field, as determined by intracellular injection of biocytin, an intracellular marker that completely fills axonal and dendritic arbors so that they can be examined and measured (Khazipov et al. 2001). The results of this unique study indicate that the dendritic arbors of CA1 neurons reach the stratum lacunosum-moleculare by one month before birth (embryonic day E154), and that, by midgestation, synaptic currents can be observed in GABAergic neurons, coincident with the extension of dendritic branches into stratum radiatum, while glutamatergic synapses are associated with the refinement of the dendritic arbor and the appearance of spines during the last third of gestation.

The maturation of the HF is intrinsically related to declarative memory function, which is specifically related to the integrity of the medial temporal lobe (Squire et al. 2004). Different studies have shown that the postnatal development of declarative memory in humans is sensitive to lesions and matures slowly, which is also the case in nonhuman primates (Bachevalier and Beauregard 1993; Overman et al. 1992; Bachevalier et al. 1993). The postnatal development of the HF is an exuberant phase of growth that has been also observed in the nonhuman primate (Duffy and Rakic 1983; Lavenex et al. 2007). Our description of the postnatal development of the human HF, although based only on thionin-stained material, is along the same lines, as most of the morphological changes take place during the first postnatal year. However, not all of the functions dependent on the HF develop at the same time (Bachevalier and Beauregard 1993), and so the maturation of the anatomical substrate needs to be followed by the sculpting actions of other intervening brain systems that are ultimately needed to be fully functional. An example in nonhuman primates is provided by Bachevalier and Mishkin (1984), where the ability to learn an object recognition task such as the delayed non-match to sample (DNMS) task is not present in infant rhesus monkeys until

four months of age, and it does not reach a level equivalent to that of adults until two years of age. Lesions of the MTL (including the HF and amygdala) versus visual unimodal association cortex (area TE of Bailey and von Bonin 1951) performed in infant rhesus monkeys only resulted in impaired performance of the DNMS task with medial temporal lobe lesions, but not after area TE lesions (Bachevalier 1990). These results suggest that visual association cortex has considerable plasticity, as similar lesions in adults impair the DNMS task.

In human infants there is evidence that the postnatal development of these functions parallels that observed in nonhuman primates. Overman (1990) and Overman et al. (1992) have shown that it is not until two years of age that infants learn the DNMS task, although their memory abilities are time limited and are highly dependent on the load of information. In contrast, some form of recognition is already present in six month old infants, as demonstrated by a strong preference for novel objects. Other memory functions such as spatial memory develop even more slowly (Aadland et al. 1985), and do not seem not to be fully developed until four years of age.

6.2 Hippocampal Growth

Our results indicate that the HF grows steadily from birth to the age of 14 years. Our qualitative studies and the determination of the lengths of the HF structures suggest that this growth is not uniform and is located mainly in the EC and in the caudal two-thirds of the hippocampus.

Several studies on the growth of the hippocampus, using MRI longitudinal analysis in particular, have been reported in the last decade (Giedd et al. 1996a, b; Gogtay et al. 2004; Sowell et al. 2004a, b; Evans 2006; Gogtay et al. 2006; Shaw et al. 2008). In addition, the HF has been found to have a protracted maturation, especially for the myelination process (Benes 1989).

Experimental evidence comes from studies in other primate species, such as the baboon (Kroenke et al. 2007), where the gestational development of the cerebral cortex has been examined with surface-based visualization methods (Van Essen 2004) in fixed, postmortem fetal cases. Although the HF is not included as such since it does not show up in structural MRI, it has been shown that diffusion anisotropy (determined by high-resolution diffusion tensor imaging, DTI) is low in allocortical and periallocortical regions (the paleocortex and peripaleocortex of Filiminoff 1947) by midgestation. Moreover, the periallocortical regions included in this study (subiculum, presubiculum, parasubiculum, and EC) display lower diffusion anisotropies than the six-layered isocortex, especially at midgestation. The cortex near the lateral fissure and the precentral gyrus shows relatively low anisotropy at the beginning of the second half of gestation; in addition, near full-term gestation, the relative anisotropy shows less variation. The growth of the cerebral cortex is not uniform, and the rostral

cortical surface grows faster than more caudal regions. Our findings on the enhanced growth of the body and tail of the hippocampus compared to the more rostral portions are shown in Fig. 5.4. However, these results must be approached with caution because of the low number of cases, the lack of definition of the anatomical structures under development, the loss of tissue for neuropathological diagnosis, the possibility of error in the plane of section of MRI compared to the anatomical series, and other variables, so these results are only an approximation of real values. Moreover, data in the literature (Gogtay et al. 2004, 2006) support this finding of nonuniform growth in some regions of the brain.

Thus, it can be concluded that the cortex progresses from low diffusion anisotropy regions that coincide with the border between the periallocortex and the neocortex to high diffusion anisotropy areas. It can be assumed that the allocortical regions (olfactory and hippocampal regions) mark a trend in the progressive development of the cerebral cortex. This technique can be applied to clinical situations such as prematurely born infants (Deipolyi et al. 2005).

Earlier references in the literature posit that the human postnatal development of the HF shows differences in growth, with the right hippocampus being significantly bigger in females than in males, although males had a larger left amygdala (Giedd et al. 1996a, b). More detailed longitudinal studies based on MRI scans in children and young adults aged 4–25 years every two years for a period of between six and ten years have been reported by Gogtay et al. (2006). In these studies it was shown that the hippocampus is regionally heterochronous, with the posterior hippocampus volume increasing over time and the anterior hippocampus decreasing (relatively speaking) over time. Overall, between the ages of 4 and 25 years, the total hippocampal volume did not change. Our findings are in accordance with these studies, and so our data indicate that there is little difference in the MRI longitudinal extent of the HF between the two older specimens (5 and 14 years). However, the relative reduction in volume of the hippocampal head is not easily explained, although the limited number of cases in our series precludes any definitive conclusion on this aspect. Any assessment of the growth of the hippocampal head must take into account the fact that this is a very heterogeneous region, made up of different hippocampal fields, each with its own selective connectivity, beginning with the DG that receives the perforant path input, and continuing with the CA fields of the hippocampus proper and the subiculum. At present, it can be only ascertained that the subiculum accounts for the largest single cytoarchitectonic field in the hippocampal head, although a detailed volumetric assessment of the volume of each HF field is needed. In contrast, the gain in volume in the body and tail seems to be associated with the DG and CA3, although resolution limitations mean that further studies are needed to clarify this issue. Our description at rather fixed time points of neurodevelopment neither supports nor refutes the contention of Gogtay et al. (2006).

A correlation between the size of the hippocampus and the verbal intellectual quotient (IQ) has been demonstrated by Schumann et al. (2007), who found such a

correlation in children and adolescents between 8 and 18 years of age. In the same vein, Shaw et al. (2006) studied how the thickness varies in different regions of the cerebral cortex, and showed that a rapid phase of cortical thickness increase followed by a strong cortical thinning in early adolescence correlated with higher intelligence.

Initiatives such as the NIH MRI study of normal brain development (Evans et al. 2006) will provide data on a large population, balanced demographically, that will help to define the normal parameters of brain development using more controlled clinical and behavioral data.

Postnatal cortical development has been also considered in a number of studies. Gogtay et al. (2004) studied cortical development in children between four years of age and early adulthood (21 years) using MRI scans performed every two years. Their findings reveal that the cortical volume increases during the early years, and then decreases around puberty in a nonhomogeneous manner, which lasts until the end of the adolescence. In particular, the temporal lobe shows a late maturation pattern, except for the temporal poles, which mature (gray matter loss) as early as the frontal and occipital poles. In turn, the frontal and occipital poles present a similar pattern of maturation to the pre- and postcentral gyri, the earliest regions to show cortical maturation. The presumptive EC exhibits early maturation and does not seem to change thereafter. Our results, similar to those for the hippocampal growth, are mainly based on the early years, and from a structural point of view the EC presents an adult-like appearance by the end of the first year (Graterón et al. 2002), while the changes observed between the subsequent time points (5 and 14 years) show little change, in agreement with the results of Gogtay et al. (2004). Shaw et al. (2008) elaborate the change in cortical thickness and describe a linear model for the neurodevelopmental trajectories of relatively simple regions in terms of lamination complexity. In contrast, the isocortex, including higher-order association cortex, follows a cubic trajectory that is developmentally much more complex than that of limbic structures. These findings are in agreement with the linear neurodevelopmental trajectory reported for the hippocampus (Gogtay et al. 2006).

A relevant recent study by Shaw et al. (2007) shows an association between the thickness of the EC and the presence of the allele ε4 in the apolipoprotein E. In this study, based on an extensive sample of children (239 healthy children and 530 MRI scans), a stepwise correlation was found between the thickness of the EC such that ε2 allele carriers present a thicker EC while ε4 carriers show a thinner EC. As the ε4 allele for apolipoprotein E correlates with an increased risk for Alzheimer's disease, ε4 allele carriers of apolipoprotein E may have a higher susceptibility for damage to the EC, one of the hallmarks of Alzheimer's disease.

Those findings underscore the contention that the postnatal growth of the HF specific neurological or psychiatric diseases in which the HF as a whole or in some of its components is measurable, and therefore volumetric data based on clear recognition of HF landmarks on MRI scans are meaningful in the diagnosis/prognosis of different neurodevelopmental disorders.

6.3 Hypoxia and Memory

The hippocampus can be damaged in different conditions that ultimately produce hypoxia of the brain. For a long time, the hippocampus has been known to be a labile structure with defined neuropathological patterns of hippocampal damage. Among its clinical effects, perinatal anoxia can lead to a sustained deficit of episodic memory, which is termed "developmental amnesia" (Vargha-Kadem et al. 1997), and found in children with hippocampal damage. Despite the fact that an enormous amount of development takes place during the first postnatal year, the plasticity and reorganization abilities of the injured brain are not able to overcome a lesion of the hippocampus (Bachevalier and Vargha-Kadem 2005). The almost complete sparing of semantic memory (i.e., memory for facts and events that do not have a personal context, as in episodic memory) offers deep insights into the memory functions performed exclusively by the hippocampus. It should be kept in mind that this period involves a great deal of synaptic development along with dendritic and glial growth, myelination of the main tract that connects the EC and the hippocampus, and the enhancement of the connectivity with the remainder of the neocortex, but the effects of the lesion are irreversible.

6.4 Epilepsy and Medial Temporal Sclerosis

Some of the most prevalent pathologies related to the development of the human HF are epileptic disorders related to the temporal lobe. The hallmark hippocampal lesion is so-called hippocampal sclerosis or mesial sclerosis, which ultimately means "hardening" that stands out as an intense atrophy of the hippocampus. After such a lesion the hippocampus reorganizes, particularly the mossy fibers (Babb et al. 1991), probably due to the modifications in the DG (Houser 1990; Armstrong 1993; Sloviter 1994). In addition, neuronal losses in CA1 and other HF fields are constantly present (Mathern et al. 1996).

Structural MRI studies show a decrease in the hippocampal volume that is instrumental in diagnosis and surgical treatment (Trenerry et al. 1993). This decrease in volume affects not only the hippocampus proper but the parahippocampal gyrus and white matter abnormalities too (Bernasconi et al. 2000). Recently, the involvement of pathology in the EC has been studied by Novak et al. (2002), who stress the importance of EC in mesial sclerosis, where cell loss preferentially takes place in layer III neurons (Du et al. 1993). The importance of EC damage is highlighted by the fact that surgical removal of the EC is considered an indicator of good clinical outcome—even more so than hippocampal resection (Novack et al. 2002). Importantly, the surgical treatment of hippocampal sclerosis may lead to pervasive memory deficits (Noulhiane et al. 2007).

6.5 Schizophrenia, Bipolar Disorder, Autism, and Attention-Deficit/ Hyperactivity Disorder

Schizophrenia is considered a neurodevelopmental disorder with a strong genetic predisposition and HF abnormalities. Early anatomical studies (reviewed in Insausti 1996) indicate that dendritic orientation is altered in some HF components (Kovelman and Scheibel 1984), although further studies gave only partially confirmatory results (Altshuler et al. 1987; Christison et al. 1989).

It has also been claimed that schizophrenia is a neurodevelopmental disorder in which there is a neuronal migration disorder (Jacob and Beckmann 1986, 1994). In addition, a 37% decrease in the number of neurons in layers II and III has also been reported (Falkai et al. 1988). Arnold et al. (1991a, b) report aberrant invaginations in the EC (heterotopia) and a decrease in cellularity in superficial layers, mainly in layer II. Moreover, a distorted morphology in those regions as well as a decrease in microtubule-associated proteins 2 and 5 (MAP2 and MAP5) have been reported in the EC and subiculum, and the normal pattern of structural integrity of the cytoskeleton may also be altered (Arnold et al. 1991a, b)

A decrease in the number of neurons in the hippocampus has been also reported, although with contradictory results (Falkai et al. 1988; Heckers et al. 1990a, b; Benes et al. 1991; Benes 2000; Benes and Berretta 2000). In addition, unbiased methods of evaluating numbers of neurons have yielded no differences in the number of cortical neurons between controls and schizophrenics (Pakkenberg 1993b), so the issue of possible variations in neuron number in schizophrenia as a result of a neurodevelopmental disorder remains open.

At a more gross anatomic level of analysis, both a loss of cortical gray matter (Thompson et al. 2001; Gogtay et al. 2008; Gogtay 2008) and decreased hippocampal volume (Rapoport et al. 1999; Nugent et al. 2007) have been described for this disorder. Gogtay et al. (2008) extended their study to the entity named childhood-onset schizophrenia (COS) using the longitudinal trajectory of the thickness of cortical gray matter development in COS cases (Gogtay 2008) and in their non-psychotic siblings (Gogtay et al. 2008). These studies, although not specifically intended to examine the HF, have determined the level of white matter involvement in the volume reduction described in the literature. Controls showed a pervasive growth of 2.6% in white matter compared to 1.3% in childhood-onset schizophrenia, with statistical difference for the right hemisphere. Siblings of COS patients do not present differences from controls (Gogtay 2008). It appears that cortical gray matter thickness loss occurs in adolescence. Thus, the normal phenomenon of maturation is exaggerated and excessive synapse loss and dendritic pruning takes place (Huttenlocher and Dabholkar 1997; Feinberg 1982). Establishing whether or not these synaptic and dendritic changes also affect the HF specifically during its postnatal development, including late transformations during adolescence, would require further studies.

Bipolar disorder is another major psychosis that is suspected of involving a neurodevelopmental disorder. Several pathological phenomena have been described. For instance, deviations from the normal pattern of Timm staining for mossy fibers (Dowlatshahi et al. 2000), a hippocampal decrease in CA2 cell number (Benes et al. 1998), dendritic abnormalities in the subiculum (Rosoklija et al. 2000), a reduction in reelin immunoreactivity (Fatemi et al. 2000), and synaptic proteins (Fatemi et al. 2000, 2001) have been reported. A trend towards a reduction in hippocampal volume has been noted, while the same study reports a decrease in amygdala volume in juvenile bipolar disorder (Blumberg 2003). A recent report, however, confirms that hippocampal volume is reduced by a significant 9.2% compared to controls (Bearden et al. 2008). These pathological findings suggest a variety of possible neurodevelopmental abnormalities that ultimately lead to the clinical expression of this disease.

Attention-deficit/hyperactivity disorder (ADHD) is a common disorder that affects a significant percentage of children (Shaw et al. 2007a). Longitudinal studies suggest a developmental delay, as they show that the time at which 50% of the points have reached maximal cortical thickness is 7.5 years for controls and 10.5 years for ADHD, although no specific measurements were taken for the HF. The greatest delay occurs in the polymodal association cortex of the frontal and temporal lobes, and so, as the temporal association cortex is considered one of the main sources of cortical input to the EC and thus to the HF (Insausti et al. 1987; Insausti and Amaral 2008; Mohedano et al. 2008), a developmental delay in cortical association areas anatomically linked to the HF would probably affect the development and maturation of the transfer of highly processed cortical information to the hippocampus. In addition, this delay in cortical maturation also affects also the onset of decline in cortical growth that is typical of adolescence.

6.6 Developmental Delay

Developmental delay is a condition that is responsible for many of the physical and intellectual disabilities that occur in children. Ischemic episodes, especially during delivery, can damage the white matter (periventricular leukomalacia) and thus the connective system that transfers information within hemispheres and between hemispheres. With the main aim of studying axonal maturation from midgestation until 2.5 years, Haynes et al. (2005) studied white matter maturation with a series of immunohistochemical markers at the level of the parietal cortex in order to determine the maturation of white matter at the time when corticocortical and corticosubcortical connections expand and elongate, a period when periventricular leukomalacia—a hallmark of prematurity with cerebral palsy and cognitive or behavioral disturbances—appears (Haynes et al. 2003). They found that white matter markers such as Bielschowsky stain, SMI 31 (to demonstrate high

molecular weight phosphorylated neurofilaments), and myelin basic protein all reach adult-like levels of expression by one year of age.

Abernethy et al. (2002) examined structural MRI scans of 15–16 year old children that had survived a very low birth weight and reported decreased volumes in the left hippocampus and a smaller hippocampal ratio, in addition to a smaller right caudate nucleus. Further studies based on DTI reveal a reduction in the entire corpus callosum and a lack of correlation with the volume of the corresponding cortical white matter (Cascio et al. 2006). Those findings are extended in the work of Skranes et al. (2007), who studied the correlation of perceptual and cognitive abilities with fractional anisotropy using DTI. Fractional anisotropy values were lower in different brain white matter tracts, including the internal and external capsules, the corpus callosum, and longitudinal associational fasciculi such as the superior, middle superior and inferior fasciculi, thus indicating white matter injury (periventricular leukomalacia) in children with very low birth weights, and a susceptibility to mental retardation.

There is the possibility that poor growth in the early postnatal period—a time of rapid growth in brain structures, as determined by neurodevelopmental trajectories (Shaw et al. 2008)—may heavily influence the postnatal development of the HF and related functions of learning and memory.

Abnormal hippocampal morphologies are also associated with other brain developmental disorders (Sato et al. 2001), thus indicating that disorders of neuronal migration (e.g., in cortical dysplasia) result in concurrent abnormalities in HF development. Among these are holoprosencephaly, lissencephaly, tuberous sclerosis, Fukuyama muscular dystrophy and agenesis of the corpus callosum, which are associated with an abnormal shape (globular), orientation (vertical), or a reduction in the size of the hippocampus (Baker and Barkowich 1992; Sato et al. 2001).

Mutations in the human doublecortin gene leading to Type I lissencephaly and subcortical laminar heterotopia as well as hippocampal malformation, particular in relation to the migration of cells that disturb the development of the neocortex, corpus callosum and hippocampus, have been also reported (Kappeler et al. 2007; Forman et al. 2005; Montenegro et al. 2006).

References

Aadland J, Beatty WW, Maki RH (1985) Spatial memory of children and adults assessed in the radial maze. Develop Psychobiol 18:163–172

Abel LA, Levin S, Holzman PS (1992) Abnormalities of smooth pursuit and saccadic control in schizophrenia and affective disorders. Vision Res 32:1009–1014

Abernethy LJ, Palaniappan M, Cooke RW (2002) Quantitative magnetic resonance imaging of the brain in survivors of very low birth weight. Arch Disease Child 87:279–283

Altshuler LL, Conrad A, Kovelman JA, Scheibel A (1987) Hippocampal pyramidal cell orientation in schizophrenia. A controlled neurohistologic study of the Yakovlev collection. Arch Gen Psychiatry 44:1094–1098

Amaral DG, Lavenex P (2007) Hippocampal neuroanatomy. In: Per Andersen, Richard Morris, David Amaral, Tim Bliss, John O'Keefe (eds) The hippocampus book, pp 37–114

Amaral DG, Witter MP (1989) The three-dimensional organization of the hippocampal formation: a review of anatomical data. Neuroscience 31:571–591

Amaral DG, Insausti R, Cowan WM (1987) The entorhinal cortex of the monkey: I Cytoarchitectonic organization. J Comp Neurol 264:326–355

Amaral DG, Scharfman HE, Lavenex P (2007) The dentate gyrus: fundamental neuroanatomical organization (dentate gyrus for dummies). Prog Brain Res 163:3–22

Armstrong DD (1993) The neuropathology of temporal lobe epilepsy. J Neuropathol Exp Neurol 52:433–443

Arnold SE, Trojanowski JQ (1996) Human fetal hippocampal development: I. Cytoarchitecture, myeloarchitecture, and neuronal morphologic features. J Comp Neurol 367:274–292

Arnold SE, Hyman BT, Van Hoesen GW, Damasio AR (1991a) Some cytoarchitectural abnormalities of the entorhinal cortex in schizophrenia. Arch Gen Psychiatry 48:625–632

Arnold SE, Lee VM, Gur RE, Trojanowski JQ (1991b) Abnormal expression of two microtubule-associated proteins (MAP2 and MAP5) in specific subfields of the hippocampal formation in schizophrenia. PNAS 88:10850–10854

Arnold SE, Franz BR, Gur RC, Gur RE, Shapiro RM, Moberg PJ, Trojanowski JQ (1995) Smaller neuron size in schizophrenia in hippocampal subfields that mediate cortical-hippocampal interactions. Am J Psychiatry 152:738–748

Babb TL, Kupfer WR, Pretorius JK, Crandall PH, Levesque MF (1991) Synaptic reorganization by mossy fibers in human epileptic fascia dentata. Neuroscience 42:351–363

Bachevalier J (1990) Ontogenetic development of habit and memory formation in primates. Ann NY Acad Sci 608:457–477; discussion 477–484

Bachevalier J, Beauregard M (1993) Maturation of medial temporal lobe memory functions in rodents, monkeys and humans. Hippocampus 3 Spec No: 191–201

Bachevalier J, Mishkin M (1984) An early and a late developing system for learning and retention in infant monkeys. Behav Neurosci 98:770–778

Bachevalier J, Vargha-Khadem F (2005) The primate hippocampus: ontogeny, early insult and memory. Curr Opinion Neurobiol 15:168–174

Bachevalier J, Brickson M, Hagger C (1993) Limbic-dependent recognition memory in monkeys develops early in infancy. NeuroReport 4:77–80

Bailey PA, Bonin GV (1951) The isocortex of man. University of Illinois Press VI:1–301
Bailey A, Luthert P, Dean A, Harding B, Janota I, Montgomery M, Rutter M, Lantos P (1998) A clinicopathological study of autism. Brain 121(Pt 5):889–905
Baker LL, Barkovich AJ (1992) The large temporal horn: MR analysis in developmental brain anomalies versus hydrocephalus. Amer J Neurorad 13:115–122
Bauman M, Kemper TL (1985) Histoanatomic observations of the brain in early infantile autism. Neurology 35:866–874
Bayer SA, Altman J (2004) Atlas of human central nervous system development. Volume 2. The human brain during the third trimester. CRC Press, LLC USA
Bearden CE, van Erp TG, Dutton RA, Lee AD, Simon TJ, Cannon TD, Emanuel BS, McDonald-McGinn D, Zackai EH, Thompson PM (2008) Alterations in midline cortical thickness and gyrification patterns mapped in children with 22q11.2 deletions. Cereb Cortex 19:115–126
Benes FM (1989) Myelination of cortical-hippocampal relays during late adolescence. Schizo Bull 15:585–593
Benes FM (2000) Emerging principles of altered neural circuitry in schizophrenia. Brain Res Brain Res Rev 31:251–269
Benes FM, Berretta S (2000) Amygdalo-entorhinal inputs to the hippocampal formation in relation to schizophrenia. Ann NY Acad Sci 911:293–304
Benes FM, Sorensen I, Bird ED (1991) Reduced neuronal size in posterior hippocampus of schizophrenic patients. Schizoph Res 17:597–608
Benes FM, Kwok EW, Vincent SL, Todtenkopf MS (1998) A reduction of nonpyramidal cells in sector CA2 of shizophrenics and manic depressives. Biol Psychiatry 44:88–97
Bernasconi N, Bernasconi A, Caramanos Z, Andermann F, Dubeau F, Arnold DL (2000) Morphometric MRI analysis of the parahippocampal region in temporal lobe epilepsy. Ann NY Acad Sci 911:495–500
Blumberg HP, Kaufman J, Martin A, Whiteman R, Zhang JH, Gore JC, Charney DS, Krystal JH, Peterson BS (2003) Amygdala and hippocampal volumes in adolescents and adults with bipolar disorder. Arch Gen Psychiatry 60:1201–1208
Bobinski M, de Leon MJ, Wegiel J, Desanti S, Convit A, Saint Louis LA, Rusinek H, Wisniewski HM (2000) The histological validation of post mortem magnetic resonance imaging-determined hippocampal volume in Alzheimer's disease. Neuroscience 95:721–725
Bonilha L, Kobayashi E, Cendes F, Min Li L (2004) Protocol for volumetric segmentation of medial temporal structures using high-resolution 3-D magnetic resonance imaging. Human Brain Map 22:145–154
Braak H (1980) Architectonics of the human telencephalic cortex. Stud Brain Funct 4
Brisse H, Fallet C, Sebag G, Nessmann C, Blot P, Hassan M (1997) Supratentorial parenchyma in the developing fetal brain: in vitro MR study with histologic comparison. Amer J Neurorad 18:1491–1497
Brodmann (1909) Vergleichende Lokalisationslehre. Leipzig JA Barth. In: Charles R Noback, William Montagna (eds) The primate brain advances in primatology, vol 1
Cannon TD, Mednick SA, Parnas J, Schulsinger F, Praestholm J, Vestergaard A (1994) Developmental brain abnormalities in the offspring of schizophrenic mothers. II. Structural brain characteristics of schizophrenia and schizotypal personality disorder. Arch Gen Psychiatry 51:955–962
Cascio C, Styner M, Smith RG, Poe MD, Gerig G, Hazlett HC, Jomier M, Bammer R, Piven J (2006) Reduced relationship to cortical white matter volume revealed by tractography-based segmentation of the corpus callosum in young children with developmental delay. Am J Psychiatry 163:2157–2163
Christison GW, Casanova MF, Weinberger DR, Rawlings R, Kleinman JE (1989) A quantitative investigation of hippocampal pyramidal cell size, shape, and variability of orientation in schizophrenia. Arch Gen Psychiatr 46:1027–1032
Conrad AJ, Abebe T, Austin R, Forsythe S, Scheibel AB (1991) Hippocampal pyramidal cell disarray in schizophrenia as a bilateral phenomenon. Arch Gen Psychiatry 48:413–417

de la Monte SM, Hedley-Whyte ET (1990) Small cerebral hemispheres in adults with Down's syndrome: contributions of developmental arrest and lesions of Alzheimer's disease. J Neuropathol Exp Neurol 49:509–520

Debbane M, Glaser B, David MK, Feinstein C, Eliez S (2006a) Psychotic symptoms in children and adolescents with 22q11.2 deletion syndrome: Neuropsychological and behavioral implications. Schizoph Res 84:187–193

Debbane M, Schaer M, Farhoumand R, Glaser B, Eliez S (2006b) Hippocampal volume reduction in 22q11.2 deletion syndrome. Neuropsychologia 44:2360–2365

Deipolyi AR, Mukherjee P, Gill K, Henry RG, Partridge SC, Veeraraghavan S, Jin H, Lu Y, Miller SP, Ferriero DM, Vigneron DB, Barkovich AJ (2005) Comparing microstructural and macrostructural development of the cerebral cortex in premature newborns: diffusion tensor imaging versus cortical gyration. NeuroImage 27:579–586

Dowlatshahi D, MacQueen G, Wang JF, Chen B, Young LT (2000) Increased hippocampal supragranular Timm staining in subjects with bipolar disorder. NeuroReport 11:3775–3778

Du F, Whetsell WO Jr, Abou-Khalil B, Blumenkopf B, Lothman EW, Schwarcz R (1993) Preferential neuronal loss in layer III of the entorhinal cortex in patients with temporal lobe epilepsy. Epilepsy Res 16:223–233

Duffy CJ, Rakic P (1983) Differentiation of granule cell dendrites in the dentate gyrus of the rhesus monkey: a quantitative Golgi study. J Comp Neurol 214:224–237

Eriksson PS, Perfilieva E, Bjork-Eriksson T, Alborn AM, Nordborg C, Peterson DA, Gage FH (1998) Neurogenesis in the adult human hippocampus. Nat Med 4:1313–1317

Evans AC (2006) The NIH MRI study of normal brain development. NeuroImage 30:184–202

Falkai P, Bogerts B, Rozumek M (1988) Limbic pathology in schizophrenia: the entorhinal region–a morphometric study. Biol Psychiatry 24:515–521

Fatemi SH, Earle JA, McMenomy T (2000) Reduction in Reelin immunoreactivity in hippocampus of subjects with schizophrenia, bipolar disorder and major depression. Mol Psychiatry 5 (654–663):571

Fatemi SH, Earle JA, Stary JM, Lee S, Sedgewick J (2001) Altered levels of the synaptosomal associated protein SNAP-25 in hippocampus of subjects with mood disorders and schizophrenia. NeuroReport 12:3257–3262

Feinberg I (1982) Schizophrenia: caused by a fault in programmed synaptic elimination during adolescence? J Psych Res 17:319–334

Ferrer I, Gullotta F (1990) Down's syndrome and Alzheimer's disease: dendritic spine counts in the hippocampus. Acta Neuropathol 79:680–685

Filiminoff IN (1947) A rational subdivision of the cerebral cortex. In: Charles R Noback, William Montagna (eds) The primate brain advances in primatology, vol 1, pp 296–311

Forman MS, Squier W, Dobyns WB, Golden JA (2005) Genotypically defined lissencephalies show distinct pathologies. J Neuropathol Exp Neurol 64:847–857

Galaburda AM, Wang PP, Bellugi U, Rossen M (1994) Cytoarchitectonic anomalies in a genetically based disorder: Williams syndrome. NeuroReport 5:753–757

Gertz SD (1972) Structural variations in the rostral human hippocampus. Johns Hopkins Med J 130:367–376

Giedd JN, Snell JW, Lange N, Rajapakse JC, Casey BJ, Kozuch PL, Vaituzis AC, Vauss YC, Hamburger SD, Kaysen D, Rapoport JL (1996a) Quantitative magnetic resonance imaging of human brain development: ages 4–18. Cereb Cortex 6:551–560

Giedd JN, Vaituzis AC, Hamburger SD, Lange N, Rajapakse JC, Kaysen D, Vauss YC, Rapoport JL (1996b) Quantitative MRI of the temporal lobe, amygdala, and hippocampus in normal human development: ages 4–18 years. J Comp Neurol 366:223–230

Gogtay N (2008) Cortical brain development in schizophrenia: insights from neuroimaging studies in childhood-onset schizophrenia. Schizoph Res 34:30–36

Gogtay N, Giedd JN, Lusk L, Hayashi KM, Greenstein D, Vaituzis AC, Nugent TF 3rd, Herman DH, Clasen LS, Toga AW, Rapoport JL, Thompson PM (2004a) Dynamic mapping of human cortical development during childhood through early adulthood. PNAS 101:8174–8179

Gogtay N, Sporn A, Clasen LS, Nugent TF 3rd, Greenstein D, Nicolson R, Giedd JN, Lenane M, Gochman P, Evans A, Rapoport JL (2004b) Comparison of progressive cortical gray matter loss in childhood-onset schizophrenia with that in childhood-onset atypical psychoses. Arch Gen Psychiatry 61:17–22

Gogtay N, Nugent TF 3rd, Herman DH, Ordonez A, Greenstein D, Hayashi KM, Clasen L, Toga AW, Giedd JN, Rapoport JL, Thompson PM (2006) Dynamic mapping of normal human hippocampal development. Hippocampus 16:664–672

Gogtay N, Lu A, Leow AD, Klunder AD, Lee AD, Chavez A, Greenstein D, Giedd JN, Toga AW, Rapoport JL, Thompson PM (2008) Three-dimensional brain growth abnormalities in childhood-onset schizophrenia visualized by using tensor-based morphometry. PNAS 105: 15979–15984

Gonçalves-Pereira PM, Insausti R, Artacho-Perula E, Salmenpera T, Kalviainen R, Pitkanen A (2005) MR volumetric analysis of the piriform cortex and cortical amygdala in drug-refractory temporal lobe epilepsy. Amer J Neurorad 26:319–332

Graterón L, Insausti AM, García-Bragado F, Arroyo-Jiménez MM, Marcos P, Martínez-Marcos A, Blaizot X, Artacho-Pérula E, Insausti R (2002) Postnatal development of the human entorhinal cortex. In: Menno Witter, Floris Wouterlood (eds) The parahippocampal region, pp 21–31

Hanke J (1997) Sulcal pattern of the anterior parahippocampal gyrus in the human adult. Annals Anat 179:335–339

Haynes RL, Folkerth RD, Keefe RJ, Sung I, Swzeda LI, Rosenberg PA, Volpe JJ, Kinney HC (2003) Nitrosative and oxidative injury to premyelinating oligodendrocytes in periventricular leukomalacia. J Neuropathol Exp Neurol 62:441–450

Haynes RL, Borenstein NS, Desilva TM, Folkerth RD, Liu LG, Volpe JJ, Kinney HC (2005) Axonal development in the cerebral white matter of the human fetus and infant. J Comp Neurol 484:156–167

Heckers S, Heinsen H, Heinsen Y, Beckmann H (1990a) Morphometry of the parahippocampal gyrus in schizophrenics and controls. Some anatomical considerations. J Neural Transm Gen Sect 80:151–155

Heckers S, Heinsen H, Heinsen YC, Beckmann H (1990b) Limbic structures and lateral ventricle in schizophrenia. A quantitative postmortem study. Arch Gen Psychiatry 47:1016–1022

Heckers S, Heinsen H, Geiger B, Beckmann H (1991) Hippocampal neuron number in schizophrenia. A stereological study. Arch Gen Psychiatry 48:1002–1008

Hevner RF, Kinney HC (1996) Reciprocal entorhinal-hippocampal connections established by human fetal midgestation. J Comp Neurol 372:384–394

Houser CR (1990) Granule cell dispersion in the dentate gyrus of humans with temporal lobe epilepsy. Brain Res 535:195–204

Huttenlocher PR, Dabholkar AS (1997) Regional differences in synaptogenesis in human cerebral cortex. J Comp Neurol 387:167–178

Insausti R (1996) Alteraciones estructurales de la corteza entorrinal e hipocampo en la esquizofrenia. Evidencia o sospecha? Boletín SENC Sociedad Española de Neurociencia 5:17–19

Insausti R, Amaral DG (2004) Hippocampal formation. In: Paxinos and Mai (eds) The human nervous system, pp 871–906

Insausti R, Amaral DG (2008) Entorhinal cortex of the monkey: IV. Topographical and laminar organization of cortical afferents. J Comp Neurol 509:608–641

Insausti R, Muñoz M (2001) Cortical projections of the non-entorhinal hippocampal formation in the cynomolgus monkey (*Macaca fascicularis*). Eur J NeuroSci 14:435–451

Insausti R, Amaral DG, Cowan WM (1987) The entorhinal cortex of the monkey: III. Subcortical afferents. J Comp Neurol 264:396–408

Insausti R, Tunon T, Sobreviela T, Insausti AM, Gonzalo LM (1995) The human entorhinal cortex: a cytoarchitectonic analysis. J Comp Neurol 355:171–198

Insausti R, Insausti AM, Sobreviela MT, Salinas A, Martinez-Penuela JM (1998a) Human medial temporal lobe in aging: anatomical basis of memory preservation. Microsc Res Tech 43:8–15

Insausti R, Juottonen K, Soininen H, Insausti AM, Partanen K, Vainio P, Laakso MP, Pitkanen A (1998b) MR volumetric analysis of the human entorhinal, perirhinal, and temporopolar cortices. Amer J Neurorad 19:659–671

Insausti AM, Megias M, Crespo D, Cruz-Orive LM, Dierssen M, Vallina IF, Insausti R, Florez J (1998c) Hippocampal volume and neuronal number in Ts65Dn mice: a murine model of Down syndrome. Neurosci Lett 253:175–178

Jakob H, Beckmann H (1986) Prenatal developmental disturbances in the limbic allocortex in schizophrenics. J Neural Trans 65:303–326

Jakob H, Beckmann H (1994) Circumscribed malformation and nerve cell alterations in the entorhinal cortex of schizophrenics. Pathogenetic and clinical aspects. J Neural Trans Gen Sect 98:83–106

Judas M, Rados M, Jovanov-Milosevic N, Hrabac P, Stern-Padovan R, Kostovic I (2005) Structural, immunocytochemical, and MR imaging properties of periventricular crossroads of growing cortical pathways in preterm infants. Amer J Neurorad 26:2671–2684

Kappeler C, Dhenain M, Phan Dinh Tuy F, Saillour Y, Marty S, Fallet-Bianco C, Souville I, Souil E, Pinard JM, Meyer G, Encha-Razavi F, Volk A, Beldjord C, Chelly J, Francis F (2007) Magnetic resonance imaging and histological studies of corpus callosal and hippocampal abnormalities linked to doublecortin deficiency. J Comp Neurol 500:239–254

Khazipov R, Esclapez M, Caillard O, Bernard C, Khalilov I, Tyzio R, Hirsch J, Dzhala V, Berger B, Ben-Ari Y (2001) Early development of neuronal activity in the primate hippocampus in utero. J Neurosci 21:9770–9781

Klingler J (1948) Die makroskopische anatomi der Ammonsformation. Denkschr Schweiz Naturforch Ges 78:1–80

Kostovic I, Petanjek Z, Judas M (1993) Early areal differentiation of the human cerebral cortex: entorhinal area. Hippocampus 3:447–458

Kostovic I, Judas M, Rados M, Hrabac P (2002) Laminar organization of the human fetal cerebrum revealed by histochemical markers and magnetic resonance imaging. Cereb Cortex 12:536–544

Kovelman JA, Scheibel AB (1984) A neurohistological correlate of schizophrenia. Biol Psychiatry 19:1601–1621

Kraus C (1962) Changes in paraffin sections caused by the microtome and the resulting distortion (a contribution to the technical treatment of the brain). J Hirnforsch 5:23–38

Kroenke CD, Van Essen DC, Inder TE, Rees S, Bretthorst GL, Neil JJ (2007) Microstructural changes of the baboon cerebral cortex during gestational development reflected in magnetic resonance imaging diffusion anisotropy. J Neurosci 27:12506–12515

Lavenex P, Banta Lavenex P, Amaral DG (2007) Postnatal development of the primate hippocampal formation. Develop Neurosci 29:179–192

Lorente de Nó R (1934) Studies on the structure of the cerebral cortex II. Continuation of the study of the ammonic system. J Physiol Neurol 46:113–177

Mathern GW, Babb TL, Mischel PS, Vinters HV, Pretorius JK, Leite JP, Peacock WJ (1996) Childhood generalized and mesial temporal epilepsies demonstrate different amounts and patterns of hippocampal neuron loss and mossy fibre synaptic reorganization. Brain 119(Pt 3):965–987

Mohedano M, Martinez-Marcos A, Pro-Sistiaga P, Blaizot X, Arroyo-Jimenez MM, Marcos P, Artacho-Pérula E, Insausti R (2008) Convergence of unimodal and polymodal sensory input to the entorhinal cortex in the fascicularis monkey. Neuroscience 151:255–271

Montenegro MA, Kinay D, Cendes F, Bernasconi A, Bernasconi N, Coan AC, Li LM, Guerreiro MM, Guerreiro CA, Lopes-Cendes I, Andermann E, Dubeau F, Andermann F (2006) Patterns

of hippocampal abnormalities in malformations of cortical development. J Neurol Neurosurg Psychiatry 77:367–371
Mouritzen-Dam A (1979) Shrinkage of the brain during histological procedures with fixition in formaldehhyde solutions of different concentrations. J Hirnforsch 20:115–119
Mouritzen-Dam A (1992) The possible pathological importance of dysgenesis, heterotopia and other cellular displacements in the brain. Epilepsy Res Suppl 9:61–65
Noulhiane M, Piolino P, Hasboun D, Clemenceau S, Baulac M, Samson S (2007) Autobiographical memory after temporal lobe resection: neuropsychological and MRI volumetric findings. Brain 130:3184–3199
Novak K, Czech T, Prayer D, Dietrich W, Serles W, Lehr S, Baumgartner C (2002) Individual variations in the sulcal anatomy of the basal temporal lobe and its relevance for epilepsy surgery: an anatomical study performed using magnetic resonance imaging. J Neurosurgery 96:464–473
Nugent TF 3rd, Herman DH, Ordonez A, Greenstein D, Hayashi KM, Lenane M, Clasen L, Jung D, Toga AW, Giedd JN, Rapoport JL, Thompson PM, Gogtay N (2007) Dynamic mapping of hippocampal development in childhood onset schizophrenia. Schizoph Res 90:62–70
Overman WH (1990) Performance on traditional matching to sample, non-matching to sample, and object discrimination tasks by 12- to 32-month-old children. A developmental progression. Ann NY Acad Sci 608:365–385; discussion 385–393
Overman W, Bachevalier J, Turner M, Peuster A (1992) Object recognition versus object discrimination: comparison between human infants and infant monkeys. Behav Neurosci 106:15–29
Pakkenberg B (1993) Total nerve cell number in neocortex in chronic schizophrenics and controls estimated using optical disectors. Biol Psychiatr 34:768–772
Pruessner JC, Li LM, Serles W, Pruessner M, Collins DL, Kabani N, Lupien S, Evans AC (2000) Volumetry of hippocampus and amygdala with high-resolution MRI and three-dimensional analysis software: minimizing the discrepancies between laboratories. Cereb Cortex 10:433–442
Pruessner JC, Kohler S, Crane J, Pruessner M, Lord C, Byrne A, Kabani N, Collins DL, Evans AC (2002) Volumetry of temporopolar, perirhinal, entorhinal and parahippocampal cortex from high-resolution MR images: considering the variability of the collateral sulcus. Cereb Cortex 12:1342–1353
Quester R, Schroder R (1997) The shrinkage of the human brain stem during formalin fixation and embedding in paraffin. J Neurosci Meth 75:81–89
Rados M, Judas M, Kostovic I (2006) In vitro MRI of brain development. Eur J Radiol 57:187–198
Rakic P, Nowakowski RS (1981) The time of origin of neurons in the hippocampal region of the rhesus monkey. J Comp Neurol 196:99–128
Rapoport JL, Giedd JN, Blumenthal J, HamburgerS JN, Fernandez T, Nicholson R, Bedwell J, Lenane M, Zijdenbos A, Paus T, Evans A (1999) Progressive cortical change during adolescence in childhood-onset schizophrenia. A longitudinal magnetic resonance imaging study. Arch Gen Psychiatry 56:649–654
Raymond GV, Bauman ML, Kemper TL (1996) Hippocampus in autism: a Golgi analysis. Acta Neuropathol 91:117–119
Raz N, Torres IJ, Briggs SD, Spencer WD, Thornton AE, Loken WJ, Gunning FM, McQuain JD, Driesen NR, Acker JD (1995) Selective neuroanatomic abnormalities in Down's syndrome and their cognitive correlates: evidence from MRI morphometry. Neurology 45:356–366
Rose M (1927) Der Allocortex bei Mensch und Tier. I und II. J F Psych u Neur 34:1–111
Rosene DL, Hoesen Van GW (1987) The hippocampal formation of the primate brain. A review of some comparative aspects of cytoarchitecture and connections. In: EG Jones and A Peters (eds) Cerebral Cortex, vol 6, pp 345–456

Rosoklija G, Toomayan G, Ellis SP, Keilp J, Mann JJ, Latov N, Hays AP, Dwork AJ (2000) Structural abnormalities of subicular dendrites in subjects with schizophrenia and mood disorders: preliminary findings. Arch Gen Psychiatry 57:349–356

Saitoh O, Karns CM, Courchesne E (2001) Development of the hippocampal formation from 2 to 42 years: MRI evidence of smaller area dentata in autism. Brain 124:1317–1324

Sato N, Hatakeyama S, Shimizu N, Hikima A, Aoki J, Endo K (2001) MR evaluation of the hippocampus in patients with congenital malformations of the brain. Amer J Neurorad 22:389–393

Schumann CM, Buonocore MH, Amaral DG (2001) Magnetic resonance imaging of the post-mortem autistic brain. J Autism Developm Dis 31:561–568

Schumann CM, Hamstra J, Goodlin-Jones BL, Kwon H, Reiss AL, Amaral DG (2007) Hippocampal size positively correlates with verbal IQ in male children. Hippocampus 17:486–493

Seress L (2001) Morphological changes of the human hippocampal formation from midgestation to early childhood. In: Nelson AA, Luciana M (eds) Handbook of developmental cognitive neuroscience. MIT Press, Cambridge, MA, pp 45–47

Seress L, Mrzljak L (1987) Basal dendrites of granule cells are normal features of the fetal and adult dentate gyrus of both monkey and human hippocampal formations. Brain Res 405:169–174

Seress L, Ribak CE (1995a) Postnatal development and synaptic connections of hilar mossy cells in the hippocampal dentate gyrus of rhesus monkeys. J Comp Neurol 355:93–110

Seress L, Ribak CE (1995b) Postnatal development of CA3 pyramidal neurons and their afferents in the Ammon's horn of rhesus monkeys. Hippocampus 5:217–231

Seress L, Abraham H, Tornoczky T, Kosztolanyi G (2001) Cell formation in the human hippocampal formation from mid-gestation to the late postnatal period. Neuroscience 105:831–843

Shaw P, Eckstrand K, Sharp W, Blumenthal J, Lerch JP, Greenstein D, Clasen L, Evans A, Giedd J, Rapoport JL (2007a) Attention-deficit/hyperactivity disorder is characterized by a delay in cortical maturation. PNAS 104:19649–19654

Shaw P, Greenstein D, Lerch J, Clasen L, Lenroot R, Gogtay N, Evans A, Rapoport J, Giedd J (2006) Intellectual ability and cortical development in children and adolescents. Nature 440:676–679

Shaw P, Lerch JP, Pruessner JC, Taylor KN, Rose AB, Greenstein D, Clasen L, Evans A, Rapoport JL, Giedd JN (2007b) Cortical morphology in children and adolescents with different apolipoprotein E gene polymorphisms: an observational study. Lancet Neurol 6:494–500

Shaw P, Kabani NJ, Lerch JP, Eckstrand K, Lenroot R, Gogtay N, Greenstein D, Clasen L, Evans A, Rapoport JL, Giedd JN, Wise SP (2008) Neurodevelopmental trajectories of the human cerebral cortex. J Neurosci 28:3586–3594

Sidman RL, Rakic P (1973) Neuronal migration, with special reference to developing human brain: a review. Brain Res 62:1–35

Skranes J, Vangberg TR, Kulseng S, Indredavik MS, Evensen KA, Martinussen M, Dale AM, Haraldseth O, Brubakk AM (2007) Clinical findings and white matter abnormalities seen on diffusion tensor imaging in adolescents with very low birth weight. Brain 130:654–666

Sloviter RS (1994) The functional organization of the hippocampal dentate gyrus and its relevance to the pathogenesis of temporal lobe epilepsy. Ann Neurol 35:640–654

Sowell ER, Thompson PM, Leonard CM, Welcome SE, Kan E, Toga AW (2004) Longitudinal mapping of cortical thickness and brain growth in normal children. J Neurosci 24:8223–8231

Squire LR, Stark CE, Clark RE (2004) The medial temporal lobe. Ann Rev Neurosci 27: 279–306

Stephan H, Andy OJ (1970) The allocortex in primates. In: Noback and Montana (eds) The primate brain, vol 1, pp 109–134

Tanzi RE (1996) Neuropathology in the Down's syndrome brain. Nat Med 2:31–32

Thompson PM, Vidal C, Giedd JN, Gochman P, Blumenthal J, Nicolson R, Toga AW, Rapoport JL (2001) Mapping adolescent brain change reveals dynamic wave of accelerated gray matter loss in very early-onset schizophrenia. PNAS 98:11650–11655

Trenerry MR, Jack CR Jr, Sharbrough FW, Cascino GD, Hirschorn KA, Marsh WR, Kelly PJ, Meyer FB (1993) Quantitative MRI hippocampal volumes: association with onset and duration of epilepsy, and febrile convulsions in temporal lobectomy patients. Epilepsy Res 15:247–252

Uecker A, Obrzut JE (1993) Hemisphere and gender differences in mental rotation. Brain Cogn 22:42–50

Van Essen DC (2004) Surface-based approaches to spatial localization and registration in primate cerebral cortex. NeuroImage 23(Suppl 1):S97–S107

Vargha-Khadem F, Isaacs E, Mishkin M (1994) Agnosia, alexia and a remarkable form of amnesia in an adolescent boy. Brain 117(Pt 4):683–703

Vargha-Khadem F, Gadian DG, Watkins KE, Connelly A, Van Paesschen W, Mishkin M (1997) Differential effects of early hippocampal pathology on episodic and semantic memory. Science 277:376–380

Weiss S (1991) Morphometry and magnetic resonance imaging of the human brain in normal controls and Down's syndrome. Anat Rec 231:593–598

West JR, Chen WJ, Pantazis NJ (1994) Fetal alcohol syndrome: the vulnerability of the developing brain and possible mechanisms of damage. Met Brain Dis 9:291–322

Witter MP, Amaral DG (2004) Hippocampal formation. In: George Paxinos (ed) The rat nervous system, pp 635–393

Witter MP, Groenewegen HJ, Lopes da Silva FH, Lohman AH (1989) Functional organization of the extrinsic and intrinsic circuitry of the parahippocampal region. Prog Neurobiol 33: 161–253

Subject Index